Doctoral Dissertation

Intratumor bacterium *Cutibacterium acnes*-functionalized graphene oxide nanocomplexes for cancer photothermo-chemo-immunotherapy

Soudamini Chintalapati Sai Vimala Veera

Supervisor: Eijiro Miyako

Division of Advanced Science and Technology,

Japan Advanced Institute of Science and Technology

Materials Science

September 2025

Abstract

The traditional perception of intratumoral bacteria as harmful agents that contribute to cancer progression and metastasis is being increasingly challenged by emerging evidence suggesting their potential therapeutic value. This thesis explores the underappreciated anticancer potential of bacteria isolated from the tumor microenvironment and aims to redefine their role from passive residents or malignancy promoters to active therapeutic agents. During a broader investigation into bacterial anticancer properties, three bacterial strains—*Cutibacterium acnes*, *Acinetobacter radioresistens*, and *Bacillus thuringiensis*—were isolated from tumor tissues and evaluated for their tumor-suppressive capabilities. Among them, *C. acnes*, a non-pathogenic anaerobe from the *Propionibacteriaceae* family, exhibited superior tumor growth inhibition when administered intravenously in murine models. Histological and molecular analyses indicated immune cell infiltration and activation in response to the bacterial presence, suggesting that *C. acnes* exerts its antitumor effects, at least in part, through immune stimulation. Moreover, colony assays confirmed its specific localization within the hypoxic tumor microenvironment, reinforcing its natural tumor-homing ability and biocompatibility.

Despite its promise, monotherapy with *C. acnes* did not achieve complete tumor regression. It could only facilitate tumor growth suppression, underscoring the need for a multimodal approach to tackle cancer's complexity. To address this, the study integrated bacterial immunotherapy with nanotechnology and chemotherapy. Leveraging the amphiphilic and immunogenic nature of bacterial components, a nanohybrid platform was developed by functionalizing graphene oxide (GO) with *C. acnes* biomolecules and loading it with camptothecin (CPT), a hydrophobic chemotherapeutic agent. The resulting CPT–CA–GO complex exhibited improved aqueous dispersibility and was designed to exploit GO's photothermal properties upon near-infrared (NIR) laser exposure. Upon systemic administration and targeted irradiation, this multifunctional nanocomposite facilitated enhanced tumor accumulation, localized heating, chemotherapeutic drug release, and immune system activation, collectively contributing to marked tumor suppression.

This thesis highlights two major insights: first, that certain intratumoral bacteria possess intrinsic therapeutic properties and can serve as safe, cost-effective agents for immunomodulation; and second, that combining biologically derived agents with smart nanomaterials and classical drugs can synergistically enhance therapeutic outcomes. By avoiding genetically modified organisms and relying instead on naturally occurring bacterial strains, this approach offers translational promise with fewer biosafety concerns. Overall, the study presents a novel paradigm in cancer therapy, where intratumoral bacteria—once considered merely opportunistic or pathogenic—are re-envisioned as key elements in a multimodal therapeutic arsenal. These findings not only expand the landscape of oncolytic and immunotherapeutic strategies but also encourage the broader scientific community to revisit the tumor microbiome as a resource for cancer treatment innovation.

Keywords- Cancer, tumor-isolated bacteria, tumor suppression, immunology, Hybrid nanoarchitectonics, photothermal therapy, graphene oxide, drug delivery

Referee-in-Chief - **Dr. Eijiro Miyako,**

Japan Advanced Institute of Science and Technology, Japan

Referees - **Dr. Kazuaki Matsumura**,

Japan Advanced Institute of Science and Technology, Japan

Dr. Motoichi Kurisawa,

Japan Advanced Institute of Science and Technology, Japan

Dr. Takumi Yamaguchi,

Japan Advanced Institute of Science and Technology, Japan

Dr. Eiji Yuba

Osaka Metropolitan University, Japan

Table of contents

List of Tables and Figures

TABLES

CHAPTER 2

CHAPTER 3

FIGURES

CHAPTER 1

CHAPTER 2

CHAPTER 3

CHAPTER 4

CHAPTER 1

General Introduction

Introduction

1.1. Research Interest

This research is positioned at the convergence of cancer biology, tumor immunology, and microbiome science, with a primary focus on investigating the therapeutic potential of intratumoral bacteria in cancer treatment. While tumor-associated bacteria have often been implicated in promoting cancer aggressiveness and aiding metastasis, recent findings indicate that certain intratumoral bacterial species may possess intrinsic anticancer properties.[1-4] This work challenges the conventional perception of bacteria as solely pathogenic in the tumor microenvironment by isolating and evaluating native bacterial strains from within tumors for their tumor-suppressive efficacy.

The study explores three such bacteria—*Cutibacterium acnes*, *Acinetobacter radioresistens*, and *Bacillus thuringiensis*—isolated directly from tumors. Among them, *C. acnes* demonstrated superior tumor suppression through immune system activation, as confirmed by qPCR and IHC analysis. However, while *C. acnes* was effective in suppressing tumor progression, but monotherapy was insufficient for complete tumor regression, highlighting the complexity and multifaceted nature of cancer.

To address these limitations, the research integrates bacterial therapy with chemotherapeutic and photothermal strategies through a nanomedicine platform.[5] Functionalized graphene oxide (GO), modified with components of *C. acnes*, was used to enhance immune activation and drug delivery efficiency. Combined with the natural chemotherapeutic agent camptothecin and near-infrared radiation (NIR)-induced photothermal therapy, the resulting nanoarchitecture enabled targeted tumor ablation. This multimodal approach yielded complete tumor regression in preclinical models,

demonstrating the synergistic effects of combining immune stimulation, chemotherapy, and photothermal therapy.

This research emphasizes the therapeutic promise of tumor-resident bacteria not only as direct anticancer agents but also as bioactive modifiers in nanotechnology platforms. It contributes to a growing field aimed at developing safe, effective, and biologically integrated strategies for tackling cancer through immune-mediated and localized therapeutic interventions.

1.2. Bacterial therapy

Cancer is often framed as a battle, with the immune system and medical interventions fighting against a relentless enemy. Bacterial therapy is an emerging and promising cancer treatment approach that leverages the unique properties of certain bacteria to selectively target and destroy tumors. Historically rooted in the pioneering work of William Coley in the late 19th century, this concept has evolved significantly with advancements in microbiology, immunology, and genetic engineering. Unlike traditional therapies, bacteria—especially facultative or obligate anaerobes—can preferentially colonize the hypoxic and immunosuppressive tumor microenvironment, where many conventional treatments fail. These microbes can stimulate robust immune responses, secrete anticancer enzymes or toxins, and disrupt tumor vasculature. Genetically engineered strains such as *Salmonella, Listeria*, and *Clostridium* have demonstrated the ability to deliver therapeutic payloads directly into tumors while minimizing systemic toxicity.

More recently, intratumoral bacteria—those naturally residing within tumors—have shown intrinsic anticancer and immunostimulatory properties. Traditionally viewed as harmful accomplices in cancer progression, contributing to drug resistance, metastasis, and immune evasion, these microbes are now being re-evaluated. Emerging evidence reveals that certain

bacterial species may actively shape the tumor microenvironment by competing for nutrients, modulating immune pathways, or producing tumor-suppressive metabolites. This suggests a more nuanced relationship between tumors and their resident microbes, reframing the tumor as a complex and dynamic ecosystem rather than a sterile battlefield.

In our laboratory, several intratumoral bacteria displaying unexpected tumor-suppressive capabilities were serendipitously isolated, forming what we now refer to as an AUN consortium (*Rhodopseudomonas palustris* (A-gyo) and *Proteus mirabilis* (UN-gyo)).[6] These findings raise critical questions: Are we overlooking the functional roles of bacteria in cancer biology? Could these microbial communities be harnessed for therapeutic gain? Rather than universally targeting tumor-associated bacteria as threats, it is time to distinguish the harmful from the beneficial and explore their untapped therapeutic potential. By mapping the microbial composition of tumors and elucidating the specific contributions of individual bacterial strains, we may unlock a novel dimension of cancer therapy rooted in microbial biology.

1.3.**Research background**

Cancer remains one of the leading causes of death globally, accounting for nearly 10 million deaths in 2020, which is approximately one in every six deaths worldwide.[7] The most commonly diagnosed cancers include breast, lung, colorectal, and prostate cancer, with lung cancer being the leading cause of cancer-related mortality. Factors such as tobacco use, high body mass index, alcohol consumption, dietary imbalances, and environmental pollution significantly contribute to cancer risk, alongside infectious agents like human papillomavirus (HPV), hepatitis B and C, and *Helicobacter pylori*, which are particularly prevalent in low- and middle-income countries (LMICs). Despite advances in screening and treatment, cancer continues to impose a substantial

global health and economic burden, especially in LMICs where access to early diagnosis and effective therapy remains limited.

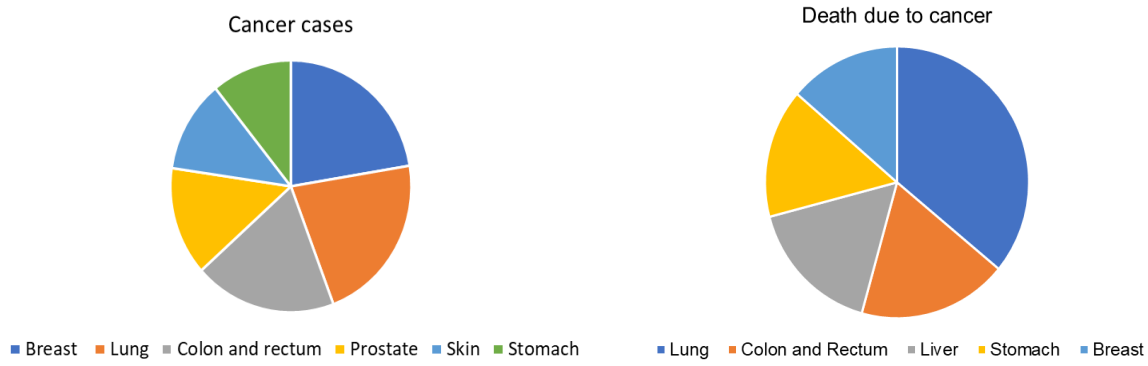

Figure 1.1- Global Cancer Burden Chart- top cancers by incidence and mortality (Source-WHO)

Traditional treatments—chemotherapy, radiotherapy, and surgery—though effective in many cases, are often associated with high costs, systemic toxicity, and limited accessibility. In response to these challenges, emerging strategies such as bacterial therapy have gained attention for their innovative and potentially transformative approach. Bacterial therapy utilizes genetically engineered or naturally tumor-targeting bacteria to localize within cancerous tissues, particularly hypoxic and necrotic tumor cores that are often resistant to standard treatments. These bacteria can directly lyse tumor cells, modulate the immune response, or deliver therapeutic agents like cytokines or gene-editing tools precisely within the tumor microenvironment. Early-phase clinical studies using strains like *Clostridium novyi*-NT and *Salmonella typhimurium* have shown encouraging results.[8,9] Notably, bacterial therapy holds promise as a cost-effective alternative to more complex and expensive therapies such as CAR-T cell therapy or monoclonal antibodies.[10,11] Its potential for low-cost production, ease of storage, and reduced systemic toxicity makes it especially appealing for resource-limited settings. Therefore, bacterial therapy represents a novel and practical frontier in cancer treatment, aligning scientific innovation with the pressing need for accessible, affordable, and effective oncological care worldwide.

1.4.Future scope

With the continuous advancement of science and biotechnology, cancer therapy is entering an exciting new phase of innovation. While conventional treatments such as chemotherapy, radiation, and surgery have significantly evolved over the past decades, survival rates for many cancers remain suboptimal. One major obstacle is the intrinsic heterogeneity of cancer; each tumor—and even each cell within a tumor—can possess distinct mutations, making it difficult for standard monotherapies to offer a universally effective solution. This complexity demands a more dynamic, targeted, and adaptive approach. Bacterial therapy, also referred to as "living drug therapy," represents a promising frontier in this regard. Contrary to the long-standing perception of bacteria as purely harmful agents, recent research has highlighted their ability to selectively target tumor environments, particularly hypoxic and necrotic cores, and to stimulate robust anti-tumor immune responses. Several bacterial strains have demonstrated not only tumor localization abilities but also the potential to deliver therapeutic agents and activate host immunity, thereby enhancing therapeutic outcomes.

However, bacterial therapy is not without its challenges. Risks such as systemic toxicity, unwanted inflammation, and off-target effects underscore the need for precise control over bacterial dose and strain specificity. Personalized bacterial therapies tailored to individual tumor profiles may help overcome these barriers. Furthermore, due to the complex nature of cancer, the integration of bacterial therapy with other treatment modalities—such as chemotherapy, radiation, immunotherapy, or even surgery when applicable—offers a synergistic approach that could significantly enhance efficacy. Ongoing research is increasingly focused on such combinatorial strategies to address the multifaceted nature of cancer. The future of bacterial therapy lies in

refining bacterial engineering, improving targeting mechanisms, and conducting rigorous clinical trials to establish safety, effectiveness, and scalability. With continued interdisciplinary collaboration and technological progress, bacterial therapy holds significant promise as a cost-effective, accessible, and transformative component of next-generation cancer treatment strategies.

1.5. References

[1] S. Xiao, M. Mu, C. Feng, S. Pan, N. Chen, The application of bacteria-nanomaterial hybrids in antitumor therapy, Journal of Nanobiotechnology 2024 22:1 22 (2024) 1–24. https://doi.org/10.1186/S12951-024-02793-X.

[2] F. Rommasi, Bacterial-Based Methods for Cancer Treatment: What We Know and Where We Are, Oncol Ther 10 (2022) 23–54. https://doi.org/10.1007/s40487-021-00177-x.

[3] K.H. Gupta, C. Nowicki, E.F. Giurini, A.L. Marzo, A. Zloza, Bacterial-based cancer therapy (Bbct): Recent advances, current challenges, and future prospects for cancer immunotherapy, Vaccines (Basel) 9 (2021). https://doi.org/10.3390/vaccines9121497.

[4] M.G. Kramer, M. Masner, F.A. Ferreira, R.M. Hoffman, Bacterial Therapy of Cancer: Promises, Limitations, and Insights for Future Directions, Front Microbiol 9 (2018) 16. https://doi.org/10.3389/FMICB.2018.00016.

[5] A. Upadhyay, Cancer: An unknown territory; rethinking before going ahead, Genes Dis 8 (2021) 655–661. https://doi.org/10.1016/j.gendis.2020.09.002.

[6] Y. Goto, S. Iwata, M. Miyahara, E. Miyako, Discovery of Intratumoral Oncolytic Bacteria Toward Targeted Anticancer Theranostics, Advanced Science 10 (2023). https://doi.org/10.1002/advs.202301679.

[7] Cancer, (n.d.). https://www.who.int/news-room/fact-sheets/detail/cancer (accessed April 30, 2025).

[8] V. Staedtke, N.J. Roberts, R.Y. Bai, S. Zhou, Clostridium novyi-NT in cancer therapy, Genes Dis 3 (2016) 144. https://doi.org/10.1016/J.GENDIS.2016.01.003.

[9] Y. Zhang, S. Miwa, N. Zhang, R.M. Hoffman, M. Zhao, Tumor-targeting Salmonella typhimurium A1-R arrests growth of breast-cancer brain metastasis, Oncotarget 6 (2014) 2615. https://doi.org/10.18632/ONCOTARGET.2811.

[10] R.C. Sterner, R.M. Sterner, CAR-T cell therapy: current limitations and potential strategies, Blood Cancer Journal 2021 11:4 11 (2021) 1–11. https://doi.org/10.1038/s41408-021-00459-7.

[11] C.H. June, R.S. O'Connor, O.U. Kawalekar, S. Ghassemi, M.C. Milone, CAR T cell immunotherapy for human cancer, Science (1979) 359 (2018) 1361–1365. https://doi.org/10.1126/SCIENCE.AAR6711/ASSET/373C3262-9A02-44E9-AF18-3A3ACA77E131/ASSETS/GRAPHIC/359_1361_F4.JPEG.

CHAPTER 2

Tumor-isolated Cutibacterium acnes as an effective tumor suppressive living drug

Abstract

The two major challenges in cancer treatment are reducing the side effects and minimizing the cost of cancer treatment. A better therapy to treat cancer remains to be developed despite the presence of many therapeutic options. Here, we present bacterial therapy for treating cancer using tumor-isolated *Cutibacterium acnes*, which is safe to use, has minimal side effects compared to chemotherapeutic drugs, and most importantly, targets the tumor microenvironment due to the bacterium's anaerobic nature. It activates the immune system, and the immune cells effectively penetrate through the tumor tissue and form an immunologic hub inside, explicitly targeting the tumor and destroying the cells. This bacterial therapy is a new, cost-effective, innovative treatment.

Tumor-isolated *Cutibacterium acnes* as an effective tumor suppressive living drug

2.1 Keywords: Intratumoral bacteria; *Cutibacterium acnes*; tumor suppression; immunology

Highlights

- Tumor-resident bacteria possess unexplored, strong anticancer properties.
- Bacteria-mediated cancer therapy demonstrates excellent tumor suppression.
- *Cutibacterium acnes* attracts cytotoxic immune cells.
- Bacteria could be a cost-effective modality to effectively treat cancer.

2.2 Introduction

Receiving cancer treatment is a pressing issue nowadays, not only for patients with cancer but also for their close friends and family members. Dealing with cancer is challenging and severely painful both physically and mentally. The financial burden is another major pitfall in this whole story. The World Health Organization estimates approximately 19 million newly diagnosed cancer cases annually, out of which approximately 9.9 million cases face death.[1] All available knowledge needs to be applied in the search for cancer treatment. A few possible reasons why more treatment options remain needed today despite the availability of many therapeutics are the heterogeneous nature of the tumor environment, the presence of foolproof mechanisms to suppress the host immune system, and the constant DNA mutation in the cancer cells which creates new cancer cells with new modifications.[2]

Among many cutting-edge remedies, cancer immunotherapy has revolutionized treatment as a forth pillar after traditional major therapies and rejuvenated the field of tumor immunology.[3–8] Sir William B. Coley first performed immunotherapy for cancer in the 1890s, after a thorough literature review, when he injected heat-killed bacteria, *Streptococcus pyogenes* and *Serratia*

marcescens (the Coley's toxin), into patients with severe metastatic cancer. Most of the patients had a good prognosis.[9] Today, we use immunotherapy in the form of antibody therapy, T-cell transfer therapy, etc., to treat cancer and various other diseases.[10] However, the rigid stromal barrier and hypoxic area of the solid tumor is poorly infiltrated by antibodies and anti-tumor immune cells.[11–14] Because of specific characteristics, bacteria have promising advantages in the field of tumor therapy. Indeed, facultative and obligate anaerobic bacteria selectively accumulate to and colonize solid tumor tissues as these have hypoxic and immunosuppressive tumor microenvironments (TME).[15,16] As the result, proliferated bacteria can effectively recruit and stimulate cytotoxic immune cells to suppress cancerous tumor cells in TME.[17–20] For a long time, only the probiotic bacteria have been, in our opinion, the most useful bacteria, but today, many virulent engineered bacteria, such as *Listeria*, *Clostridium*, *Salmonella,* etc., are being attenuated and genetically modified to help treat cancer. Attenuated *Salmonella* sps. reached till clinical trials as well.[17–20] Therefore, bacterial therapy is in its renaissance phase, and these living materials should be considered for actual cancer treatment after studying and analyzing their effective anticancer properties.[21–24] However, the efficacy and tumor targeting of conventional bacterial cancer therapy still remain challenging.

To overcome the drawbacks of conventional bacterial cancer therapy, nanoengineered bacterial therapy is in its implementation phase.[25–35] In fact, some nanoparticle-coupled bacterial therapies bring synergistic effects on the tumor and its development. In particular, simple nanoengineering amplifies the physicochemical activities of bacteria or crosslinking surface molecules of the bacterium with particles, such as functional pigment indocyanine green, polydopamine, and therapeutic polymer that induce effective hyperthermia for photothermal cancer therapy.[36–38] Indeed, the easily manipulatable nature of bacteria by nanoengineering and/or genetic engineering

has a great scope. However, the development of the ultimate natural bacterial chassis, which has stronger anticancer efficacy, excellent tumor targeting effect, and higher biocompatibility, is essential for development of future innovative nanoengineering of bacteria.

To that end, intratumoral bacteria could be a useful tool in the fight against cancer.[39–44] We recently reported the discovery and first demonstrated the effective anticancer properties of isolated intratumoral bacteria, which are associated with natural purple photosynthetic bacteria.[45] In fact, bacteria, including *Proteus mirabilis* and *Rhodopseudomonas paulistris,* grow and proliferate within the tumor microenvironment which effectively modulates the immune system and provokes strong anticancer responses in various syngeneic mice models. However, much more work and understanding of the anticancer efficacy of various intratumoral bacteria is required before it can be applied to personalized medicine. Several studies have been conducted on bacteria inside the tumor and how they could contribute to the development of cancer,[39–44] but the current study aimed to investigate whether intratumoral bacteria, when isolated from the tumor and used to cure the tumor, could cure cancer. We believe that higher biocompatible and stronger therapeutic oncolytic bacteria still remain in a tumor.

This study explored the anticancer efficacy of three native strains of bacteria, including *Acinetobacter radioresistens, Bacillus thuringiensis,* and *Cutibacterium acnes,* isolated from the tumors. Out of these three bacteria, *C. acnes* showed excellent tumor-suppressing ability. Additionally, *C. acnes* species could be safely injected intravenously into the target and colonize the hypoxic tumor microenvironment. Further, we compared the efficacy demonstrated by this bacterium to the immune checkpoint inhibitor (ICI) drug, the programmed cell-death ligand 1 (PD-L1) inhibitor (Anti-PD-L1 antibody), and the antineoplastic drug, paclitaxel (Taxol). *C. acnes* has demonstrated impressive tumor suppression with its oncolytic, as well as immunostimulant

properties, compared to the antineoplastic drug and ICI. This study describes our results about the anticancer properties of these intratumoral bacteria and their strategy in inducing the immune response. This study elucidates the mystery of intratumoral bacteria and its immunology.

2.3 Materials and Methods

2.3.1 Bacterial strains

This investigation used bacteria, including *A. radioresistens*, *B. Thuringiensis*, and *C. acnes*, which were isolated from mice bearing breast cancer EMT6/AR1 and Meth-A sarcoma-derived cell lines, respectively. *A. radioresistens* were grown aerobically in the *Luria Bertani* (*LB*) broth (Nacalai Tesque, Kyoto, Japan) at 37°C inside the incubator (i-CUBE FCI-280HG; AS ONE, Osaka, Japan) for not >3 days. *B. Thuringiensis* and *C. acnes* were grown anaerobically in Pearl Core E-MC64 medium (Eiken Chemical, Tokyo, Japan) at 37°C inside the incubator for not >3 days. This experiment obtained all the chemicals used from Nacalai Tesque, Tokyo Chemical Industry (Tokyo, Japan), and FUJIFILM Wako Pure Chemical (Osaka, Japan).

2.3.2 Antineoplastic and ICI drugs

The antineoplastic drug, paclitaxel (Nacalai Tesque) at 1 mg/mL, was sonicated in 10% Cremophor EL® (Nacalai Tesque) in phosphate-buffered saline (PBS) for 5 min to dissolve into the solution and was stored for 1 week at 4°C. It was sonicated for 1 min before every use to make sure that the suspension was maintained. ICI drug, anti-PD-L1 (Leinco Technologies, MO, USA) (6 mg/mL) was stored at −80°C, diluted in PBS, and used for further tests.

2.3.3 Isolation of functional bacteria from solid tumors

The animal experiments followed the protocols approved by the Institutional Animal Care and Use Committee of Japan Advanced Institute of Science and Technology (JAIST) (No. 04-007). We obtained female BALB/cCrSlc mice (n = 3; 4 weeks old; average weight = 15 g) from Japan SLC

(Hamamatsu, Japan). We generated a mouse bearing the EMT6/AR1-derived tumors by injecting 100 µL of the culture medium/Matrigel (Dow Corning, Corning, NY) mixture (v/v = 1:1) containing 1×10^6 cells into the right flank region of the mouse. The tumors were carefully excised after 14 days when the tumor volumes reached approximately 300 mm^3. The mixture was shaken for 20 min at a speed of 380 rpm/min at 15°C after homogenizing thoroughly with a homogenizer pestle in 2 mL of PBS solution at 4°C. The supernatant (100 µL) was inoculated onto four different agar plates, namely, desoxycholate agar (with sodium desoxycholate, iron ammonium citrate, sodium chloride, dipotassium phosphate, lactose, peptone, and neutral red) (Nissui Pharmaceutical); mannitol salt agar (with mannitol, sodium chloride, phenol red, meat extract, and peptone) (Nissui Pharmaceutical); standard method agar (with yeast, peptone, and glucose) (Nissui Pharmaceutical); and LB agar (tryptone, Sodium chloride and yeast extract) (Nacalai tesque). A few colonies developed on the LB agar plate and the standard method agar plate after incubation for 3 days anaerobically under tungsten lamps. They were carefully picked using a syringe needle and stereomicroscope. The colorless colonies were sub-cultured aerobically and anaerobically in the LB broth (Nacalai Tesque) and Pearl Core E-MC64 medium (Eiken Chemical, Tokyo, Japan) at 37°C inside the incubator (i-CUBE FCI-280HG; AS ONE). The best growth of this bacteria was observed in aerobic conditions in the LB broth. The media was spread on an LB agar plate and sent for identification. The BEX Co. (Tokyo, Japan) identified it as *A. radioresistens* (listed in **Table 2.1**).

Two more bacteria were similarly identified from the sarcoma-Meth-A derived solid tumors (ca. 300 mm^3). Female BALB/cCrSlc mice (n = 3; 4 weeks old; average weight = 15 g) were injected on the right flank with 100 µL of the culture medium/Matrigel (Dow Corning, Corning, NY) mixture (v/v = 1:1) containing 1×10^6 cells into the right flank region of the mouse. We excised

the tumor after 14 days. The solution was spread on four different agar plates anaerobically at 26°C–30°C under tungsten lamps after thoroughly homogenizing the tumor in PBS. Two different colonies of bacteria were isolated using a syringe needle and stereomicroscope. The colorless colonies of *B. thuringiensis* were carefully picked from the deoxycholate agar plate and standard method agar plate and demonstrated the best growth in the anaerobic condition in the Pearl Core E-MC64 medium (Eiken Chemical, Tokyo, Japan) at 37°C inside the incubator (i-CUBE FCI-280HG; AS ONE). Thus, Pearl Core E-MC64 medium was used for further cultures of *B. thuringiensis*. The colorless colonies of *C. acnes* were carefully picked from the standard method agar plate and presented the best growth in the anaerobic condition in the Pearl Core E-MC64 medium (Eiken Chemical, Tokyo, Japan) at 37°C inside the incubator. Thus, Pearl Core E-MC64 medium was used for further cultures of *C. acnes.* These bacteria were sent for identification at the BEX Co. (listed in **Tables 2.2 and 2.3**).

Table 2.1. Obtained 16S rRNA gene sequences of *Acinetobacter radioresisten*s

<Partial gene sequence (758 bp)>

GATTGAACGCTGGCGGCAGGCTTAACACATGCAAGTCGAGCGGATGAAAGTAGCTT
GCTACyGGATTCAGCGGCGGACGGGTGAGTAATGCTTAGGAATCTGCCTATTAGTGGGGG
ACAACGTTCCGAAAGGGGCGCTAATACCGCATACGTCCTACGGGAGAAAGCAGGGGACC
TTTGGGCCTTGCGCTAATAGATGAGCCTAAGTCGGATTAGCTAGTTGGTAGGGTAAAGGC
CTACCAAGGCGACGATCTGTAGCGGGTCTGAGAGGATGATCCGCCACACTGGGACTGAGA
CACGGCCCAGACTCCTACGGGAGGCAGCAGTGGGGAATATTGGACAATGGGGGGAACCC
TGATCCAGCCATGCCGCGTGTGTGAAGAAGGCCTTTTGGTTGTAAAGCACTTTAAGCGAG
GAGGAGGCTACCTAGATTAATACTTTAGGATAGTGGACGTTACTCGCAGAATAAGCACCG
GCTAACTCTGTGCCAGCAGCCGCGGTAATACAGAGGGTGCGAGCGTTAATCGGATTTACT
GGGCGTAAAGCGTGCGTAGGCGGCCAATTAAGTCAAATGTGAAATCCCCGAGCTTAACTT
GGGAATTGCATTCGATACTGGTTGGCTAGAGTATGGGAGAGGATGGTAGAATTCCAGGTG
TAGCGGTGAAATGCGTAGAGATCTGGAGGAATACCGATGGCGAAGGCAGCCATCTGGCCT
AATACTGACGCTGAGGTACGAAAGCATGGGGAGCAAACAGGATT

<Complete gene sequence (1,459 bp)>

ATTGAACGCTGGCGGCAGGCTTAACACATGCAAGTCGAGCGGATGAAAGTAGCTTG
CTACyGGATTCAGCGGCGGACGGGTGAGTAATGCTTAGGAATCTGCCTATTAGTGGGGGA
CAACGTTCCGAAAGGGGCGCTAATACCGCATACGTCCTACGGGAGAAAGCAGGGGACCTT
TGGGCCTTGCGCTAATAGATGAGCCTAAGTCGGATTAGCTAGTTGGTAGGGTAAAGGCCT
ACCAAGGCGACGATCTGTAGCGGGTCTGAGAGGATGATCCGCCACACTGGGACTGAGACA
CGGCCCAGACTCCTACGGGAGGCAGCAGTGGGGAATATTGGACAATGGGGGGAACCCTG
ATCCAGCCATGCCGCGTGTGTGAAGAAGGCCTTTTGGTTGTAAAGCACTTTAAGCGAGGA
GGAGGCTACCTAGATTAATACTTTAGGATAGTGGACGTTACTCGCAGAATAAGCACCGGC
TAACTCTGTGCCAGCAGCCGCGGTAATACAGAGGGTGCGAGCGTTAATCGGATTTACTGG
GCGTAAAGCGTGCGTAGGCGGCCAATTAAGTCAAATGTGAAATCCCCGAGCTTAACTTGG
GAATTGCATTCGATACTGGTTGGCTAGAGTATGGGAGAGGATGGTAGAATTCCAGGTGTA
GCGGTGAAATGCGTAGAGATCTGGAGGAATACCGATGGCGAAGGCAGCCATCTGGCCTA
ATACTGACGCTGAGGTACGAAAGCATGGGGAGCAAACAGGATTAGATACCCTGGTAGTCC
ATGCCGTAAACGATGTCTACTAGCCGTTGGGGCCCTTGAGGCTTTAGTGGCGCAGCTAAC
GCGATAAGTAGACCGCCTGGGGAGTACGGTCGCAAGACTAAAACTCAAATGAATTGACG
GGGGCCCGCACAAGCGGTGGAGCATGTGGTTTAATTCGATGCAACGCGAAGAACCTTACC
TGGCCTTGACATACAGAGAACTTTCCAGAGATGGATTGGTGCCTTCGGGAACTCTGATAC
AGGTGCTGCATGGCTGTCGTCAGCTCGTGTCGTGAGATGTTGGGTTAAGTCCCGCAACGA
GCGCAACCCTTTTCCTTATTTGCCAGCACTTCGGGTGGGAACTTTAAGGATACTGCCAGTG
ACAAACTGGAGGAAGGCGGGGACGACGTCAAGTCATCATGGCCCTTACGGCCAGGGCTA
CACACGTGCTACAATGGTCGGTACAAAGGGTTGCTACACAGCGATGTGATGCTAATCTCA
AAAAGCCGATCGTAGTCCGGATTGGAGTCTGCAACTCGACTCCATGAAGTCGGAATCGCT
AGTAATCGCGGATCAGAATGCCGCGGTGAATACGTTCCCGGGCCTTGTACACACCGCCCG
TCACACCATGGGAGTTTGTTGCACCAGAAGTAGGTAGTCTAACCTTAGGGGGGACGCTTA
CCACGGTGTGGCCGATGACTGGGGTG

Table 2.2. Obtained 16S rRNA gene sequences of *Bacillus thuringiensis*.

<Partial gene sequence (767 bp)> GGATGAACGCTGGCGGCGTGCCTAATACATGCAAGTCGAGCGAATGGATTAAGAGC TTGCTCTTATGAAGTTAGCGGCGGACGGGTGAGTAACACGTGGGTAACCTGCCCATAAGA CTGGGATAACTCCGGGAAACCGGGGCTAATACCGGATAACATTTTGAACCGCATGGTTCG AAATTGAAAGGCGGCTTCGGCTGTCACTTATGGATGGACCCGCGTCGCATTAGCTAGTTG GTGAGGTAACGGCTCACCAAGGCAACGATGCGTAGCCGACCTGAGAGGGTGATCGGCCA CACTGGGACTGAGACACGGCCCAGACTCCTACGGGAGGCAGCAGTAGGGAATCTTCCGCA ATGGACGAAAGTCTGACGGAGCAACGCCGCGTGAGTGATGAAGGCTTTCGGGTCGTAAAA CTCTGTTGTTAGGGAAGAACAAGTGCTAGTTGAATAAGCTGGCACCTTGACGGTACCTAA CCAGAAAGCCACGGCTAACTACGTGCCAGCAGCCGCGGTAATACGTAGGTGGCAAGCGTT ATCCGGAATTATTGGGCGTAAAGCGCGCGCAGGTGGTTTCTTAAGTCTGATGTGAAAGCC CACGGCTCAACCGTGGAGGGTCATTGGAAACTGGGAGACTTGAGTGCAGAAGAGGAAAG TGGAATTCCATGTGTAGCGGTGAAATGCGTAGAGATATGGAGGAACACCAGTGGCGAAG GCGACTTTCTGGTCTGTAACTGACACTGAGGCGCGAAAGCGTGGGGAGCAAACA
<Complete gene sequence (1,474 bp)> GATGAACGCTGGCGGCGTGCCTAATACATGCAAGTCGAGCGAATGGATTAAGAGCT TGCTCTTATGAAGTTAGCGGCGGACGGGTGAGTAACACGTGGGTAACCTGCCCATAAGAC TGGGATAACTCCGGGAAACCGGGGCTAATACCGGATAACATTTTGAACCGCATGGTTCGA AATTGAAAGGCGGCTTCGGCTGTCACTTATGGATGGACCCGCGTCGCATTAGCTAGTTGGT GAGGTAACGGCTCACCAAGGCAACGATGCGTAGCCGACCTGAGAGGGTGATCGGCCACA CTGGGACTGAGACACGGCCCAGACTCCTACGGGAGGCAGCAGTAGGGAATCTTCCGCAAT GGACGAAAGTCTGACGGAGCAACGCCGCGTGAGTGATGAAGGCTTTCGGGTCGTAAAACT CTGTTGTTAGGGAAGAACAAGTGCTAGTTGAATAAGCTGGCACCTTGACGGTACCTAACC AGAAAGCCACGGCTAACTACGTGCCAGCAGCCGCGGTAATACGTAGGTGGCAAGCGTTAT CCGGAATTATTGGGCGTAAAGCGCGCGCAGGTGGTTTCTTAAGTCTGATGTGAAAGCCCA CGGCTCAACCGTGGAGGGTCATTGGAAACTGGGAGACTTGAGTGCAGAAGAGGAAAGTG GAATTCCATGTGTAGCGGTGAAATGCGTAGAGATATGGAGGAACACCAGTGGCGAAGGC GACTTTCTGGTCTGTAACTGACACTGAGGCGCGAAAGCGTGGGGAGCAAACAGGATTAGA TACCCTGGTAGTCCACGCCGTAAACGATGAGTGCTAAGTGTTAGAGGGTTTCCGCCCTTTA GTGCTGAAGTTAACGCATTAAGCACTCCGCCTGGGGAGTACGGCCGCAAGGCTGAAACTC AAAGGAATTGACGGGGGCCCGCACAAGCGGTGGAGCATGTGGTTTAATTCGAAGCAACG CGAAGAACCTTACCAGGTCTTGACATCCTCTGAAAACCCTAGAGATAGGGCTTCTCCTTCG GGAGCAGAGTGACAGGTGGTGCATGGTTGTCGTCAGCTCGTGTCGTGAGATGTTGGGTTA AGTCCCGCAACGAGCGCAACCCTTGATCTTAGTTGCCATCATTAAGTTGGGCACTCTAAGG TGACTGCCGGTGACAAACCGGAGGAAGGTGGGGATGACGTCAAATCATCATGCCCCTTAT GACCTGGGCTACACACGTGCTACAATGGACGGTACAAAGAGCTGCAAGACCGCGAGGTG GAGCTAATCTCATAAAACCGTTCTCAGTTCGGATTGTAGGCTGCAACTCGCCTACATGAAG CTGGAATCGCTAGTAATCGCGGATCAGCATGCCGCGGTGAATACGTTCCCGGGCCTTGTA CACACCGCCCGTCACACCACGAGAGTTTGTAACACCCGAAGTCGGTGGGGTAACCTTTTT GGAGCCAGCCGCCTAAGGTGGGACAGATGATTGGGGTG

Table 2.3. Obtained 16S rRNA gene sequences of *Cutibacterium acnes*.

<Partial gene sequence (736 bp)>

GGACGAACGCTGGCGGCGTGCTTAACACATGCAAGTCGAACGGAAAGGCCCTGCTT
TTGTGGGGTGCTCGAGTGGCGAACGGGTGAGTAACACGTGAGTAACCTGCCCTTGACTTT
GGGATAACTTCAGGAAACTGGGGCTAATACCGGATAGGAGCTCCTGCTGCATGGTGGGGG
TTGGAAAGTTTCGGCGGTTGGGGATGGACTCGCGGCTTATCAGCTTGTTGGTGGGGTAGTG
GCTTACCAAGGCTTTGACGGGTAGCCGGCCTGAGAGGGTGACCGGCCACATTGGGACTGA
GATACGGCCCAGACTCCTACGGGAGGCAGCAGTGGGGAATATTGCACAATGGGCGGAAG
CCTGATGCAGCAACGCCGCGTGCGGGATGACGGCCTTCGGGTTGTAAACCGCTTTCGCCT
GTGACGAAGCGTGAGTGACGGTAATGGGTAAAGAAGCACCGGCTAACTACGTGCCAGCA
GCCGCGGTGATACGTAGGGTGCGAGCGTTGTCCGGATTTATTGGGCGTAAAGGGCTCGTA
GGTGGTTGATCGCGTCGGAAGTGTAATCTTGGGGCTTAACCCTGAGCGTGCTTTCGATACG
GGTTGACTTGAGGAAGGTAGGGGAGAATGGAATTCCTGGTGGAGCGGTGGAATGCGCAG
ATATCAGGAGGAACACCAGTGGCGAAGGCGGTTCTCTGGGCCTTTCCTGACGCTGAGGAG
CGAAAGCGTGGGGAGCGAACA

<Complete gene sequence (1,447 bp)>

GACGAACGCTGGCGGCGTGCTTAACACATGCAAGTCGAACGGAAAGGCCCTGCTTT
TGTGGGGTGCTCGAGTGGCGAACGGGTGAGTAACACGTGAGTAACCTGCCCTTGACTTTG
GGATAACTTCAGGAAACTGGGGCTAATACCGGATAGGAGCTCCTGCTGCATGGTGGGGGT
TGGAAAGTTTCGGCGGTTGGGGATGGACTCGCGGCTTATCAGCTTGTTGGTGGGGTAGTG
GCTTACCAAGGCTTTGACGGGTAGCCGGCCTGAGAGGGTGACCGGCCACATTGGGACTGA
GATACGGCCCAGACTCCTACGGGAGGCAGCAGTGGGGAATATTGCACAATGGGCGGAAG
CCTGATGCAGCAACGCCGCGTGCGGGATGACGGCCTTCGGGTTGTAAACCGCTTTCGCCT
GTGACGAAGCGTGAGTGACGGTAATGGGTAAAGAAGCACCGGCTAACTACGTGCCAGCA
GCCGCGGTGATACGTAGGGTGCGAGCGTTGTCCGGATTTATTGGGCGTAAAGGGCTCGTA
GGTGGTTGATCGCGTCGGAAGTGTAATCTTGGGGCTTAACCCTGAGCGTGCTTTCGATACG
GGTTGACTTGAGGAAGGTAGGGGAGAATGGAATTCCTGGTGGAGCGGTGGAATGCGCAG
ATATCAGGAGGAACACCAGTGGCGAAGGCGGTTCTCTGGGCCTTTCCTGACGCTGAGGAG
CGAAAGCGTGGGGAGCGAACAGGCTTAGATACCCTGGTAGTCCACGCTGTAAACGGTGGG
TACTAGGTGTGGGGTCCATTCCACGGGTTCCGTGCCGTAGCTAACGCTTTAAGTACCCCGC
CTGGGGAGTACGGCCGCAAGGCTAAAACTCAAAGGAATTGACGGGGCCCCGCACAAGCG
GCGGAGCATGCGGATTAATTCGATGCAACGCGTAGAACCTTACCTGGGTTTGACATGGAT
CGGGAGTGCTCAGAGATGGGTGTGCCTCTTTTGGGGTCGGTTCACAGGTGGTGCATGGCT
GTCGTCAGCTCGTGTCGTGAGATGTTGGGTTAAGTCCCGCAACGAGCGCAACCCTTGTTCA
CTGTTGCCAGCACGTTATGGTGGGGACTCAGTGGAGACCGCCGGGGTCAACTCGGAGGAA
GGTGGGGATGACGTCAAGTCATCATGCCCCTTATGTCCAGGGCTTCACGCATGCTACAATG
GCTGGTACAGAGAGTGGCGAGCCTGTGAGGGTGAGCGAATCTCGGAAAGCCGGTCTCAGT
TCGGATTGGGGTCTGCAACTCGACCTCATGAAGTCGGAGTCGCTAGTAATCGCAGATCAG
CAACGCTGCGGTGAATACGTTCCCGGGGCTTGTACACACCGCCCGTCAAGTCATGAAAGT
TGGTAACACCCGAAGCCGGTGGCCTAACCGTTGTGGGGGAGCCGTCGAAGGTGGGACTGG
TGATTAGGACT

2.3.4 Cell culture

This experiment obtained the murine colon carcinoma cell line (Colon-26) from the Japanese Collection of Research Bioresources Cell Bank (Tokyo, Japan). We purchased murine skin sarcoma (Meth-A) cell lines from the Cell Resource Center for Biomedical Research, Institute of Development, Aging and Cancer Tohoku University (Sendai, Japan). Drug-resistant mouse mammary tumor (EMT6/AR1) cell line was obtained from KAC Co., Ltd. (Tokyo, Japan). The Colon-26 and Meth-A cell line was cultured in the Roswell Park Memorial Institute 1640 Medium (Gibco, Grand Island, NY) containing 10% fetal bovine serum and 1% penicillin-streptomycin, while the EMT6/AR1 cell line was cultured in cell growth medium No.104 (KAC Co., Ltd.) containing doxorubicin (1 μg mL^{-1}). Cells were maintained at 37°C in a humidified incubator containing 5% CO_2 and were cryopreserved in multiple vials and stored in liquid nitrogen. Cell stocks were regularly revived to avoid the genetic instabilities that are associated with high passage numbers.

2.3.5 Bacterial anticancer therapy

Female BALB/cCrSlc mice (n = 20; 4 weeks old; average weight = 17 g) were obtained from Japan SLC (Hamamatsu, Japan) to study the anticancer efficacy of bacteria. Mice bearing the Colon-26 cell-derived tumors were generated by injecting 100 μL of the culture medium/Matrigel (Dow Corning, Corning, NY) mixture (v/v = 1:1) containing 5×10^6 cells into the right flank of the mice. As the average tumor size reached approximately 100 mm^3 (n = 5 in each group; 7 weeks old; average weight = 17 g) in approximately 10 days, they were intravenously injected in the tail vein with culture medium (200 μL) containing *A. radioresistens* (1×10^7 CFU/mL), *B. thuringiensis* (1×10^9 CFU/mL), and *C. acnes* (1×10^9 CFU/mL). The control experiments were also performed using PBS (200 μL) which was also intravenously injected into the tail. Changes in tumor volume

and overall health (Viability and body weight) were monitored daily. The tumor volume was calculated using $V = L \times W^2/2$, where L and W stand for the length and width of the tumor, respectively. The survival ratio of Colon-26 tumor-bearing mice (n = 20, biologically independent mice) was also measured during treatment for 40 days. The mice were euthanized as the endpoint was reached according to the guidelines of the Institutional Animal Care and Use Committee of JAIST when the tumor volumes reached >2000 mm^3. The values of median lethal dose (LD_{50}) were measured using ten female BALB/cCrSlc mice (6 weeks old; average weight = 20 g) for each bacterium at different concentration.

2.3.6 Colony assay

The Colon-26 tumor-bearing BALB/c mice (female, 7weeks; n = 3; average tumor size = 200 mm^3; average weight = 20 g; BALB/cCrSIc; Japan SLC) were intravenously injected in the tail vein with culture medium (200 μL) containing *C. acnes* (1×10^9 CFU/mL). After 24 and 72 h, the tumors and organs were carefully excised and weighed. After homogenizing thoroughly with a pestle in 1 mL of PBS solution at 4 °C, the mixture was shaken for 20 min at a 380 rpm/min speed at 15 °C. The supernatant was diluted 10 times with PBS, and a sample (100 μL) was then inoculated onto an agar plate. After anaerobically incubated, the formed bacterial colonies were imaged. For counting bacterial colonies, the supernatant was diluted 0, 10, 100, and 1000 times with PBS, and then a sample (5 μL) was inoculated onto an agar plate as above-mentioned. Finally, formed bacterial colonies were manually counted. The control experiment was also performed using PBS solution for normal BALB/c mice (female, 7 weeks; n = 3; average weight = 20 g; BALB/cCrSIc; Japan SLC) without tumors because tumor-resident bacteria might cause misreading the actual number of colonies derived from *C. acnes*.

2.3.7 Anticancer therapy using ICI drug and antineoplastic drug

Female BALB/cCrSlc mice (n = 10; 4 weeks old; average weight = 17 g) were obtained from Japan SLC (Hamamatsu, Japan) to study the anticancer efficacy of these drugs. Mice bearing the Colon-26 cell-derived tumors were generated by injecting 100 µL of the culture medium/Matrigel (Dow Corning, Corning, NY) mixture (v/v = 1:1) containing 5×10^6 cells into the right flank of the mice. When the average tumor size reached approximately 100 mm^3 (n = 5 in each group; 7 weeks old; average weight = 18g) in approximately 10 days, they were intravenously injected in the tail vein with PBS (200 µL) containing paclitaxel (Nacalai Tesque) (2.5 mg/kg body weight of mice) and anti-PD-L1 (Leinco Technologies, MO, USA) (2.5 mg/kg body weight of mice). Tumor formation and the health of the mice were closely observed daily (viability and body weight). The tumor volume was calculated using $V = L \times W^2/2$, where L and W stand for the length and width of the tumor, respectively. The survival ratio of Colon-26 tumor-bearing mice (n = 10, biologically independent mice) was also measured during treatment for 40 days. The mice were euthanized as the endpoint was reached following the guidelines of the Institutional Animal Care and Use Committee of JAIST when the tumor volumes reached >2000 mm^3.

2.3.8 Immunohistochemistry staining of tumor tissues

The Colon-26 tumor-bearing mice (female; approximately 7 weeks; n = 2; average weight = 18 g; average tumor size = 400 mm^3; BALB/cCrSIc; Japan SLC) were euthanized 2 days after the administration of 200 µL of PBS and 200 µL of *C. acnes* (1×10^9 CFU/mL) injection intravenously. Tumor tissues from the treated and the control mice were then harvested for immunohistochemical (IHC) staining. Analysis was performed by Biopathology Institute Co., Ltd. (Oita, Japan) using standard protocols. Primary tumors were surgically removed, fixed in 10% formalin, processed for paraffin embedding, and cut into 3–4 µm thick sections. The sections were

stained with hematoxylin and examined using light microscopy (IX73; Olympus, Tokyo, Japan) after incubation with primary antibodies (listed in **Table 2.4**). The areas showing positive staining in tumor tissues were analyzed using a light microscopy system (BZ-X810; Keyence, Tokyo, Japan) and hybrid cell count and microcell count software (Keyence).

Table 2.4. Antibodies used in this study.

Antibody	Type	Source	Catalog No.	Application
CD4	Rabbit Monoclonal	Cell Signaling Technology	25229	IHC (1:100)
CD8	Rabbit Monoclonal	Cell Signaling Technology	98941	IHC (1:200)
F4/80	Mouse Monoclonal	BMA Biomedicals	T-2028	IHC (1:50)
CD3	Rabbit Monoclonal	Abcam	ab16669	IHC (1:100)
CD19	Rabbit Polyclonal	Bioss	bs-0079R	IHC (1:100)
CXCR4	Goat Polyclonal	Abcam	ab1670	IHC (1:100)
NKp46	Rabbit Polyclonal	Affinity Biosciences	DF7599	IHC (1:100)
Caspase-3	Rabbit Polyclonal	Cell Signaling Technology	9661S	IHC (1:100)
TNF-α	Rabbit Polyclonal	Abcam	ab6671	IHC (1:100)
Anti-digoxigenin-peroxidase	Sheep Polyclonal	Merck Millipore	S7100	Tunel

2.3.9 Quantitative polymerase chain reaction (qPCR)

The Colon-26 tumor-bearing mice (female; about 6 weeks; n = 6; average weight = 18 g; average tumor size = 200 mm^3; BALB/cCrSIc; Japan SLC) were euthanized the next day after administration of *C. acnes* (200 μL, 1×10^9 CFU/mL) intravenously. To analyze the immune cells and cytokines in tumors, tumors were collected from mice in different groups after intravenous (I.V.) injection of sample for 24 h, and then homogenized by a handy homogenizer (Thermo Fisher Scientific) before qPCR. qPCR was performed using QuantStudio 1 PCR system (Thermo Fisher Scientific) to study the relative gene expression of CD3, CD19, CXCR4, F4/80, NKp46, IFN-γ, and TNF-α, using gene specific primer-probe combinations (Thermo Fisher Scientific) (**listed in Table 2.5**), by Taqman chemistry. Endogenous control was determined using TaqMan™ Array Mouse Endogenous Control Plate 96 well (Thermo Fisher Scientific). The reactions were run in triplicate using ACTB (β-actin) as an endogenous control. The thermal cycling parameters, 50 °C for 2 min for AmpErase UNG activation, 95 °C for 2 min for AmpliTaq Gold DNA Pol. activation and 40 cycles of each 95 °C for 15 s for denaturation/melting and 60 °C for 1 min for annealing and extension, yielded optimum amplification. For the test genes and endogenous control standards 10-fold serial dilutions were run in the study to estimate the efficiency of PCR and the percentage efficiency ranged between 90 to 100%. Results were analyzed and shown as fold change (log10 relative quantification) relative to the control group.

Table 2.5. TaqMan™ Primers for qPCR.

Target	Assay ID	Gene Symbol	Source
F4/80	Mm00802529_m1	Adgre1	Thermo Fisher Scientific
CD3	Mm00442746_m1	Cd3d	Thermo Fisher Scientific
CD19	Mm00515420_m1	Cd19	Thermo Fisher Scientific
CXCR4	Mm01996749_s1	Cxcr4	Thermo Fisher Scientific
NKp46	Mm01337324_g1	Ncr1	Thermo Fisher Scientific
IFN-γ	Mm01168134_m1	Ifng	Thermo Fisher Scientific
TNF-α	Mm00443258_m1	Tnf	Thermo Fisher Scientific
ACTB	Hs01060665_g1	Actb	Thermo Fisher Scientific

2.3.10 Blood tests

This study used the Celltac α blood cell counting machine (Nihon Kohden, Tokyo, Japan) to measure the complete blood count (CBC) of the mice and investigated the biochemical parameters with Japan SLC and Oriental Yeast Co. (Tokyo, Japan). BALB/c mice (female; 7 weeks; n = 10 in each group; average weight = 18 g; Japan SLC) were injected in the tail vein with culture medium containing bacteria (200 μL, 5×10^7 CFU/mL) or PBS (200 μL). The blood samples were collected from the inferior vena cava of the mouse after 14 days.

2.3.11 Statistical analysis

This study performed all experiments in triplicates and repeated them three or more times. Quantitative values are expressed as means ± standard error of the mean (SEM) of at least three independent experiments. Statistical differences were identified using Student's one-way t-test and one-way or two-way analysis of variance.

2.4 Results and Discussion

2.4.1 Isolation of tumor-suppressing bacteria from tumors

We previously reported the isolation of three bacteria, including *Proteus mirabilis* (A-gyo), *Rhodopseudomonas palustris* (UN-gyo), and its bacterial consortium (AUN; the mixture of A-gyo and UN-gyo) from the tumor, which demonstrated highly effective oncolytic properties and strong immune stimulation to completely eradicate the tumor and to have good immunological memory in preventing the relapse of the same tumor.[45] However, it was just the beginning of understanding the oncolytic properties of intratumoral bacteria. Numerous studies have been conducted to explore the contribution of bacteria inside tumors to cancer progression,[46] but our study focuses on how these bacteria, with their immune stimulant and oncolytic properties, could be our friends and not our opponents. This study successfully isolated three more bacteria (**Figure 2.1a**), including *A. radioresistens*, which is a gram-negative, aerobic, pleomorphic, coccobacilli shaped bacteria of the family *Moraxellaceae*; *B. thuringiensis*, which is a gram-positive, rod-shaped, facultative anaerobe of the family *Bacillaceae*; and *C. acnes*, which is a gram-positive, rod-shaped, and aerotolerant anaerobe of the family *Propionibacteriaceae*. We obtained 16S rRNA gene sequences of *A. radioresistens*, *B. thuringiensis*, and *C. acnes* using Basic Local Alignment Search Tool analyses (**Tables 2.1 – 2.3**). *A. radioresistens* was isolated from the EMT6/AR1-derived tumor in BALB/c mice while *B. thuringiensis* and *C. acnes* were isolated from the Meth-A sarcoma-derived

tumor in BALB/c mice (**Figure 2.1b**). All the isolated bacteria had no pigments and hence appeared as white colonies. *B. thuringiensis* colonies were observed on the deoxycholate agar and standard method agar plate. *C. acnes* colonies were observed on the standard method agar plate while the *A. radioresistens* colonies were observed on the LB agar and the standard method agar plate. We used the Pearl Core E-MC64 medium for the liquid culture because the composition of the standard method agar plate and Pearl Core E-MC64 medium is similar. The media in which the best growth of the bacteria was observed was used for further cultures after growing all three bacteria in both LB media and Pearl Core E-MC64 medium at 37°C. *A. radioresistens* demonstrated the best growth in aerobic conditions in the LB media while *B. thuringiensis* and *C. acnes* indicated the best growth in anaerobic conditions in the Pearl core trypto soy broth **(Figure 2.1b)**.

(a)

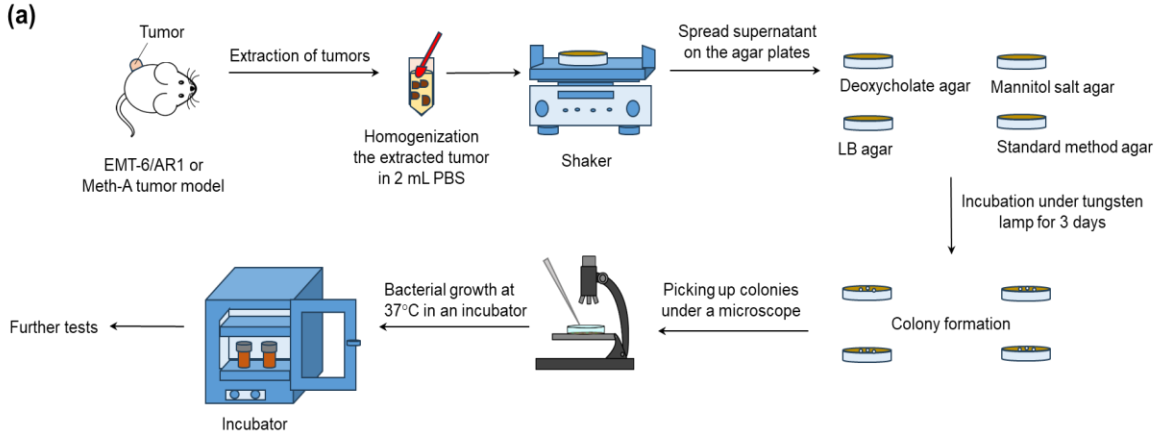

(b)

Name of bacteria	Agar plate colonies observed	Suitable media for liquid culture	Tumor
Acinetobacter radioresistens	LB agar or Standard method agar	LB Media	EMT6/AR1
Bacillus thuringiensis	Deoxycholate agar or Standard method agar	Pearl core Trypto soy broth	Meth-A
Cutibacterium acnes	Standard method agar	Pearl core Trypto soy broth	Meth-A

Figure 2.1. **Schematic illustration of isolations of intratumoral oncolytic bacteria.** (a) A brief depiction of the entire process involved in isolating three bacteria from the tumor models, EMT6/AR1 and Meth-A sarcoma. (b) Summary of isolation of bacteria. The isolated bacteria showing their best growth in only one or two of the agar plates or liquid media.

2.4.2 Tumor-suppressing ability of tumor-isolated bacteria

We verified the anticancer efficacy of the three isolated intratumoral bacteria. The basic idea was to implant a tumor into the right flank of the mice and intravenously inject the bacteria when the tumors reached about 100 mm^3 and to observe the tumor volume (**Figure 2.2a**). The mice given the I.V. injection of *C. acnes*, *B. thuringiensis*, and *A. radioresistens* demonstrated suppressed tumor growth compared to the mice in the control group (PBS administration) (**Figures 2.2b and 2.2c**). None of these bacteria demonstrated an overall effect on the health of the mice (**Figures 2.2d and 2.2e**). Among them, *C. acnes* indicated stronger tumor suppression and a longer survival rate probably because of its excellent anticancer efficacy and targeting effect. 75% of the mice treated with *A. radioresistens* died immediately (within 5 days) after the PBS group died. The *B. thuringiensis* could survive longer than the *A. radioresistens* group, and the tumor volume of the *Bacillus* group kept increasing steadily, thereby making these bacteria not a good option for studying tumor suppression, over the *C. acnes*. (**Figure 2.2c)** The cells in the tumor divided continuously but with reduced cell growth and division in the tumors treated with *C. acnes*, which appear to be strongly targeted by the immune system and the bacteria itself. The images indicate the morphology and size of the observed tumors on the day the bacterial treatment was administered (day 0) and 18 days thereafter (**Figure 2.2b).** Indeed, *C. acnes* displayed significant cytotoxicity against Colon-26 in a concentration dependent manner (**Figure 2.2e**). Meanwhile, the body weight of mice after any bacterial administrations showed no differences, indicating no side effects by bacterial injection (**Figure 2.2f**). The values of LD_{50} of *C. acnes*, *B. thuringiensis*, and *A. radioresistens* were 2×10^9 CFU/mL, 2×10^9 CFU/mL, and 2×10^7 CFU/mL, respectively. By confirming with colony assay, *C. acnes* also showed tumor targeting and it was gradually

proliferated in a tumor over time (**Figure 2.2g**). In the control PBS group, vital organs did not exhibit any colonies derived from *C. acnes* at all.

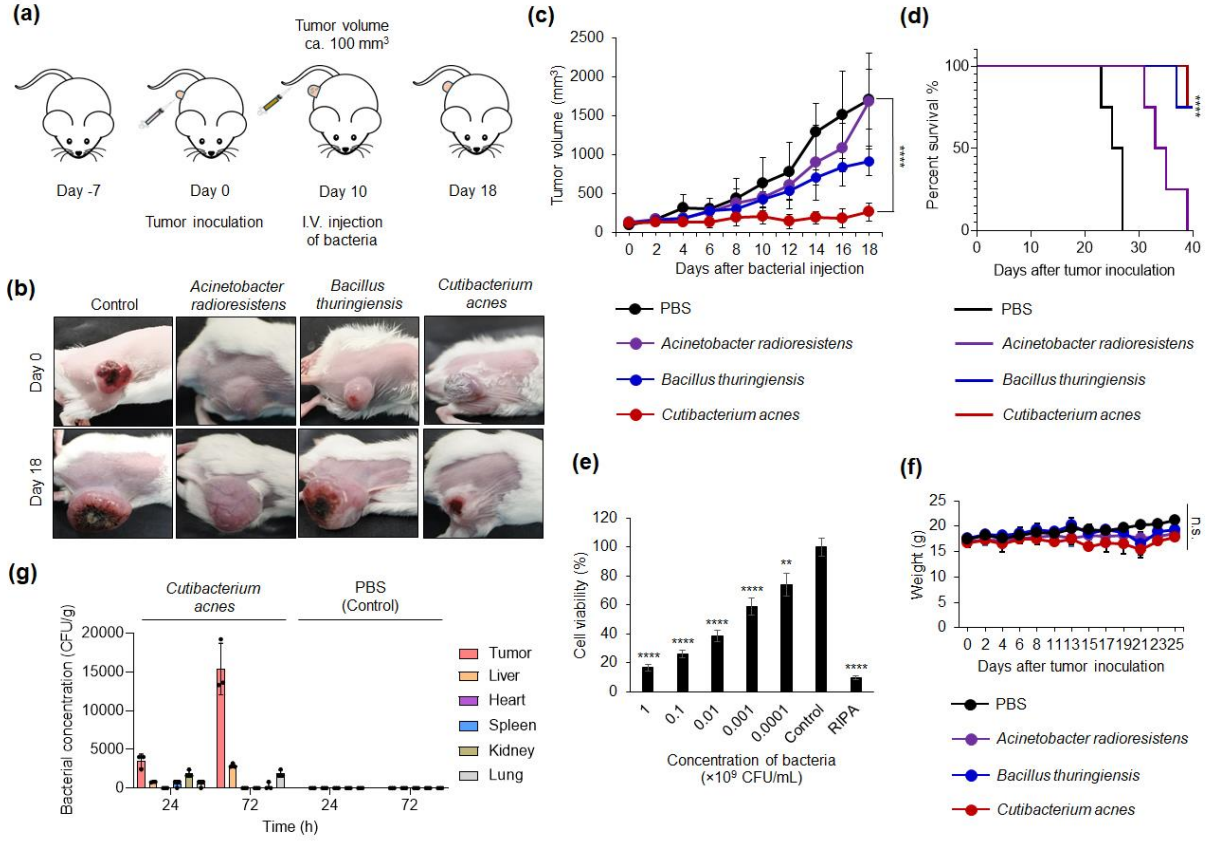

Figure 2.2 Anticancer efficacy of tumor-isolated bacteria. (a) An idea of the work plan from injecting the tumor to giving a tail intravenous injection of the bacteria being assessed. (b) The comparative images of the mice on day 0 before treatment and day 18 after treatment. The *Cutibacterium acnes* group shows suppressed tumor growth while most others almost reached approximately 2000 mm^3. (c) Graph showing the variation in tumor volume of each of the mice groups (n = 4), the control, the *Cutibacterium acnes*, the *Bacillus thuringiensis*, and the *Acinetobacter radioresistens*. Survival curve of the three different bacteria tested for tumor-suppressing activity. Data are expressed as means ± standard error of the mean (SEM) (n = 4 biologically independent tests). ****$p < 0.0001$, by one-way Student's *t-test*. (d) Kaplan–Meier survival curves of Colon 26 tumor-bearing mice (n = 4 biologically independent mice) after tumor implantation. Statistical significance was calculated in comparison with the PBS group. ****$P < 0.0001$ by Log-rank (Mantel–Cox) test. (e) Cytotoxicity of AUN. The viability of Colon 26 cell was tested after 24 h of treatment with *Cutibacterium acnes* at different bacterial concentrations. Data are represented as means ± SEM; n = 5 independent experiments. Statistical significance was calculated in comparison with the control group without bacterial treatment. **, $p < 0.01$ and ****, $p < 0.0001$, by Student's two-sided t-test. (f) Variation

in body weight of the mice vs. days after tumor inoculation. (g) Numbers of the bacterial colony of tumors and organs in Colon-26-tumor-bearing BALB/c mice after I.V. injection of *Cutibacterium acnes* (1×10^9 CFU/mL) for 24 and 72 h. Data are represented as mean ± SEM; n = 3 independent experiments.

A. radioresistens is one of the bacteria causing severe nosocomial infections and spreading antibiotic resistance.[47] Little is known about the pathogenicity of this bacterium that causes bacteremia and severe pulmonary infection. The higher dose (1×10^9 CFU/mL) of this bacterial injection was toxic to the mice. The mice treated with 1×10^9 CFU/mL died a couple of days after administration. Hence, the optimal concentration (1×10^7 CFU/mL) of this bacterium was determined by standardization and used for further tests. We consider that *A. radioresistens* could not effectively inhibit tumor hypoxia and induce an immune response against it because of the aerobic nature of the bacterium.

C. acnes maintained the suppressed volume at approximately 200 mm^3 for an extended period, making it an excellent tumor-suppressing biomaterial, while both *B. thuringiensis* and *C. acnes* groups showed obvious tumor volume suppression. They are both anaerobic bacteria, thus they could actively reside inside the tumor due to the hypoxic nature of the tumor microenvironment and proliferate to attract the attention of a few immune cells. These immune cells that infiltrate into the tumor tissue to target the bacteria also eliminate the surrounding tumor cells, thereby hindering the tumor tissue from further development. This makes these bacteria effective tumor-suppressing materials along with their inherent superpowers in destroying the tumor tissue.

The tumor suppression that could be achieved in this case of *B. thuringiensis* could be solely credited to recognizing the pattern recognition receptors (PRR) on the surface of the bacterial membrane.[48] Additionally, the bacterium could survive in both oxygenic and anoxygenic environments because it is a facultative anaerobe; hence, the total distribution of this bacterium

inside the tumor could be minimal after considering its clear up from other parts of the mice's body. However, it shows a better contribution in tumor suppression compared to the control as well as the aerobic bacterium *A. radioresistens.*

Conversely, *C. acnes* is commensal and helps in other bacterial-colonization resistance, antioxidant activity, and immunomodulatory properties. It is also an opportunistic pathogen that most commonly causes acne vulgaris and implant-associated shoulder infections. Its pathogenicity is caused by the secretion of various host tissue-dissolving enzymes, such as lipases, sialidases, and hyaluronidase. Enzymes, such as lipases, dissolve the lipid-rich particles that surround the bacteria. It also produces prominent porphyrin levels that lead to skin inflammation and acne. Radical oxygenase, the RoxP enzyme of this bacterium, helps it to survive in the oxygen-rich environment because it is an aerotolerant anaerobe.[49] This is a slow-growing bacterium that takes up to 5 h for one division.[50] We consider that *C. acnes* can safely reside inside the tumor because it is an anaerobic bacterium. A tumor could be a comfortable place to reside for this bacterium because the tumor has a high metabolism rate and attracts lots of nutrients which the bacterium can use to multiply. Additionally, it is a good place for the bacteria to hide and resist any attack from the immune system because a tumor shields itself from the immune system,[51] and most importantly, it is favorable for the growth of this anaerobic bacterium because the tumor environment is low with oxygen. *C. acnes* is considered probiotic because it is a common resident of the cutis, with three different phylotypes of itself, that maintain the homeostasis of the skin. However, they are also opportunistic pathogens when their concentration is high in a lipid-rich environment, and their enzymes and proinflammatory secretions cause inflammation and scars. Its amazing tumor-suppressing ability might come from two major properties: one is the enzymes that it produces to dissolve the surrounding tumor tissue, and the other is its immunomodulatory

properties. It can also attract the immune system toward it because of the PRRs on its surface as well as the proinflammatory secretions of these bacteria because it can grow well inside the tumor. The PRR could induce an immune response and produce an overall harsh effect on the tumor cells. Indeed, two of the mice in this group showed approximately 75% tumor reduction after 12 days of treatment although the tumor regrew in a suppressed manner in their further days. Another important feature of this bacterium is its gram positivity. It contains peptidoglycan and lipoteichoic acid on its surface, which is good at attracting the immune system. Toll-like receptors 2 or 6 recognize bacterial lipopeptides, which in turn release inflammatory cytokines and upregulate co-stimulatory molecules on antigen-presenting cells. Lipopeptides are also considered a natural adjuvant.[52] The various characteristics of *C. acnes*, such as having peptidoglycan and lipoteichoic acid membrane, the ability to secrete therapeutic molecules to dissolve host tissue, and the common feature of any bacteria to attract the immune system, make it a viable choice for tumor growth-suppressing bacterial therapy. In any case, we used *C. acnes*, which demonstrated the best anticancer efficacy, as a model bacterium for further experiments.

2.4.3 Anticancer efficacies of oncolytic bacteria and conventional drug

This study compared the efficacy reflected by the bacterium in suppressing tumor growth to the effect of the ICI drug, anti-PD-L1 Antibody, and antineoplastic drug, paclitaxel, in the Colon 26 tumor model to better understand the role of *C. acnes* in terms of tumor suppression. I.V. injection of both drugs was given in four shots each (each administration: 2.5 mg/kg of body weight of mice) every other day, and a single shot of bacterium at 1×10^9 CFU/mL was given intravenously. The results indicate that *C. acnes* displayed better tumor suppression compared to the other two tested drugs (**Figures 2.3a – 2.3c**). The immune system acts locally around the tumor since the bacterium resides inside the tumor and acts as an immunomodulant, as previously explained. The

effect of these particles is seen throughout the body in the case of these drugs because they are not tumor-cell specific. This makes the tumor cells one of the targets but not the sole target as in anaerobic bacteria-based therapy. The observed results could also be explained in terms of bacterial ability to amplify the immune response. Once any of the immune cells are activated, long downstream signaling involves various other cells. The mosaic of immune cells together brings out bacteria-based immunotherapy.

A single shot of *C. acnes* produced a much more effective tumor suppression when compared to four shots of paclitaxel and anti-PD-L1 antibody, as seen in the graph in **Figure 2.3a**. In principle, paclitaxel acts by arresting the cells from mitotic division by targeting the microtubules. The dynamic nature of the tubules is affected, and they can no longer participate in cell division. This stops the cancer cells from dividing. Longer paclitaxel exposure of cancer cells induces apoptosis.[53] The cancer cells can no longer proliferate but it acts nonspecifically because it is not tumor-specific, and the drug may not be able to target many cancer cells. The anti-PD-L1 antibody targets the T-cell surface PD-L1 receptors and restricts the cancer cells from evading the immune system attack in the case of ICI therapy.[54] This is one of the good strategies for modulating the immune response, but our results revealed that we could not achieve either extended tumor growth suppression or complete recovery from tumors even after four shots of anti-PD-L1 at 2.5 mg/kg body weight of mice. Once again, a single shot of *C. acnes* has made its way into being a better tumor growth suppressor compared to ICI drugs. We need a therapy that targets as many cancer cells as possible. For such a situation, a few anaerobic bacteria like *C. acnes* may be a desirable choice as their zone of attracting the immune cells begins from within the tumor environment making cancer cells more prone to recognition by the immune cells. The life expectancy of the *C. acnes*-treated mice was much better compared to other drug-treated mice **(Figure 2.3c)**. The

average body weight of the mice in different groups showed no difference compared to the control depicting that there is no side effect to the health of the mice because of the treatments **(Figure 2.3d)**.

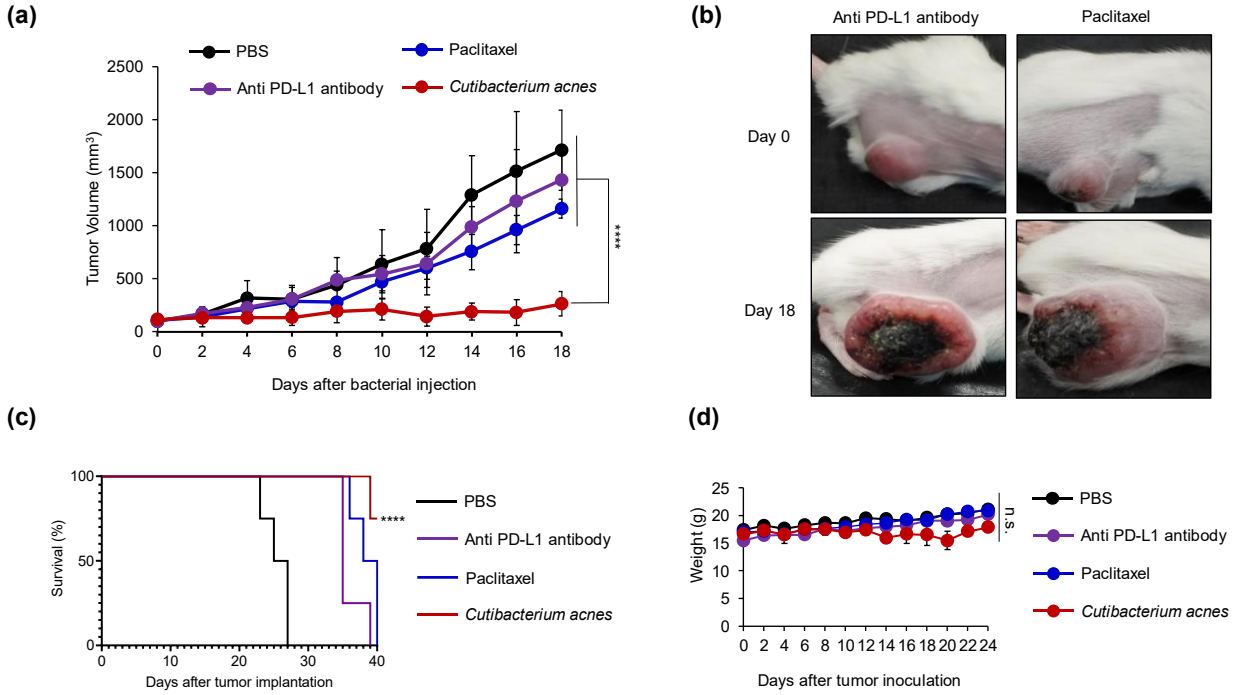

Figure 2.3. Anticancer efficacy of conventional drugs and *Cutibacterium acnes*. (a) A graph depicting the variation in tumor volume of mice treated with *Cutibacterium acnes* and the drugs, including paclitaxel and anti-PD-L1 antibody. Data are expressed as means ± standard error of the mean (SEM) (n = 4 biologically independent tests). ****$p < 0.0001$, by one-way Student's *t-test*. (b) Image reference of tumor volume on day 0, before treatment, and day 18 after treatment of anti-PD-L1 antibody or paclitaxel. (c) Kaplan–Meier survival curves of Colon 26 tumor-bearing mice (n = 4 biologically independent mice) after tumor implantation. Statistical significance was calculated in comparison with the PBS group. ****$P <$ 0.0001 by Log-rank (Mantel–Cox) test. (d) Variation in the body weight of mice after tumor inoculation and treatment.

2.4.4 Mechanistic insights into bacterial treatment

Finally, IHC staining was performed on both the control and the treated groups to understand the immunological mechanism that made the suppression feasible in the *C. acnes*-treated group

(**Figures 2.4a and 2.4b**). Most of the tumor-suppressing activity was performed by the cytotoxic T cells and macrophages as an overall expression. We consider that the bacterium, *C. acnes*, is strongly recognized by the innate immune systems. *C. acnes* is a commensal bacterium and is commonly present on the skin surface, although it does not make it much of a foreign invader in the body when the bacteria are present in larger amounts in the tumor, they can be specially recognized by the macrophages which is reflected in the F4/80 biomarker-based staining, which is approximately 40% higher than that of the PBS group. Other immune cells, such as neutrophils (CXCR4) and B cells (CD19) were barely noticed inside the tumor. We hypothesize that it could be the M2 type of macrophages that were stimulated [55] because the expression level of TNF-α was also hardly seen (similar that of the control group) and the F4/80 stain was not aggressive in terms of color development. The bacterium produces many proinflammatory secretions, thus it can easily attract the attention of the M2 phenotype macrophages which have an anti-inflammatory function that helps in engulfing and digesting the dead tissue and performs a key function in TH2 cell and regulatory T (Treg) cell activation and recruitment.[56]

Other important cell types that were stimulated were the T-cells. The CD3 stain demonstrated a good intensity of expression compared to the control group, pointing toward the recruitment of both cytotoxic T-cells and helper T-cells as CD3 is a common marker for both T-cell subtypes. A better expression of the CD8 markers cells was seen despite less expression of the CD4 marker cells. This indicates that the number of T helper cells was less compared to that of cytotoxic T cells that were recruited probably because the number of antigen-presenting cells was dominated by the macrophages, which could bring in only a few T cells.

We could conclude a little influence of the cytotoxic natural killer (NK) cells as well as T cells and macrophages on tumor suppression after comparing the Nkp46 staining intensity between the

two groups. Therefore, we propose a strategy that the contribution of macrophages and cytotoxic T cells and NK cells achieved tumor suppression for an extended period in the mice treated with *C. acnes*. The terminal deoxynucleotidyl transferase dUTP nick end labeling (TUNEL) and cleaved caspases-3 staining have proved that the number of apoptotic cells was higher in the *C. acnes* bacteria-treated mice compared to the minimal apoptosis observed in the control groups. The Hematoxylin and eosin (H&E) stain of the bacteria-treated tumor slide showed a much more distorted and degraded tumor tissue with dead tumor cells while the control group demonstrated tightly packed tumor cells probably because of oncolytic property of *C. acnes* with the immunological assistances of T-cells, NK-cells, and macrophages. Moreover, qPCR assay comprehensively supports the data of IHC staining (**Figure 2.4c**).

Altogether, we conclude that *C. acnes* represents obvious tumor suppression due to synergistic T-cell, NK-cell, and macrophage stimulations in addition to the structural degradation of cancerous tumors by the oncolytic ability of *C. acnes* itself (**Figure 2.4d**). We believe that these synergistic immunological effects and therapeutic functions of *C. acnes* have wide applicational prospects.We performed the CBC test, as well as the other biochemical parameters assays, to confirm the safety of the bacterium for intravenous injection in mice (**Table 2.6**). The results revealed no deviation from the control. Hence, our bacterium is safe to be used for in vivo experiments to inject intravenously into the mice.

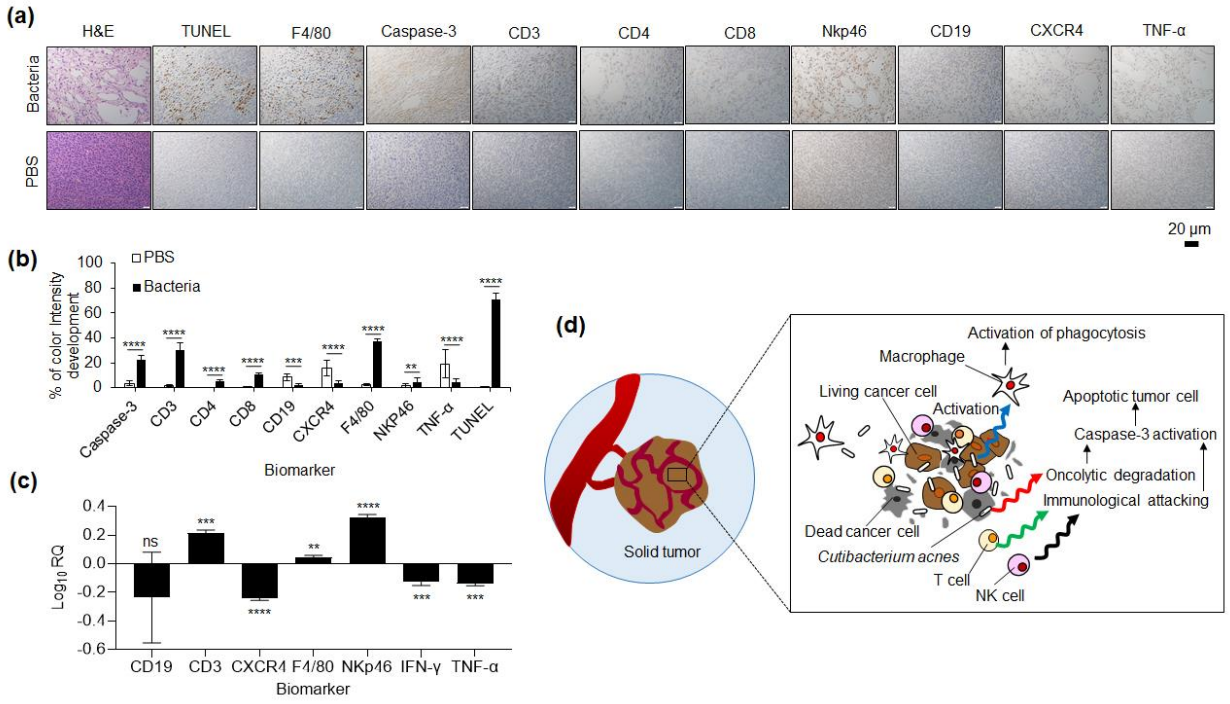

Figure 2.4. Mechanism of anticancer efficacy of *Cutibacterium acnes*. (a) IHC (F4/80, NKp46, CXCR4, CD3, CD4, CD8, CD19, TNF-α, and caspase-3), TUNEL, and hematoxylin and eosin (H&E) stained tumor tissues collected from different groups of mice after 2 days of intravenous PBS and *Cutibacterium acnes* injection. (b) Intensity of color development in various IHC slides as a comparison of control and treated samples. Data are represented as mean ± standard error of the mean (SEM); n = 10 independent areas (region of interest) in each tumor tissue collected from the groups of mice 2 days after treatments. Statistical significance was calculated in comparison with the control group. ** $p < 0.01$, ***, $p < 0.001$, and ****$p < 0.0001$, by one-way Student's t-test. (c) Quantification of immune cells related markers and cytokines by qPCR after I.V. administration with AUN for 24 h. The mRNA expression of CD19, CD3, CXCR4, F4/80, NKp46, and cytokines (IFN-γ and TNF-α) are shown as fold change [log 10 relative quantification (RQ)] relative to the control group (non-treatment). ACTB gene expression was used as an internal control. Statistical significance was calculated in comparison with the non-treatment group. ns, not significant, **, $p < 0.01$, ***, $p < 0.001$, and ****, $p < 0.0001$, by Student's two-sided t-test. Data are represented as mean ± SEM; n = 3 independent tumor tissues. (d) Scheme of the proposed mechanism.

Table 2.6. CBCs and biochemical parameters of the mice injected with PBS or *Cutibacterium acnes* suspension after 14 days.

Measured value	Entry	Unit		PBS (n = 10)	*Cutibacterium acnes* (n = 10)	P value
CBC	WBC	μL^{-1}	$\times 10^2$	95.9 ± 10.85	96.1 ± 16.41	> 0.05
	RBC	μL^{-1}	$\times 10^4$	917.5 ± 26.95	910.4 ± 22.33	> 0.05
	HGB	$g\ dL^{-1}$		14.3 ± 0.36	14.6 ± 0.42	> 0.05
	HCT		%	42.2 ± 1.19	42.8 ± 0.96	> 0.05
	MCV		fL	46.0 ± 0.42	47.1 ± 0.55	> 0.05
	MCH		pg	15.5 ± 0.16	16.0 ± 0.16	> 0.05
	MCHC	$g\ dL^{-1}$		33.8 ± 0.31	34.0 ± 0.48	> 0.05
	PLT	μL^{-1}	$\times 10^4$	89.4 ± 5.13	87.9 ± 4.95	> 0.05
Biochemical parameters	TP	$g\ dL^{-1}$		4.4 ± 0.14	4.5 ± 0.13	> 0.05
	ALB	$g\ dL^{-1}$		3.0 ± 0.08	3.1 ± 0.08	> 0.05
	BUN	dL^{-1}	mg	14.9 ± 2.95	16.9 ± 2.31	> 0.05
	CRE	dL^{-1}	mg	0.1 ± 0.01	0.1 ± 0.01	> 0.05
	Na	L^{-1}	mEq	143.6 ± 2.63	144.3 ± 1.06	> 0.05
	K	L^{-1}	mEq	22.2 ± 1.11	21.8 ± 0.56	> 0.05
	Cl	L^{-1}	mEq	103.4 ± 1.89	103.5 ± 1.08	> 0.05
	AST	$IU\ L^{-1}$		41.7 ± 5.90	36.7 ± 2.58	> 0.05
	ALT	$IU\ L^{-1}$		23.3 ± 4.49	19.8 ± 2.39	> 0.05
	LDH	$IU\ L^{-1}$		151.2 ± 21.22	128.1 ± 15.39	> 0.05
	AMY	$IU\ L^{-1}$		2490.8 ±371.36	2822.7 ± 618.42	> 0.05
	CK	$IU\ L^{-1}$		57.5 ± 11.32	42.5 ± 6.24	> 0.05

Data are represented as means ± standard errors of the mean (s.e.m.); n = 10 biologically independent mice. Statistical analyses comprise the two-way ANOVA test.

Abbreviations: ALB, albumin; ALT, alanine transaminase; AMY, amylase; AST, aspartate aminotransferase; BUN, blood urea nitrogen; Cl, chlorine; CK, creatine kinase; CRE, creatinine; HCT, hematocrit; HGB, hemoglobin; K, potassium; LDH, lactate dehydrogenase; MCH, mean corpuscular hemoglobin; MCHC, mean corpuscular hemoglobin concentration; MCV, mean corpuscular volume; Na, sodium; PLT, platelet; RBC, red blood cell; TP, total protein; WBC, white blood cell.

2.5 Conclusion

This study revealed that *C. acnes,* belonging to the *Propionibacteriaceae* family isolated from the tumor, showed good tumor-suppressing ability. We have observed that it suppresses the growth of the tumor when compared to a few other bacteria that we isolated from the tumor itself, which are *A. radioresistens*, which is an aerobe, and *B. thuringiensis*, which is a facultative anaerobe, after injecting this bacterium through the tail vein by intravenous injection. The anaerobic nature of this bacterium *C. acnes* enabled it to effectively colonize inside the tumor and produce a few proinflammatory secretions to attract the immune system toward it by infiltering immune cells into the tumor that could destroy the cancer cells, in addition to its innate ability to produce enzymes that dissolve the surrounding tissue. The IHC staining revealed a higher intensity of the stain of TUNEL and Cleaved caspases-3 indicating pronounced apoptosis.

The very first immunotherapy involved the use of bacteria to treat cancer. It was from a patient suffering from a skin-related disorder, which worked back then. With the discovery of using radiation and chemotherapy for cancer, this study was lost on its way toward scientific advancement. This form of cancer treatment may be considered after looking into the research conducted in recent past in the field of bacterial therapy.[57–59] Tumor-isolated bacteria possess anticancer properties that we could explore and look for. Today, various forms of therapy that are used contribute to further complications and diseases. Even in a few complicated cases where chemotherapy and radiation therapy cannot be used, particularly complications with other body parts, such as the cardiovascular system, the nervous system, the renal system, etc., we could use this form of bacterial therapy in a controlled way to achieve tumor suppression. It involves the bacteria alone, thus it is a very cost-effective form of therapy. There is no risk of the bacteria retrieving its virulence in the absence of genetic recombination. Hence, these natural bacteria,

which possess anticancer properties, are safe to be injected into the body and used as beneficial microbes to cure cancer, overcoming the common idea to a certain extent that most bacteria are harmful. We envision that our discovered intratumoral bacteria would overcome many problems of conventional anticancer therapies someday.

2.6 References

[1] International Agency for Research on Cancer Global cancer observatory, Cancer Fact Sheets, (2020). https://gco.iarc.fr/today/fact-sheets-populations (accessed August 4, 2023).

[2] N. Kumar, S. Fazal, E. Miyako, K. Matsumura, R. Rajan, Avengers against cancer: A new era of nano-biomaterial-based therapeutics, Materials Today, 51 (2021) 317–349. https://doi.org/10.1016/j.mattod.2021.09.020.

[3] C. Robert et al. Pembrolizumab versus ipilimumab in advanced melanoma. N. Engl. J. Med., 372 (2015) 2521–2532. https://doi: 10.1056/NEJMoa1503093.

[4] J. Larkin et al. Five-year survival with combined nivolumab and ipilimumab in advanced melanoma. N. Engl. J. Med., 381 (2019) 1535–1546. https://doi: 10.1056/NEJMoa1910836.

[5] S. Zinn, R. Vazquez-Lombardi, C. Zimmermann et al. Advances in antibody-based therapy in oncology. Nat. Cancer, 4 (2023) 165–180. https://doi: 10.1038/s43018-023-00516-z.

[6] S. Jin, Y. Sun, X. Liang et al. Emerging new therapeutic antibody derivatives for cancer treatment. Sig. Transduct. Target. Ther., 7 (2022) 39 (2022). https://doi: 10.1038/s41392-021-00868-x.

[7] K. M. Cappell, J. N. Kochenderfer, Long-term outcomes following CAR T cell therapy: what we know so far. Nat. Rev. Clin. Oncol., 20 (2023) 359–371. https://doi: 10.1038/s41571-023-00754-1.

[8] J. Yang, Y. Chen, Y. Jing et al. Advancing CAR T cell therapy through the use of multidimensional omics data. Nat. Rev. Clin. Oncol., 20 (2023) 211–228. https://doi: 10.1038/s41571-023-00729-2.

[9] Edward F. McCarthy, THE TOXINS OF WILLIAM B. COLEY AND THE TREATMENT OF BONE AND SOFT-TISSUE SARCOMAS, Iowa Orthop J. 26 (2006) 154–158.

[10] National Cancer Institute, Immunotherapy to treat cancer, (2019). https://www.cancer.gov/about-cancer/treatment/types/immunotherapy (accessed August 4, 2023).

[11] L. A. Liotta, E. C. Kohn, The microenvironment of the tumour- host interface. Nature, 411 (2001) 375–379. https://doi.org/10.1038/35077241.

[12] Y. Matsumura, Cancerstromaltargeting（CAST）therapy. Adv. Drug Deliv. Rev., 64 (2012) 710–719. https://doi: 10.1016/j.addr.2011.12.010.

[13] G. Fucà, L. Reppel, E. Landoni, B. Savoldo, G. Dotti, Enhancing chimeric antigen receptor T-cell efficacy in solid tumors. Clin. Cancer Res., 26 (2020) 2444–2451. https://doi: 10.1158/1078-0432.CCR-19-1835.

[14] K. G. Anderson, I. M. Stromnes, P. D. Greenberg, Obstacles posed by the tumor microenvironment to T cell activity: a case for synergistic therapies. Cancer Cell, 31 (2017) 311–325. https://doi: 10.1016/j.ccell.2017.02.008.

[15] S. Zhou, C. Gravekamp, D. Bermudes, K. Liu, Tumour-targeting bacteria engineered to fight cancer. Nat. Rev. Cancer, 18 (2018) 727–743. https://doi: 10.1038/s41568-018-0070-z.

[16] N. S. Forbes, Engineering the perfect (bacterial) cancer therapy. Nat. Rev. Cancer, 10 (2010) 785–794. https://doi: 10.1038/nrc2934.

[17] M. T.-Q. Duong, Y. Qin, S.-H. You, J.-J. Min, Bacteria-cancer interactions: bacteria-based cancer therapy. Exp. Mol. Med., 51 (2019) 1–15. https://doi: 10.1038/s12276-019-0297-0.

[18] S.-R. Kang, D.-H. Nguyen, S. W. Yoo, J.-J. Min, Bacteria and bacterial derivatives as delivery carriers for immunotherapy. Adv. Drug Deliv. Rev., 181 (2021) 114085. https://doi: 10.1016/j.addr.2021.114085.

[19] Bacterial therapy of cancer: Methods and protocols (ed Hoffman, R. M.) (Humana Press, Springer, Netherlands) (2015).

[20] S. Liang, C. Wang, Y. Shao, Y. Wang, D. Xing, Z. Geng, Recent advances in bacteria-mediated cancer therapy, Front. Bioeng. Biotechnol., 10 (2022) 1026248. https://doi.org/10.3389/fbioe.2022.1026248.

[21] J. M. Brown, W. R. William, Exploiting tumour hypoxia in cancer treatment. Nat. Rev. Cancer, 4 (2004) 437–447. https://doi: 10.1038/nrc1367.

[22] M. Din, T. Danino, A. Prindle, M. Skalak, J. Selimkhanov, K. Allen, E. Julio, E. Atolia, E. L. S. Tsimring, S. N. Bhatia, J. Hasty, Synchronized cycles of bacterial lysis for in vivo delivery. Nature, 536 (2016) 81–85. https://doi: 10.1038/nature18930.

[23] R. W. Bourdeau, A. Lee-Gosselin, A. Lakshmanan, A. Farhadi, S. R. Kumar, S. P. Nety, M. G. Shapiro, Acoustic reporter genes for noninvasive imaging of microorganisms in mammalian hosts. Nature, 553 (2018) 86–90. https://doi: 10.1038/nature25021.

[24] S. Chowdhury, S. Castro, C. Coker, T. E. Hinchliffe, N. Arpaia, T. Danino, Programmable bacteria induce durable tumor regression and systemic antitumor immunity. Nat. Med., 25 (2019) 1057–1063. https://doi: 10.1038/s41591-019-0498-z.

[25] O. Felfoul, M. Mohammadi, S. Taherkhani, D. de Lanauze, X. Z. Xu, Z. D. Loghin, S. Essa, S. Jancik, D. Houle, M. Lafleur, L. Gaboury, M. Tabrizian, N. Kaou, M. Atkin, T. Vuong,

[26] G. Batist, N. Beauchemin, D. Radzioch, S. Martel, Magneto-aerotactic bacteria deliver drug-containing nanoliposomes to tumour hypoxic regions. Nat. Nanotechnol., 11 (2016) 941–947. https://doi: 10.1038/nnano.2016.137.

[27] D. Zheng, Y. Chen, Z. Li, L. Xu, C. Li, B. Li, J. Fan, S. Cheng, X. Zhang, Optically-controlled bacterial metabolite for cancer therapy. Nat. Commun., 9 (2018) 1680. https://doi: 10.1038/s41467-018-03233-9.

[28 S. Suh, A. Jo, M. A. Traore, Y. Zhan, S. L. Coutermarsh-Ott, V. M. Ringel-Scaia, I. C. Allen, R. M. Davis, B. Behkam, Nanoscale bacteria-enabled autonomous drug delivery system (NanoBEADS) enhances intratumoral transport of nanomedicine. Adv. Sci., 6 (2019) 1801309. https://doi: 10.1002/advs.201801309.

[29] W. Baicheng, P. Jingmei, Y. Ruiting, S. Binfen, W. Yi, G. Xing, Z. Shaobing, Polarization of tumor-associated macrophages by nanoparticle-loaded Escherichia coli combined with immunogenic cell death for cancer immunotherapy. Nano Lett., 21 (2021) 10, 4231-4240. https://doi: 10.1021/acs.nanolett.1c00209.

[30] J. Xing, T. Yin, S. Li, T. Xu, A. Ma, Z. Chen, Y. Luo, Z. Lai, Y. Lv, H. Pan, R. Liang, X. Wu, M. Zheng, L. Cai, Sequential magneto-actuated and optics-triggered biomicrorobots for targeted cancer therapy. Adv. Funct. Mater., 31 (2021) 2008262. https://doi.org/10.1002/adfm.202008262

[31] W. Chen, Y. Wang, M. Qin, X. Zhang, Z. Zhang, X. Sun, Z. Gu, Bacteria-driven hypoxia targeting for combined biotherapy and photothermal therapy. ACS Nano, 12 (2018) 5995−6005. https://doi: 10.1021/acsnano.8b02235.

[32] C.-H. Luo, C.-T. Huang, C.-H. Su, C.-S.; Yeh, Bacteria-mediated hypoxia-specific delivery of nanoparticles for tumors imaging and therapy. Nano Lett., 16 (2016) 3493−3499. https://doi: 10.1021/acs.nanolett.6b00262.

[33] F. Chen, Z. Zang, Z. Chen, L. Cui, Z. Chang, A. Ma, T. Yin, R. Liang, Y. Han, Z. Wu, M. Zheng, C. Liu, L. Cai, Nanophotosensitizer-engineered Salmonella bacteria with hypoxia targeting and photothermal-assisted mutual bioaccumulation for solid tumor therapy. Biomaterials, 214 (2019) 119226. https://doi: 10.1016/j.biomaterials.2019.

[34] H. Chen, Y. Li, Y. Wang, P. Ning, Y. Shen, X. Wei, Q. Feng, Y. Liu, Z. Li, C. Xu, S. Huang, C. Deng, P. Wang, Y. Cheng, An engineered bacteria-hybrid microrobot with the magnetothermal bioswitch for remotely collective perception and imaging-guided cancer treatment. ACS Nano, 16 (2022) 6118−6133. https://doi: 10.1021/acsnano.1c11601.

[35] T. Yin, Z. Diao, N. T. Blum, L. Qiu, A. Ma, P. Huang, Engineering bacteria and bionic bacterial derivatives with nanoparticles for cancer therapy. Small, 18 (2022) 2104643. https://doi: 10.1002/smll.202104643.

[36] X. Huang, J. Pan, F. Xu, B. Shao, Y. Wang, X. Guo, S. Zhou, Bacteria-based cancer immunotherapy. Adv. Sci., 8 (2021) 2003572. https://doi: 10.1002/advs.202003572.

[37] S. Reghu, E. Miyako, Nanoengineered *Bifidobacterium bifidum* with optical activity for photothermal cancer immunotheranostics, Nano Lett., 22 (2022) 1880–1888. https://doi.org/10.1021/acs.nanolett.1c04037.

[38] F. Chen, Z. Zang, Z. Chen, L. Cui, Z. Chang, A. Ma, T. Yin, R. Liang, Y. Han, Z. Wu, M. Zheng, C. Liu, L. Cai, 2019. Nanophotosensitizer-engineered *Salmonella* bacteria with hypoxia targeting and photothermal-assisted mutual bioaccumulation for solid tumor therapy, Biomaterials, 214. https://doi.org/10.1016/j.biomaterials.2019.119226.

[39] S. Reghu, S. Iwata, S. Komatsu, T. Nakajo, E. Miyako, Cancer immunotheranostics using bioactive nanocoated photosynthetic bacterial complexes. Nano Today, 52 (2023) 101966. https://doi.org/10.1016/j.nantod.2023.101966.

[40] S. Kalaora, A. Nagler, D. Nejman, et al. Identification of bacteria-derived HLA-bound peptides in melanoma. Nature, 592 (2021) 138–143. https://doi.org/10.1038/s41586-021-03368-8.

[41] G. D. Sepich-Poore, L. Zitvogel, R. Straussman, J. Hasty, J. A. Wargo, R. Knight, The microbiome and human cancer. Science, 371 (2021) eabc4552. https://doi: 10.1126/science.abc4552

[42] D. Nejman, I. Livyatan, G. Fuks, et al. The human tumor microbiome is composed of tumor type-specific intracellular bacteria. Science, 368 (2020) 973–980. https://doi: 10.1126/science.aay9189.

[43] L. T. Geller, M. Barzily-Rokni, T. Danino, et al. Potential role of intratumor bacteria in mediating tumor resistance to the chemotherapeutic drug gemcitabine. Science, 357 (2017) 1156–1160. https://doi: 10.1126/science.aah5043.

[44] A. Fu, B. Yao, T. Dong, Y. Chen, J. Yao, Y. Liu, H. Li, H. Bai, X. Liu, Y. Zhang, C. Wang, Y. Guo, N. Li, S. Cai, Tumor-resident intracellular microbiota promotes metastatic colonization in breast cancer. Cell, 185 (2022) 1356–1372. https://doi: 10.1016/j.cell.2022.02.027.

[45] T. M. Savage, R. L. Vincent, S. S. Rae, L. H. Huang, A. Ahn, K. Pu, F. Li, C. Coker, T. Danino, N. Arpaia, Chemokines expressed by engineered bacteria recruit and orchestrate antitumor immunity. Sci. Adv., 9 (2023) eadc9436. https://doi: 10.1126/sciadv.adc9436.

[46] Y. Goto, S. Iwata, M. Miyahara, E. Miyako, Discovery of intratumoral oncolytic bacteria toward targeted anticancer theranostics. Adv. Sci., 10 (2023) 2301679. https://doi.org/10.1002/advs.202301679.

[47] J. Liu, Y. Zhang, Intratumor microbiome in cancer progression: current developments, challenges and future trends. Biomark Res., 10 (2022) 37. https://doi.org/10.1186/s40364-022-00381-5.

[48] A. Lazarev, J. Hyun, J.L. Sanchez, L. Verda, Community-acquired acinetobacter radioresistens bacteremia in an immunocompetent host. Cureus., 14 (2022) e29650 https://doi.org/10.7759/cureus.29650.

[49] D. Li, M. Wu, Pattern recognition receptors in health and diseases. Signal Transduct. Target. Ther., 6 (2021) 291. https://doi.org/10.1038/s41392-021-00687-0.

[50] C. Mayslich, P.A. Grange, N. Dupin, *Cutibacterium acnes* as an opportunistic pathogen: An update of its virulence-associated factors. Microorganisms, 9 (2021) 1–21. https://doi.org/10.3390/microorganisms9020303.

[51] G. S. Hall, K. Pratt-Rippin, D. M. Meisler', J. A. Washington, T. J. Roussel', D. Mille, Current eye research growth curve for *Propionibacterium acnes*. Curr. Eye Res., 13 (1994) 465–466. https://doi.org/10.3109/02713689408999875.

[52] A. Bożyk, K. Wojas-Krawczyk, P. Krawczyk, J. Milanowski, Tumor microenvironment—A short review of cellular and interaction diversity. Biology (Basel), 11 (2022) 929. https://doi.org/10.3390/biology11060929.

[53] J. P. Mcaleer, A. T. Vella, Macrophage cytokine responses to commensal Gram-positive *Lactobacillus salivarius* strains are TLR2-independent and Myd88-dependent. Sci. Rep., 11 (2021) 5896. https://doi.org/10.1038/s41598-021-85347-7.

[54] T. B. Foland, W. L. Dentler, K. A. Suprenant, M. L. Gupta, R. H. Himes, Paclitaxel-induced microtubule stabilization causes mitotic block and apoptotic-like cell death in a paclitaxel-

sensitive strain of Saccharomyces cerevisiae. Yeast, 22 (2005) 971–978. https://doi.org/10.1002/yea.1284.

[55] F. K. Alkholifi, R. M. Alsaffar, Dostarlimab an inhibitor of PD-1/PD-L1: A new paradigm for the treatment of cancer. Medicina (Lithuania), 58 (2022) 1572. https://doi.org/10.3390/medicina58111572.

[56] C. Yunna, H. Mengru, W. Lei, C. Weidong, Macrophage M1/M2 polarization. Eur. J. Pharmacol., 877 (2022) 173090. https://doi.org/10.1016/j.ejphar.

[57] P. J. Murray, T. A. Wynn, Protective and pathogenic functions of macrophage subsets, Nat. Rev. Immunol., 11 (2011) 723–737. https://doi.org/10.1038/nri3073.

[58] X. Yang, S. Komatsu, S. Reghu, E. Miyako, Optically activatable photosynthetic bacteria-based highly tumor specific immunotheranostics, Nano Today, 37 (2021) 101100 https://doi.org/10.1016/j.nantod.2021.101100.

[59] K. H. Gupta, C. Nowicki, E. F. Giurini, A. L. Marzo, A. Zloza, Bacterial-based cancer therapy (Bbct): Recent advances, current challenges, and future prospects for cancer immunotherapy, Vaccines (Basel), 9 (2021) 1497. https://doi.org/10.3390/vaccines9121497.

[60] M. Sedighi, A. Zahedi Bialvaei, M. R. Hamblin, E. Ohadi, A. Asadi, M. Halajzadeh, V. Lohrasbi, N. Mohammadzadeh, T. Amiriani, M. Krutova, A. Amini, E. Kouhsari, Therapeutic bacteria to combat cancer; current advances, challenges, and opportunities, Cancer Med., 8 (2019) 3167–3181. https://doi.org/10.1002/cam4.2148.

CHAPTER 3

Hybrid nanoarchitectonics with bacterial component-integrated graphene oxide for cancer photothermo-chemo-immunotherapy

Abstract

The multifunctionalization of graphene oxide (GO), which is known for its unique physicochemical properties, is promising for biomedical applications. Here, we developed a bio-inspired approach to utilize the cellular components of *Cutibacterium acnes* isolated from tumors to enhance the water dispersibility, drug loading capacity, photothermal conversion efficiency, and therapeutic immunogenicity of GO for effective photothermal and chemotherapeutic cancer immunotherapy in vitro and in vivo. The proposed approach is cost-effective, requires minimal resources, such as bacterial culture media, and is easily scalable for mass production via a simple single-step sonication process.

Hybrid nanoarchitectonics with bacterial component-integrated graphene oxide for cancer photothermo-chemo-immunotherapy

3.1 Keywords: Hybrid nanoarchitectonics, photothermal therapy, graphene oxide, drug delivery

Highlights

- Cutibacterium acnes enhances the aqueous dispersibility and immunomodulatory potential of graphene oxide.
- Graphene oxide-based photothermal therapy (PTT) demonstrated significant tumor suppression efficacy
- Therapeutic effects were achieved using low concentrations of graphene oxide and low-power NIR irradiation, indicating strong clinical relevance.
- The approach represents a cost-effective therapeutic strategy with high translational potential for future cancer treatment.

3.2 Introduction

Cancer therapies have advanced beyond traditional chemotherapy and include immunotherapy, radiation therapy, and photothermal therapy. Nanomedicine is revolutionizing healthcare by enabling precise drug delivery, advanced diagnostics, and innovative therapies at the molecular level.[1] Graphene, with its unique physicochemical properties, holds immense potential in nanomedicine for targeted drug delivery, biosensing, and tissue engineering.[2,3] Researchers are exploring methods to unlock its full potential for precise and effective cancer treatments.[4] Functionalized forms of graphene, particularly graphene oxide (GO), have received considerable attention in cancer research for their potential as photothermal agents and drug delivery vehicles.[5,6] GO possess a two-dimensional planar structure, chemical and mechanical stability, high photothermal conversion ability, high surface area, and good biocompatibility.[7] Despite these

advantages, water dispersibility remains a significant challenge. In many cases, surfactants or synthetic polymers, such as lipids and polyethylene glycol, are used to disperse GO molecules in aqueous solutions for biological applications.[8,9] While these molecules may aid GO dispersion, further complicated chemical modifications with various functional molecules, such as tumor-targeting ligands, anticancer drugs, and fluorescent reporter molecules, are essential to obtain sufficient efficacy for cancer treatment.[10,11]

We recently discovered that some bacteria isolated from tumors have inherent tumor-suppressive properties.[12–14] Earlier studies have shown that intratumoral non-pathogenic *Cutibacterium acnes* (CA) exhibits tumor-suppressive efficacy owing to its anticancer properties and immune-stimulating ability.[12] However, the translational and clinical feasibility of live CA has potential limitations, such as the challenge of maintaining precise bacterial systemic efficacy and its implications for therapeutic application.

To address these issues of GO multifunctionalization and safety concerns associated with live bacteria, we utilized bacterial components including cell membranes, genes, and other structural elements acting as potent immune stimulators. Indeed, the amphiphilic nature of the bacterial components of CA mimics detergent-like formation, which enhances the water dispersibility of hydrophobic GO and triggers immune responses by behaving as an immunoactivator.[15–17] GO also possesses a strong photothermal conversion ability when exposed to laser light. This property allows for the targeted exothermic destruction of cancer cells upon laser activation. Camptothecin (CPT), a well-known natural hydrophobic chemotherapeutic DNA inhibitor widely used in traditional Chinese medicine,[18] was also incorporated into CA-modified GO (CA–GO) (CPT–CA–GO) to improve the anticancer efficacy. This synergistic

nanoarchitectonics[19] approach demonstrates its potential as a useful tool for therapeutic applications and is a step toward sustainable and biologically inspired nanotechnology.

3.3 Materials and Methods

3.3.1. Bacterial strains and growth

We used *Cutibacterium acnes* (CA) isolated from mice bearing breast cancer EMT6/AR1 and Meth-A sarcoma-derived cell lines. CA was grown anaerobically in Pearl Core E-MC64 medium (Eiken Chemical, Tokyo, Japan) at 37 °C for ≤3 days. All the chemicals were obtained from Nacalai Tesque (Kyoto, Japan), Tokyo Chemical Industry (Tokyo, Japan), and FUJIFILM Wako Pure Chemicals (Osaka, Japan).

3.3.2. Nanohybrid synthesis

The CA-integrated graphene oxide (GO) encapsulating camptothecin (CPT) (CPT–CA–GO) was prepared as follows: 5 mg GO (powder, 15–20 sheets, 4–10% edge-oxidized, avg. no. of layers, 15–20; Catalog No. 796034, Sigma-Aldrich, St. Louis, MO, USA), 5×10^7 CFU/mL CA, and 5 mg CPT (FUJIFILM Wako Pure Chemical) were sonicated together in 10 mL Roswell Park Memorial Institute (RPMI) 1640 containing 10% FBS solution by pulse-type sonication (VCX-600; Sonics, Danbury, CT, USA) for 10 min in an ice bath. CA-integrated GO (CA–GO) was prepared in a similar manner, except that CPT was not added. The 10% DMSO containing CPT (DMSO–CPT) was prepared by adding 5 mg CPT to 10% DMSO (Nacalai Tesque) in 10 mL PBS (−) (Nacalai Tesque) and sonicating for 10 min. CPT–CA–GO encapsulating indocyanine green (ICG) was also prepared in the same way as CPT–CA–GO except for adding 0.1 mg/mL ICG (Tokyo Chemical Industry, Tokyo, Japan). All nanohybrids were synthesized immediately before requirements. Fresh samples were used in this study. The weight ratio of the components in CPT–CA–GO nanohybrid was CPT:CA:GO = 1:0.15:1. The ratio was calculated by weighing the freeze-dried

CA (n=3, average weight = 0.76 mg) with consideration of the preparation weight of GO (5 mg) and CPT (5 mg) for synthesizing CPT–CA–GO. Before freeze drying, the concentration of CA was adjusted as 5×10^7 CFU/mL in medium by a bacterial counter, and the bacterial suspension was prefrozen after the solvent was replaced to Milli-Q water.

3.3.3. Nanohybrid characterization

CPT–CA–GO morphology and structure were determined using the transmission electron microscopy (TEM) images. The acceleration voltage was 200 kV using high-resolution TEM (JEM-2010; JEOL, Tokyo, Japan). The average particle size of CPT–CA–GO was manually calculated from 300 nanohybrids on a TEM grid. Absorbance was measured using an ultraviolet (UV)–visible (vis)–near-infrared (NIR) spectrometer (Jasco V 770; Jasco, Tokyo, Japan). Double-faced quartz cuvettes were used to measure absorbance over 200–900 nm. PBS (II) was used instead of RPMI with 10% FBS. The fluorescence (FL) spectra of the nanoparticles were measured using a FL spectrometer (FP8600; Jasco) equipped with four-faced quartz cuvettes. FL excitation (Ex) was performed at 700 nm, and FL emission was recorded over 720–850 nm.

3.3.4. CPT loading efficiency

The standard curve for CPT was generated using different CPT concentrations (starting from 100 µg/mL) in methanol (Nacalai Tesque). The prepared CPT–CA–GO was filtered using a 0.22 µm polyvinylidene difluoride syringe filter (Millex-GV; Merck Millipore, Burlington, MA, USA), and the filtrate was used to measure the UV absorption for CPT to calculate the amount of CPT filtered. A regression equation was used to extrapolate the CPT concentration in the filtrate. The loading efficiency was calculated as follows:

$$Loading\ efficiency\ (\%) = \left[\frac{(total\ drug\ added - free\ non - entrapped\ drug)}{total\ drug\ added}\right] \times 100$$

3.3.5. Photothermal conversion tests

CPT–CA–GO was irradiated using 808 nm NIR laser (Civil Laser, Hangzhou, Zhejiang, China) at 0.7 W (approximately 35.6 mW/mm^2; spot diameter approximately 5 mm). Then, 200 µL sample was taken in a 96-well plate and the real-time temperature change was noted for 5 min using a temperature sensor (AD-5601A; A&D, Tokyo, Japan). All measurements were conducted in four replicate samples to ensure consistency and reduce experimental error. Thermographic images were recorded using an infrared thermograph (i7; FLIR, Nashua, NH, USA). The cycling stability of the CPT–CA–GO was also tested using 200 µL sample in a 96-well plate and irradiating it with 808 nm NIR laser at 0.7 W (approximately 35.6 mW/mm^2; 6 min on and 6 min off cycle) for 60 minutes. Temperature changes were recorded and plotted every minute.

3.3.6. Control drug-releasing

Control releasing of CPT from laser-induced CPT–CA–GO was performed as follows. A 500-µL PBS containing 10% FBS and CPT–CA–GO nanohybrid (GO concentration = 0.5 mg/mL, CPT = 0.5 mg/mL, and CA = 5×10^7 CFU/mL) was irradiated with an 808-nm NIR laser at 1 W (~50.9 mW/mm^2, spot diameter ~5 mm) power for 10 min. After adding PBS containing 10% FBS (500 µL), the samples were filtered by hydrophilic polyvinylidene difluoride syringe filter (pore size = 0.22 µm) (Millex^{TM}; Merck Millipore). The filtered samples were diluted 4 times with Milli-Q water after adding 500 µL DMSO, and finally the released CPT from laser-induced CPT–CA–GO was measured using a UV–vis–NIR spectrometer. The samples without laser irradiation also were measured by the same way to the laser-induced samples.

3.3.7. Cell culture and viability assay

Murine colon carcinoma (Colon-26) and human normal diploid fibroblast (TIG-103) cells were obtained from the Japanese Collection of Research Bioresources Cell Bank (Tokyo, Japan). The Colon-26 cells were cultured in RPMI 1640 medium (Gibco, Grand Island, NY, USA) containing 10% fetal bovine serum (FBS), 2 mM L-glutamine, 1 mM sodium pyruvate, gentamycin, and 100 IU/mL penicillin–streptomycin. The TIG-103 cells were cultured in Minimum Essential Medium (Gibco, Grand Island, NY, USA) containing 10% FBS, 2 mM L-glutamine, 1 mM sodium pyruvate, gentamycin, 100 IU/mL penicillin–streptomycin. The cells were maintained at 37 °C in a humidified chamber containing 5% CO_2. The samples were then cryopreserved in liquid nitrogen in multiple vials. Cell stocks were regularly revived to avoid genetic instability associated with high passage numbers.

Cell viability was assessed using Cell Counting Kit-8 (CCK-8) (Dojindo Laboratories, Kumamoto, Japan) according to the manufacturer's instructions. The CCK-8 assay detects the amount of formazan produced when the live cell dehydrogenase enzyme reduces the tetrazolium salt (WST-8). Briefly, $3–5\times10^3$ cells/well were seeded in 96-well plates, allowed to adhere overnight, and then exposed to 100 µL 0.1, 0.5, or 0.025 mg/mL CPT–CA–GO and CA–GO. As a positive control, 100 µL RIPA buffer was added to the cells. Experiments with and without laser irradiation were conducted in 96-well plates. For laser activated condition, the 808 nm NIR laser was used at 0.7 W (approximately 35.6 mW/mm^2) for 5 min each and left for 24 h. After washing with fresh medium, the cells were incubated with CCK-8 solution for 2–4 h at 37 °C. Absorbance at 450/690 nm was measured using a microplate reader.

3.3.8. Intracellular penetration of nanohybrid

Colon-26 cells (0.3×10^6 cells/well) were seeded in poly L-lysine-coated glass bottom dishes (Matsunami Glass, Osaka, Japan), allowed to adhere overnight, and exposed to ICG–CPT–CA–GO (12.5 μg/mL ICG, GO, and CPT each) for 10 h at 37 °C in a humidified incubator containing 5% CO_2. As a control, RPMI 1640 + 10% FBS was added. After washing thoroughly with fresh PBS (−) solution, the Colon-26 cells were observed using an FL microscopy system (IX73) equipped with a mirror unit (IRDYE800-33LP-A-U01; Semrock, Lake Forest, IL, USA) and an objective (40× magnification, aperture 0.95; UPLSAPO20X, Olympus) at room temperature. For 3D FL bioimaging and image overlay, Colon-26 cells were incubated with ICG–CPT–CA–GO as described above. After three washes with PBS (−), the cells were examined and images were acquired using a fluorescence microscope (BZ-X800, Keyence, Tokyo, Japan) and 3D analysis software (BZ-X800, Keyence, Tokyo, Japan).

3.3.9. Direct observation of cancer cell destruction

The Colon-26 cells were incubated for 10 h with CPT–CA–GO (12.5 μg/mL GO and CPT each) in a glass bottom dish, and the laser-induced action was recorded. Cancer cell destruction triggered by the laser-induced nanohybrid using the laser irradiation setup was performed as follows: An 808 nm, 254 mW (approximately 129 mW mm^{-2}) NIR laser beam from a continuous-wave diode laser (Sigma Koki, Tokyo, Japan) was incorporated into the microscope (IX73, Olympus). The laser beam (spot diameter: approximately 50 μm) was focused onto the target position (40× magnification; aperture 0.95; UPLSAPO40X, Olympus) at room temperature for 3 s. Videos were recorded using an electron-multiplying charge-coupled device camera system (DP80, Olympus) before and during irradiation.

3.3.10. In vivo anticancer therapy

Animal experiments were conducted following protocols approved by the Institutional Animal Care and Use Committee of the Japan Advanced Institute of Science and Technology (JAIST) (No. 04-007). Female BALB/cCrSlc mice (n=60; 4 weeks old; average weight = 15 g) were obtained from Japan SLC (Hamamatsu, Japan). Mice bearing Colon 26 cell-derived tumors were generated by injecting 1×10^6 cells with 100 µL Matrigel culture medium (v/v = 1:1; Dow Corning, Corning, NY, USA) into the dorsal right side of the mice. After approximately 1 week, when the tumor volume reached approximately 100 mm^3, the mice (n = 6 in each group) were intravenously injected with 200 µL PBS (−), 200 µL RPMI + 10% FBS containing CPT–CA–GO (0.5 mg/mL GO and CPT, 5×10^7 CFU/mL CA), 200 µL RPMI + 10% FBS containing CA–GO (0.5 mg/mL GO, 5×10^7 CFU/mL CA, 200 µL PBS (−) containing 5% Cremophor® EL encapsulating GO (CRE–GO; 0.5 mg/mL GO), or 200 µL DMSO–CPT (0.5 mg/mL CPT). Experiments with and without laser irradiation were performed for each group. For the groups treated with the laser, the tumors were irradiated 12 h after injection, followed by four more laser irradiations every 24 h (five laser irradiation sessions) using an 808 nm NIR laser at 0.8 W (approximately 40.7 mW/mm^2). Thermographic measurements were conducted during the irradiation using infrared thermography. Changes in tumor volume and overall health (viability and body weight) were monitored every alternate day. Tumor volumes were calculated using the formula $V = L \times W^2/2$, where L and W denote tumor length and width, respectively. When the tumor volume exceeded 1500 mm^3, the mice were euthanized according to the guidelines of the JAIST Institutional Animal Care and Use Committee.

3.3.11. In vivo fluorescent imaging

To study the tumor-targeting effect of ICG–CPT–CA–GO, female BALB/cCrSIc mice (5 weeks old; n=2; average weight = 18 g; average tumor size = 200 mm^3; Japan SLC) were inoculated with Colon-26 tumor cells on the dorsal right flank. After the tumor volume was 200 mm^3, the mice were intravenously injected with 200 µL PBS or RPMI 1640 + 10% FBS containing ICG–CPT–CA–GO (0.5 mg/mL ICG, CPT, and GO; 5×10^7 CFU/mL CA). The mice were imaged using an in vivo FL imaging system (VISQUE InVivo Smart-LF, Vieworks, Anyang, Republic of Korea) with 3 s exposure time and an ICG filter (excitation, 740–790 nm; emission, 810–860 nm) 4, 8, 12, and 24 h after sample administration. After 24 h later, the mice were euthanized, and the major organs, including the heart, liver, spleen, and kidneys, in addition to the tumors, were extracted and imaged. FL images were acquired and analyzed using the CleVue software (Vieworks).

3.3.12. Immunohistochemistry

The Colon-26 tumor-bearing female BALB/cCrSIc mice (5 weeks; n=10; average weight = 18 g; average tumor size = 100 mm^3; Japan SLC) were euthanized 1 d after administering 200 µL PBS, 200 µL RPMI 1640 + 10% FBS containing CPT–CA–GO (0.5 mg/mL GO and CPT, 5×10^7 CFU/mL CA), 200 µL RPMI 1640 + 10% FBS containing CA–GO (0.5 mg/mL GO, 5×10^7 CFU/mL CA), 200 µL of PBS (−) containing CRE–GO (0.5 mg/mL GO), or 200 µL DMSO–CPT (0.5 mg/mL CPT). Tumor tissues from the mice were then harvested and stored in 4% paraformaldehyde (FUJIFILM Wako Pure Chemical) for immunohistochemical (IHC) staining. The analysis was performed by Biopathology Institute Co., Ltd. (Oita, Japan) using standard protocols. Primary tumors were fixed in 10% formalin, processed for paraffin embedding, and cut into 3–4 µm thick sections. The sections were stained with hematoxylin and examined by light microscopy (IX73; Olympus, Tokyo, Japan) after incubation with primary antibodies (**Table 3.1**).

Areas showing positive staining in the tumor tissues were analyzed using a light microscopy system (BZ-X810; Keyence, Tokyo, Japan), hybrid cell count, and microcell count software (Keyence).

3.3.13. Safety analysis

This study used a blood cell counting machine (Microsemi LC 712; Horiba Medical, Japan) to measure the complete blood count (CBC) of the mice, and investigated the biochemical parameters with Japan SLC and Oriental Yeast Co. (Tokyo, Japan). Female BALB/c mice (5 weeks; n=5 in each group; average weight = 18 g; Japan SLC) were injected with CPT–CA–GO (0.5 mg / mL GO and CPT; 5×10^7 CFU/mL CA) or 200 μL PBS in the tail vein. Blood samples were collected from the inferior vena cava of the mice after 14 d. Additionally, major organs, including the heart, liver, kidneys, spleen, and lungs, were harvested and fixed in 4% paraformaldehyde before being sent to a specialized facility for H&E staining to evaluate the safety profile of the nanohybrid.

Table 3.1. Antibodies used in this study

Antibody	Type	Source	Catalog No.	Application
F4/80	Mouse Monoclonal	BMA Biomedicals	T-2028	IHC (1:50)
CD3	Rabbit Monoclonal	Abcam	ab16669	IHC (1:100)
CD19	Rabbit Polyclonal	Bioss	bs-0079R	IHC (1:100)
CXCR4	Goat Polyclonal	Abcam	ab1670	IHC (1:100)
NKp46	Rabbit Polyclonal	Affinity Biosciences	DF7599	IHC (1:100)
Caspase-3	Rabbit Polyclonal	Cell Signaling Technology	9661S	IHC (1:100)
TNF-α	Rabbit Polyclonal	Abcam	ab6671	IHC (1:100)
Anti-digoxigenin-peroxidase	Sheep Polyclonal	Merck Millipore	S7100	Tunel

3.3.14. Quantitative polymerase chain reaction (qPCR) assay

The Colon-26 tumor-bearing mice (5 weeks; n=10; average weight = 18 g; average tumor size = 100 mm^3; BALB/cCrSIc; Japan SLC) were euthanised the day after intravenous injection of 200 µL RPMI 1640 + 10% FBS containing CPT–CA–GO (0.5 mg/mL GO and CPT, 5×10^7 CFU/mL CA), 200 µL RPMI 1640 + 10% FBS containing CA–GO (0.5 mg/mL GO, 5×10^7 CFU/mL CA), 200 µL of PBS (−) containing CRE–GO (0.5 mg/mL GO), or 200 µL PBS (−) containing (CRE–GO) (0.5 mg/mL GO). To analyze the immune cells and cytokines in tumors, tumors were collected from mice in different groups after intravenous injection of sample for 24 h and then homogenized by a handy homogenizer (Thermo Fisher Scientific) before qPCR. qPCR was performed using a QuantStudio 1 PCR system (Thermo Fisher Scientific) to study the relative gene expression of CD3, CD19, CXCR4, F4/80, NK, IFN-γ, and TNF-α, using gene-specific primer-probe combinations (Thermo Fisher Scientific) (**Table 3.2**) and Taqman chemistry. Endogenous control was determined using TaqMan^{TM} Array Mouse Endogenous Control Plate 96 well (Thermo Fisher Scientific). The reactions were run in triplicate using GAPDH as an endogenous control. The thermal cycling parameters—50 °C for 2 min for AmpErase UNG activation, 95 °C for 2 min for AmpliTaq Gold DNA Pol. activation, 40 cycles each at 95 °C for 15 s for denaturation/melting, and 60 °C for 1.0 min for annealing and extension—yielded optimum amplification. For the test genes and endogenous control standards 10-fold serial dilutions were run in the study to estimate the efficiency of PCR. The percentage efficiency ranged between 90 to 100%. Results were analyzed and shown as fold change (log_{10} relative quantification) relative to the control group.

Table 3.2. TaqMan™ Primers for qPCR.

Target	Assay ID	Gene Symbol	Source
F4/80	Mm00802529_m1	Adgre1	Thermo Fisher Scientific
CD3	Mm00442746_m1	Cd3d	Thermo Fisher Scientific
CD19	Mm00515420_m1	Cd19	Thermo Fisher Scientific
CXCR4	Mm01996749_s1	Cxcr4	Thermo Fisher Scientific
NKp46	Mm01337324_g1	Ncr1	Thermo Fisher Scientific
IFN-γ	Mm01168134_m1	Ifng	Thermo Fisher Scientific
TNF-α	Mm00443258_m1	Tnf	Thermo Fisher Scientific
GAPDH	Mm99999915_g1	Gapdh	Thermo Fisher Scientific

3.3.15. Statistical analysis

All experiments were performed in triplicate and repeated at least three times. Quantitative values are expressed as the mean ± standard error of the mean (SEM) of at least three independent experiments. Statistical differences were identified by Student's *t*-test or log-rank (Mantel-Cox) test using GraphPad Prism software, version 9.4.0 (GraphPad Software, Boston, MA, USA). Statistical significance was set at $p<0.05$.

3.4. Results and Discussion

3.4.1. Characterization of the Nanoparticles

Hybrid nanoarchitectonics with CPT–CA–GO was prepared using a one-step sonication process (**Figure 3.1a**). The water dispersibility of CPT–CA–GO was significantly improved. No GO- or CPT-derived aggregates were visible in the vials for at least 2 h (**Figure 3.1b**). Precipitation occurred in a mixture of CPT and GO without CA immediately after sonication. We believe that the simple synthesis of multi-functionalized CPT–CA–GO via sonication and economical cultivation of bacterial strains only requires inexpensive media and basic equipment, such as an incubator, further enhancing its accessibility for mass production.

The structural details of CPT–CA–GO were analyzed using transmission electron microscopy (TEM) (**Figure 3.1c and Figure 3.2a**). The TEM image of CPT–CA–GO reveals bacterial components coating the GO sheet. Isolated CPT–CA–GO nanohybrids were individually distributed on a TEM grid. The average particle size of CPT–CA–GO was about 53 nm. GO exhibited a wrinkled structure, and the bacterial component coating was evident as areas with darker contrast, indicating the presence of various bacterial ingredients. The coating was almost uniform, with possible spots due to uncoated regions. In contrast, the control image of pristine GO shows one layer of electron-dense regions, suggesting the absence of bacterial ingredients. GO also displayed many big aggregations (more than 1 μm) due to the low water-dispersibility of pristine GO without any modifications.

The absorbances of CPT–CA–GO and each of its constituents were plotted (**Figure 3.1d**). When solubilized in methanol, CPT exhibits two major peaks at approximately 253 and 359 nm (**Figure 3.2b**). After loading CPT onto CA–GO, the absorbance decreased, even though the concentration of each material was adjusted. This might be due to molecular interactions, such as hydrophobic

interactions and hydrogen bonding between CPT and the nanohybrid.[20,21] The loading efficiency of CPT was 95.6%, indicating that most CPT was conjugated to the nanohybrid. We envisioned that the drug would be predominantly delivered to the tumor site along with the nanohybrids, minimizing exposure to other body tissues, thereby Supplementary the effectiveness of targeted therapy by benefiting from the enhanced permeability and retention (EPR) effect.[22–24]

3.4.2 In vitro efficacy of the nanohybrids

Upon local laser irradiation, GO absorbs near-infrared (NIR) radiation and converts it into heat in a non-radiative process.[25] Consequently, the temperature within the tumor tissue increases sufficiently and destroys tumor cells. This study aimed to identify the optimal laser power for maximum therapeutic effect while minimizing damage to healthy tissues. To this end, the temperature elevation due to the photothermal conversion ability of GO was studied using 808 nm NIR laser with 0.7 W power (approximately 35.6 mW/mm^2) for 5 min (**Figure 3.1e**). Thermographic images illustrated the temperature variations with changing concentrations, and the temperature immediately rose from 25 °C to approximately 55 °C at the highest concentration (**Figure 3.1f**).

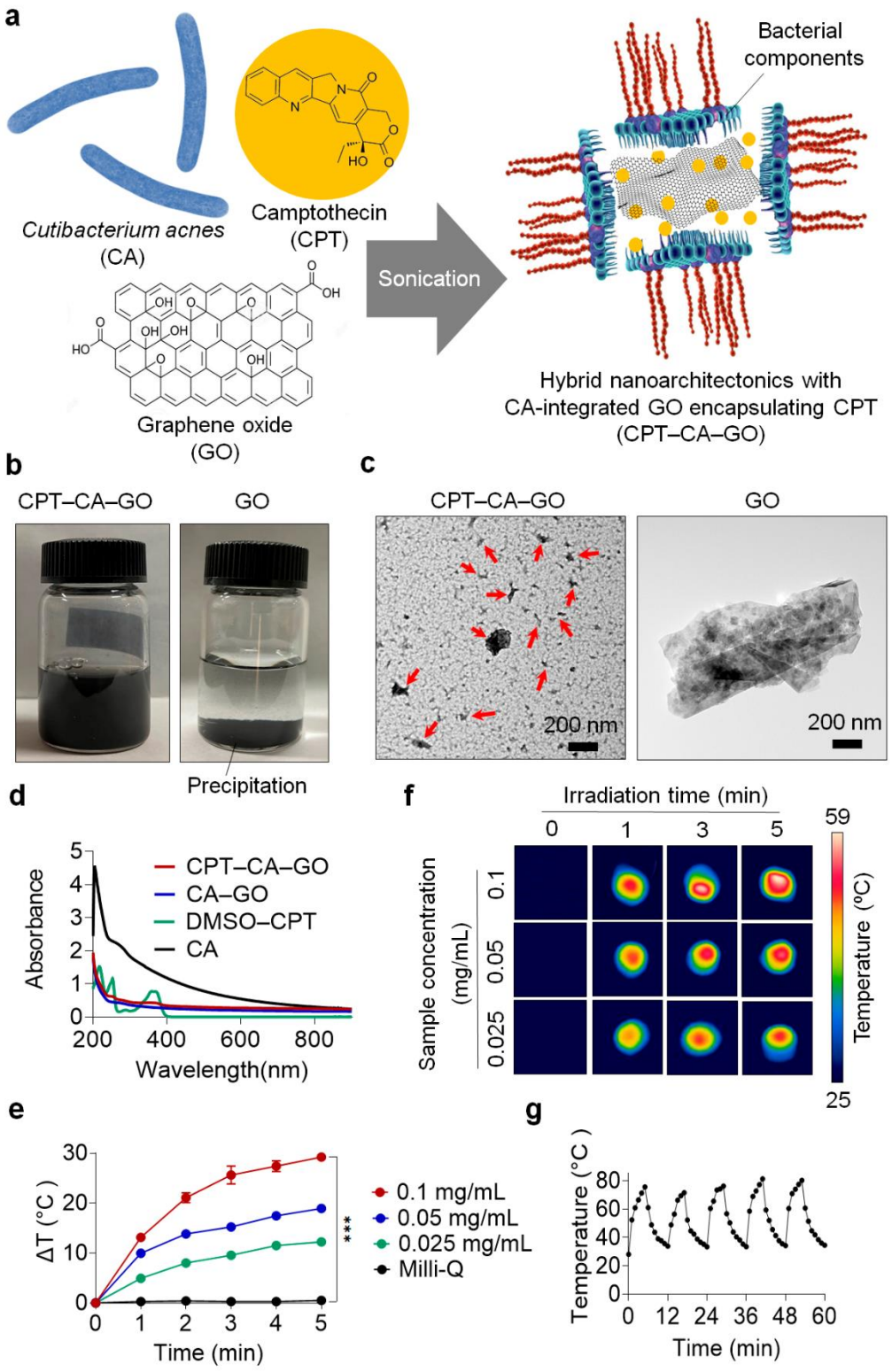

Figure 3.1. Structural and optical characterizations of the functionalized nanohybrids. (a) Schematic illustration of preparation of hybrid nanoarchitectonics with camptothecin-incorporated *Cutibacterium acnes*-modified graphene oxide (CPT–CA–GO). (b) Water dispersibility of CPT–CA–GO (left) and pristine

GO (right). (c) TEM images of CPT–CA–GO (left) and pristine GO (right). Red arrows represent CPT–CA–GO nanohybrids. (d) UV–vis–NIR absorbance spectra of CPT–CA–GO, CA–GO, 10% DMSO containing CPT (DMSO–CPT), and CA. CPT and GO concentration: 12.3 μg/mL, CA concertation: 6.25×10^6 CFU/mL. (e) Infrared thermographic images of each sample upon laser irradiation at 0, 1, 3, and 5 min. (f) Temperature elevation profile of CPT–CA–GO under 0.7 W (ca. 35.6 mW/mm^2) laser irradiation with varying concentrations. Data are presented as the mean ± SEM (n=3; biologically independent tests), ***$p<0.001$ versus the control (Milli-Q water) (Student's *t*-test). (g) Photothermal stability of CPT–CA–GO dispersion under heating and natural cooling cycles exposed to 808 nm laser irradiation at 0.7 W (~35.6 mW/mm^2) power. CPT and GO concentration: 0.1 mg/mL, CA concertation: 5×10^7 CFU/mL.

At 0.1 mg/mL and 0.7 W power (approximately 35.6 mW/mm^2), CPT–CA–GO achieved the maximum temperature difference (ΔT) of approximately 30 °C. Since 0.7 W (approximately 35.6 mW/mm^2) was sufficient to generate therapeutic heat, this power level was selected for subsequent in vivo experiments. Experiments at different laser power [1.2 W (approximately 61.1 mW/mm^2) and 0.3 W (approximately 15.3 mW/mm^2)] resulted in ΔT of approximately 60 °C and 10 °C, respectively (**Figure 3.2c**). These results clearly indicate that the photothermal conversion of CPT–CA–GO is easily controlled by changing the sample concentration and external laser power. We intended to use the laser repeatedly; hence, the photothermal stability of CPT–CA–GO as an effect of hyperthermia with repeated cycles of laser irradiation for photothermal therapy (PTT) was tested (**Figure 3.1g**). Accordingly, a CPT–CA–GO suspension was subjected to five cycles of NIR laser irradiation. Interestingly, CPT–CA–GO exhibited excellent photo-exothermic stability, and consistently reached about 80 °C in every cycle after cooling back to room temperature. The absorbance also did not change before and after 808 nm NIR laser irradiation at 0.7 W (approximately 35.6 mW/mm^2) (**Figure 3.2d**), confirming the stability and quality of CPT–CA–GO. These results demonstrate that CPT–CA–GO is highly efficient at generating therapeutic heat under NIR laser irradiation and stable over multiple cycles, making it a promising candidate for

future clinical applications in PTT. More interestingly, CPT molecules can be remotely released from the CPT–CA–GO by laser irradiation (**Figure 3.2e**). The release of CPT was spatiotemporally controllable by laser irradiation time.

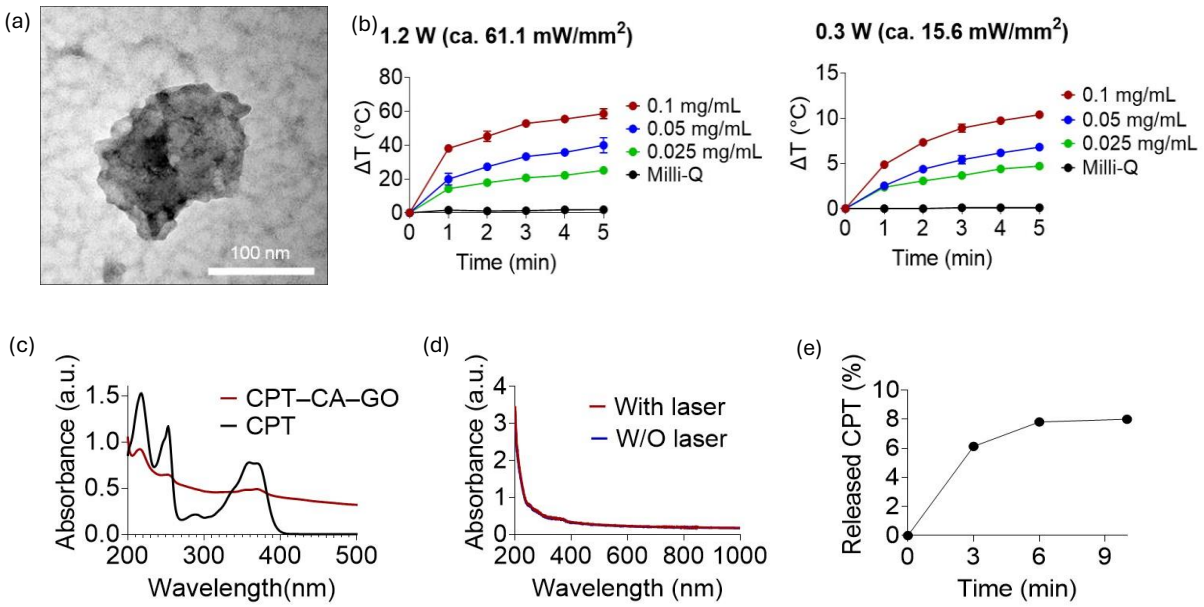

Figure. 3.2. (a) Magnified TEM image of camptothecin-incorporated *Cutibacterium acnes*-modified graphene oxide (CPT–CA–GO). (b) Magnified ultraviolet (UV)–visible (vis) absorbance spectra of camptothecin-incorporated *Cutibacterium acnes*-modified graphene oxide (CPT–CA–GO) and CPT. CPT was dissolubed in methanol. CPT and GO concentration were 12.3 µg/mL. CA concentration was 6.25×10^6 CFU/mL. (c) Temperature elevation profile of camptothecin-incorporated *Cutibacterium acnes*-modified graphene oxide (CPT–CA–GO) under 1.2 W (approximately 61.1 mW/mm^2) and 0.3 W (approximately 15.3 mW/mm^2) laser irradiation with varying concentrations. (d) Ultraviolet (UV)–visible (vis) absorbance spectra of the nanohybrids before and after 0.7 W 808 nm laser irradiation (approximately 35.6 mW/mm^2) for 5 min. Camptothecin (CPT) and graphene oxide (GO) concentration were 0.01 mg/mL. *Cutibacterium acnes* (CA) concentration was 5×10^6 CFU/mL. (e). Drug release profile from laser-induced CPT–CA–GO. Released CPT was measured by microplate reader. Data presented as means ± standard error of the mean (SEM) (n = 3; independent tests).

To verify the intracellular distribution of the nanohybrid, the fluorescent probe indocyanine green (ICG) was encapsulated in CPT–CA–GO (ICG–CPT–CA–GO) by sonication (**Figure 3.3a**). After

exciting at 700 nm, the emission peak of ICG was observed at approximately 822 nm (**Figure 3.3b**). A blue shift to 803 nm was observed for ICG–CPT–CA–GO, indicating that the molecular interactions between the nanohybrid and ICG altered the emission properties. We confirmed that ICG molecules (ca. 99%) could be tightly attached on the nanohybrids even after ultrafiltration (**Figure 3.3d**). Fluorescence (FL) imaging confirmed the intracellular nanohybrid uptake (pink dots) after 12 h, providing strong evidence of internalization (**Figure 3.3c**). The control group showed no FL. The ingestion of nanohybrids into the treated cells was also confirmed by 3D FL imaging (**Figure 3.3e**).

Next, to evaluate the cell viability upon treatment with CA–GO or CPT–CA–GO, in vitro cytotoxicity assay using the Cell Counting Kit-8 (CCK-8) was conducted on murine colorectal cancer (Colon-26) and normal human fibroblast (TIG-103) cells (**Figure 3.4**). In control experiments without laser irradiation, both CA–GO and CPT–CA–GO were more toxic to Colon-26 compared than to TIG-103. In general, cancer cells do not have healthy cellular and nuclear membranes or rigid protein and mitochondrial structures like normal cells.[26,27] Herein, CPT–CA–GO may penetrate fragile and abnormal cancer cells and cancer nuclear membranes to directly interact with DNA and destroy cancer cells by laser irradiation.[18] The increase in cytotoxicity with higher sample concentrations was also significant, indicating a clear dose-dependent response. This suggests that the nanohybrids may cause cell damage through direct cytotoxicity or interference with normal cellular functions. A radioimmunoprecipitation assay (RIPA) lysis buffer, which consistently induced strong cytotoxicity in both cell lines, was used as a positive control.

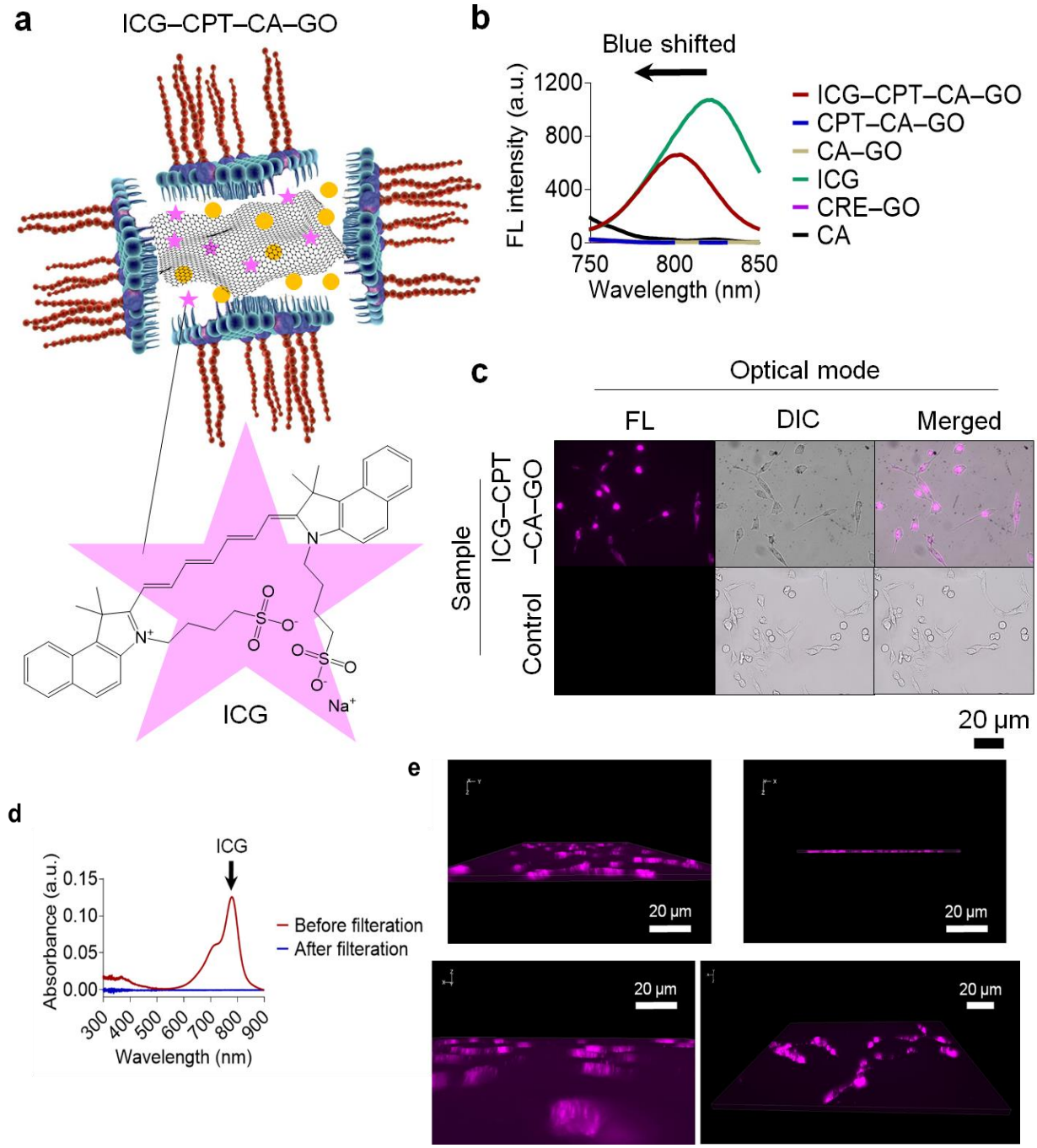

Figure 3.3. Intracellular penetration behavior and direct observation of cancer cell destruction of laser-induced nanohybrids. (a) Schematic illustration of camptothecin-incorporated *Cutibacterium acnes*-modified graphene oxide encapsulating indocyanine green (ICG–CPT–CA–GO). (b) Fluorescence (FL) emission spectra of ICG–CPT–CA–GO, CPT–CA–GO, CA–GO, ICG, 5% Cremophor® EL encapsulating GO (CRE–GO), and CA. ICG, CPT, and GO concentration: 0.1 mg/mL, CA concertation: 5×10^7 CFU/mL. (c) FL bioimaging of Colon-26 cancer cells after incubation with PBS (control) and ICG–CPT–CA–GO. The 2D pictures represent differential interference contrast (DIC), FL, and a merged image (DIC + FL).

Pink and black particles represent ICG–CPT–CA–GO. (d) UV–vis–NIR absorption spectrum of the filtrate of camptothecin-incorporated *Cutibacterium acnes*-modified graphene oxide encapsulating indocyanine green (ICG–CPT–CA–GO). The ICG–CPT–CA–GO aqueous suspension was filtered by Amicon® Ultra Centrifugal Filter (3 kDa cutting-off molecular weight; Merck Millipore) at 5000 g for 15 min at 20 ºC, and then diluted 100 times with Milli-Q water before the measurement. ICG, CPT, and GO concentration were 1 μg/mL. CA concentration was 5×10^5 CFU/mL. (e) 3D fluorescence images of Colon-26 cells after incubation with camptothecin-incorporated *Cutibacterium acnes*-modified graphene oxide encapsulating indocyanine green (ICG–CPT–CA–GO).

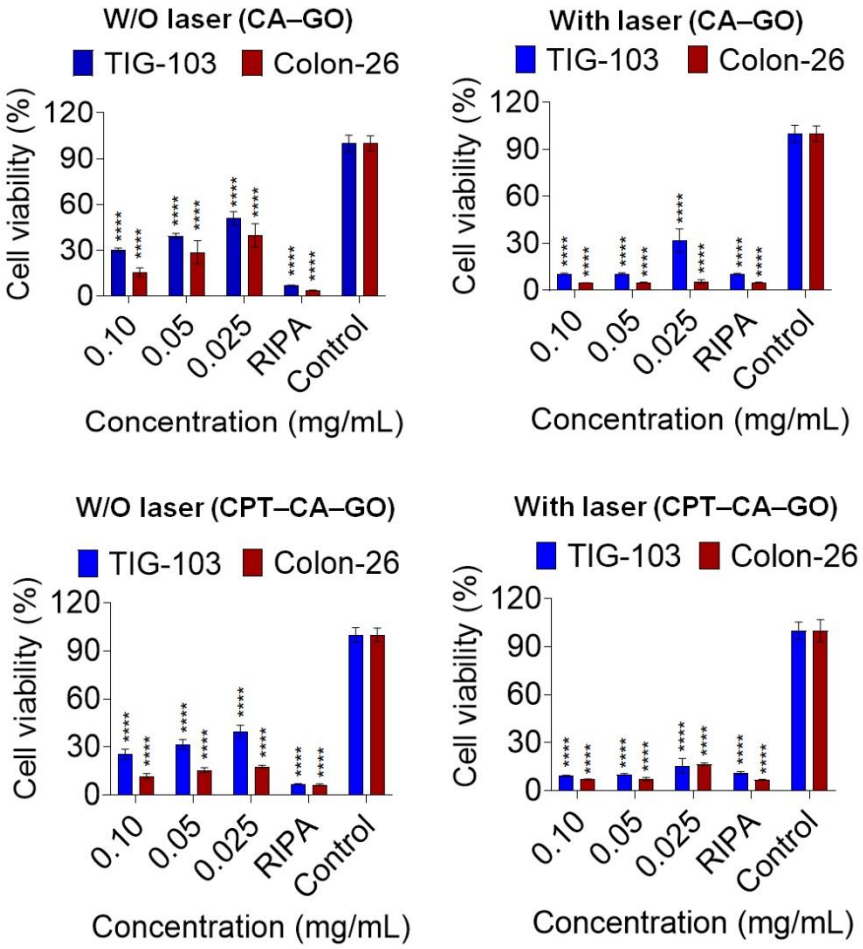

Figure 3.4. Laser-induced cytotoxicity of the nanohybrid. Viability of Colon-26 and TIG-103 cells treated with the camptothecin-incorporated *Cutibacterium acnes*-modified graphene oxide (CPT–CA–GO), CA–GO, and RIPA buffer (positive control) at various GO concentrations. Cell viability was tested 24 h after treatment with and without laser irradiation. Data presented as means ± SEM (n=5; biologically independent tests), ****p<0.0001 versus control without nanohybrids (Student's t-test).

Upon laser irradiation at 0.7 W (approximately 35.6 mW/mm^2) for 5 min, both CA–GO and CPT–CA–GO also displayed selective targeting cancer cell death. This may be attributed to the inherent heat sensitivity of cancer cells caused by selective and natural biochemical responses, such as the activation of heat-shock proteins and unique molecular signaling pathways under thermal stress.[28] In any case, the strong photothermal conversion capacity of GO demonstrated its potential as an effective exothermic agent for selective PTT.[5] The control group showed no significant reduction in cell viability both with and without laser irradiation, confirming the specificity of the nanohybrids' effectiveness. These findings indicate the potential use of nanohybrids in targeted cancer treatment.

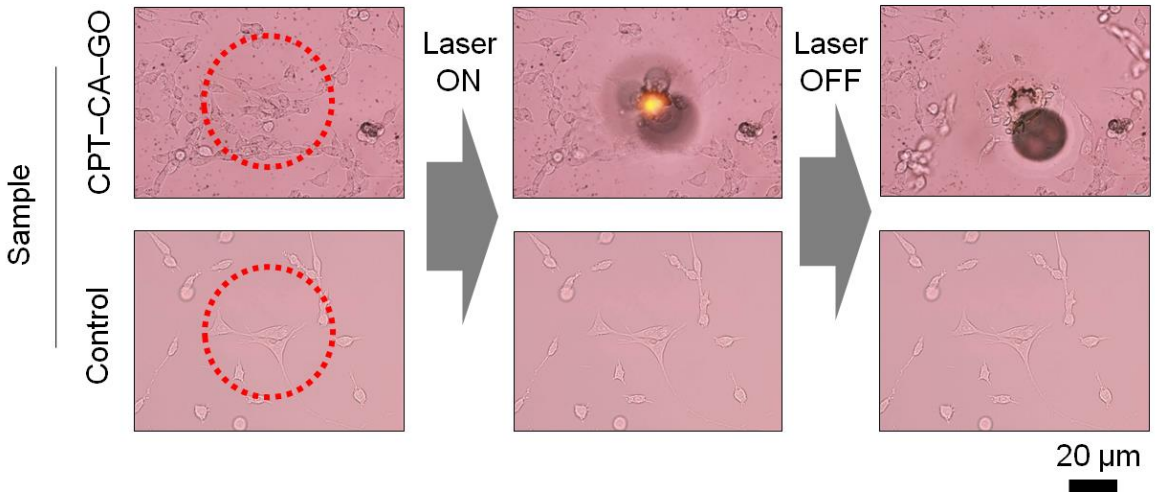

Figure 3.5. Colon-26 cancer cell destruction by laser-induced CPT–CA–GO before and after laser irradiation [wavelength = 808 nm, laser power = 254 mW (approximately 129 mW/mm^2)]. The red dashed circle represents the location of the laser irradiation.

Direct observation during NIR laser exposure (approximately 254 mW, 129 mW/mm^2) showed bursts in the cells, indicating severe heat-induced damage in CPT–CA–GO-treated cells (**Figure 3.5** and **Video 1**). The heat generated by the nanohybrids likely causes protein denaturation and membrane disruption, leading to effective cancer cell death through necrosis or apoptosis.[29,30] The control group showed no heating effect because of the absence of nanohybrids (**Video 2**).

3.4.3 In vivo efficacy of the nanohybrids

For studying the in vivo anti-tumor efficacy of the nanohybrids, the systemic ICG–CPT–CA–GO distribution in Colon-26-bearing BALB/c mice was examined using an in vivo FL bioimager (**Figure 3.6a**). FL imaging was conducted every 4 h after intravenous (i.v.) injection for 24 h, and FL derived from the nanohybrid gradually concentrated around the tumor over time. Vital organs and tumors were also extracted to assess the nanohybrid accumulation (**Figure 3.6b**). The EPR effect enabled ICG–CPT–CA–GO to accumulate in the tumor tissue due to the leaky vasculature and poor lymphatic drainage, Supplementary its use for targeted therapy.[23,24] While the tumor exhibited bright FL, the liver and kidneys showed negligible FL, likely due to nanohybrid clearance from the body, and other vital organs such as the heart, liver, and spleen showed no strong FL. When ICG is injected intravenously, it is generally taken up by liver (hepatocytes) and excreted in bile.[31,32] Herein, we consider that the obtained NIR fluorescence in the imaging is not false fluorescent signal of the isolated ICG molecules from ICG–CPT–CA–GO. A minor amount of fluorescence in the liver and kidneys suggests that the major elimination pathways for GO nanohybrids are reticuloendothelial and renal excretion.

Next, we investigated in vivo passive anticancer efficacy of various samples without laser irradiation (**Figure 3.6c and 3.6d**). CPT–CA–GO treatment exhibited a significant tumor growth suppression, followed by CA–GO treatment, presumably due to the synergistic combination of cytotoxicity of CPT and CA (**Figure 3.6c and Figure 3.7a**). 5% Cremophor® EL encapsulating GO (CRE–GO) and 10% DMSO containing CPT (DMSO–CPT) were tested as controls to verify whether each of them contributed to tumor suppression. A single dose neither exhibited inherent anticancer properties nor significantly affected tumor suppression compared with the control group (PBS injection).

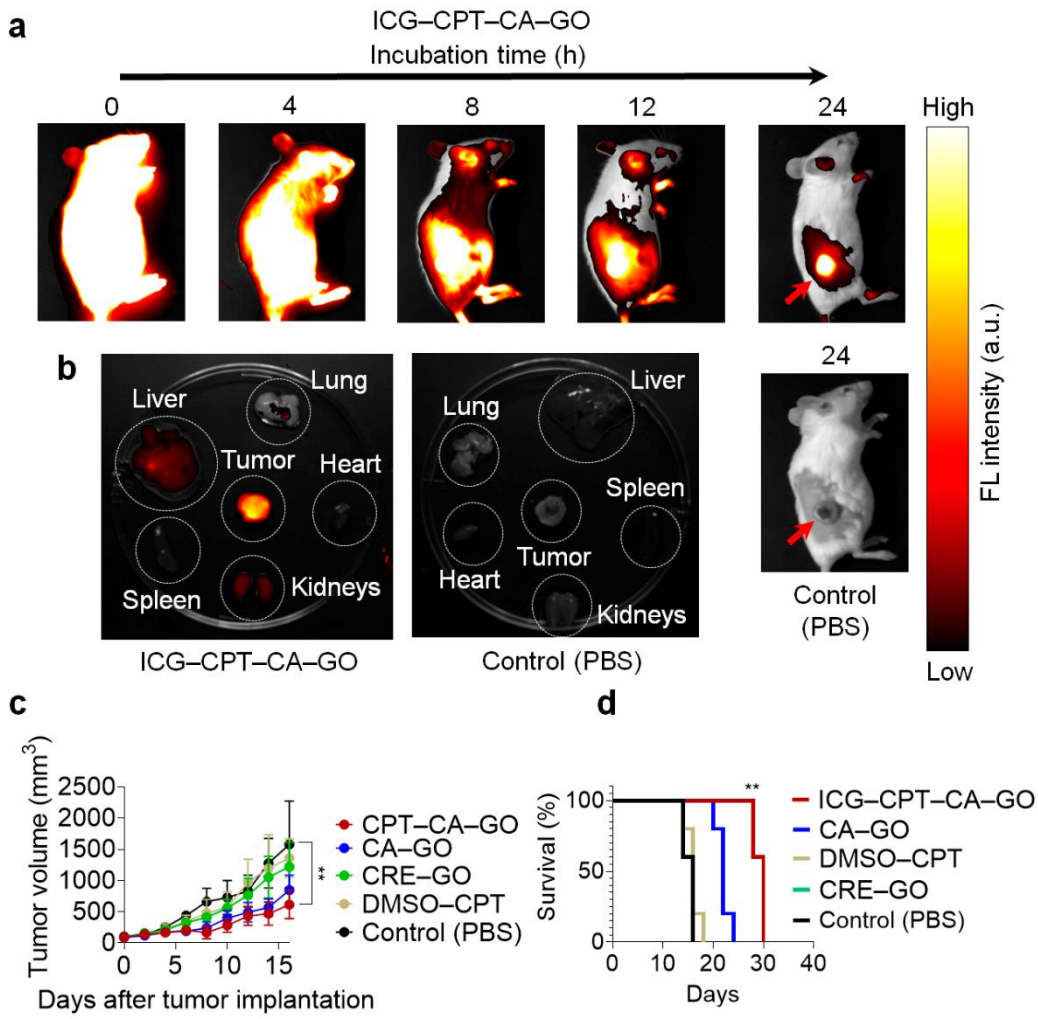

Figure 3.6. Passive anticancer performances of nanohybrids. (a) Systemic distribution of the nanohybrid in the tumor model. Fluorescence (FL) imaging of Colon-26 tumor-bearing mice after intravenous injection with PBS and camptothecin-incorporated *Cutibacterium acnes*-modified graphene oxide encapsulating indocyanine green (ICG–CPT–CA–GO). The red arrows denote the solid tumor location. (b) Extracted vital organs and tumors after intravenous injection with PBS or 200 µL ICG–CPT–CA–GO (0.5 mg/mL ICG, CPT, and GO; 5×10^7 CFU/mL CA). (c) Anticancer efficacy of various samples without laser irradiation. PBS or dispersion of CPT–CA–GO, CA–GO, 5% Cremophor® EL encapsulating GO (CRE–GO), and 10% DMSO containing CPT (DMSO–CPT), was intravenously injected into the Colon-26-bearing mice. Data are expressed as means ± SEM (n≥4 biologically independent tests). $^{**}p<0.01$ by Student's *t*-test. (d) Kaplan–Meier survival curves of Colon 26-tumor-bearing mice (n≥4 biologically independent mice) after tumor implantation for 30 d. Statistical significance was calculated in comparison with the PBS group. $^{**}p<0.01$ by Log-rank (Mantel–Cox) test.

These results indicated that the presence of CA and CPT aided the body in eliciting anticancer responses by coupling the effective intracellular uptake ability and EPR effect of the nanohybrid. All mice were euthanized when the tumor volume reached 1500 mm^3. The tumors in CPT–CA–GO- and CA–GO-treated groups reached 1500 mm^3 much slower than in the other groups because of the synergistic tumor-suppressive properties of the bacterial components and CPT. In particular, CPT–CA–GO prolonged the survival rate of the treated mice (**Figure 3.6d**). The overall health of the mice was monitored regularly and their body weight did not change significantly (**Figure 3.7b**).

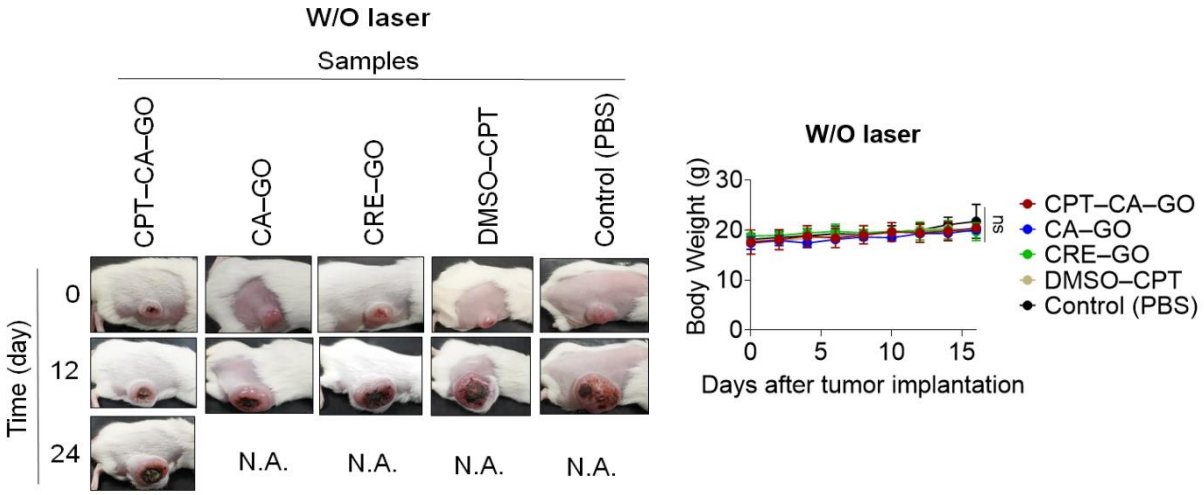

Figure 3.7. (a) Photos of the mice after each treatment without laser irradiation. (b) The average mouse body weight after treatment without laser irradiation during the treatment period. ns, not significant by Student's *t*-test versus control.

The NIR laser-activatable anti-tumor performance of CPT–CA–GO was evaluated (**Figure 3.8**). Laser irradiation at 808 nm was applied at a power of 0.8 W (approximately 40.7 mW/mm^2) for 5 min per session. Functional nanohybrids that accumulate in the tumor absorb NIR radiation, convert it into heat energy, and effectively increase the temperature of the targeted tumor tissue (**Figure 3.8a**). Mice treated with CRE–GO, CA–GO, and CPT–CA–GO exhibited a similar

temperature increase upon laser irradiation, reaching approximately 50 °C owing to the powerful photothermal conversion property of GO, whereas the other groups (PBS and DMSO–CPT) showed no significant increase in temperature (**Figure 3.8b**).

The groups treated with the laser after sample (CRE–GO, CA–GO, or CPT–CA–GO) administration demonstrated tumor disappearance (**Figure 3.8c**). Eventually, the survival curve revealed that CRE–GO, CA–GO, and CPT–CA–GO prolonged the lifetime of the mice by at least 40 d (**Figure 3.8d**). Magnified views of the first six days of the CRE–GO, CA–GO, and CPT–CA–GO treatments were carefully analyzed to assess the distinct roles of each therapeutic component (**Figure 3.8e**). Notably, CPT–CA–GO exhibited the strongest anticancer efficacy, owing to the powerful photothermal properties of GO and the anticancer properties derived from CPT and CA. No tumor regrowth was observed in the CPT–CA–GO group, whereas the CRE–GO and CA–GO groups showed tumor regrowth after a certain period (**Figure 3.8f**). These results clearly indicated that the synergistic traits of the immunological activity of CA, chemotherapeutic CPT, and photothermal conversion of GO could completely eradicate tumors with no recurrence. In addition, tumor volume did not reduce in the groups treated with PBS and DMSO–CPT even after NIR laser irradiation, because CPT or PBS do not exhibit photothermal conversion properties.

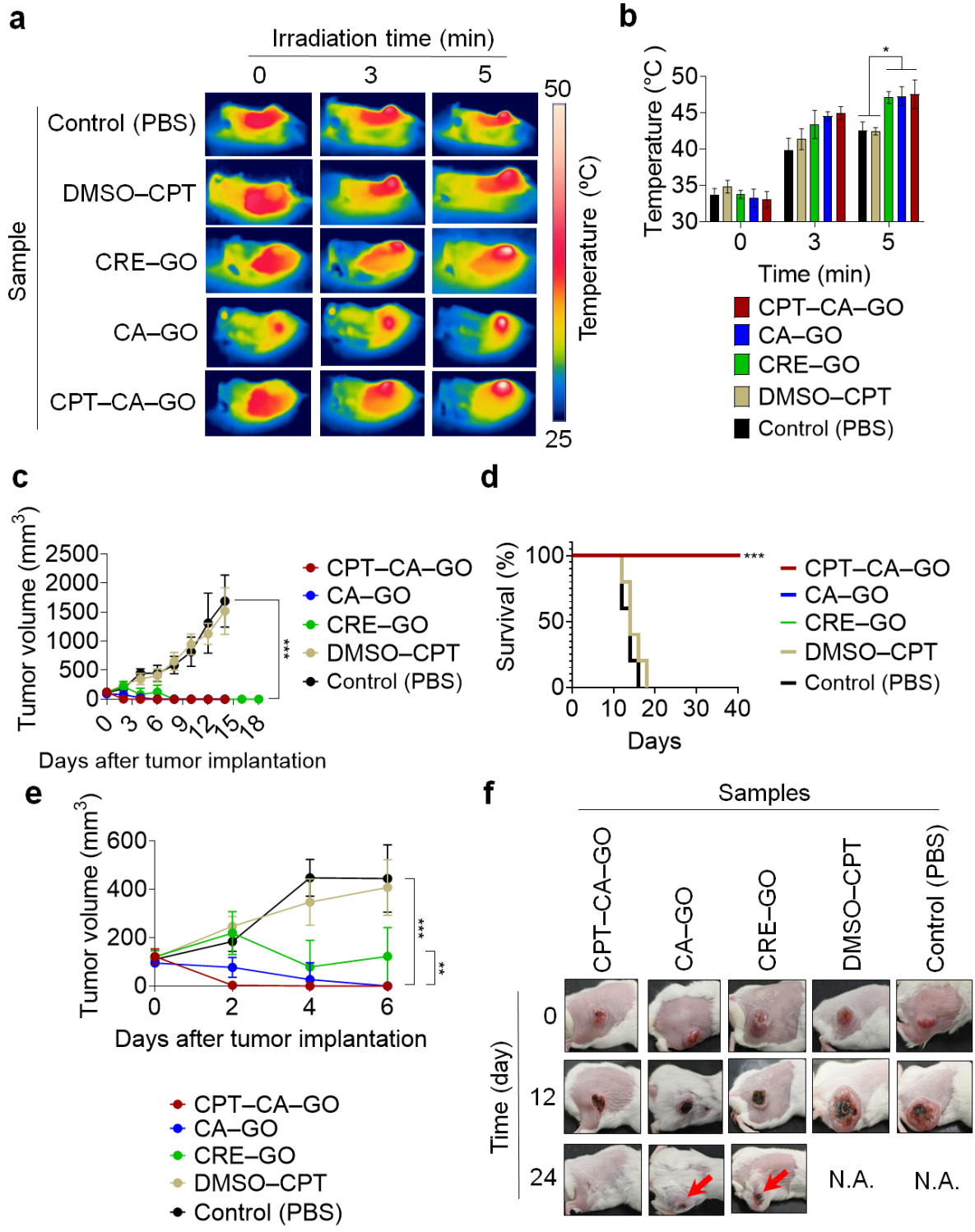

Figure 3.8. Photo-induced active anticancer efficacy of nanohybrids. (a) Thermographic measurement of the tumor surface by treatment with PBS or each sample (DMSO–CPT, CRE–GO, CA–GO, and CPT–CA–GO)-i.v. injected mice. Laser power, irradiation time, and wavelength are 0.8 W (~40.7 mW/mm^2), 5 min, and 808 nm, respectively. ICG, CPT, and GO concentration: 0.5 mg/mL; CA concertation: 5×10^7 CFU/mL.

(b) Temperature changes of tumors in Colon-26-bearing mice on day 2 after injection with each sample or PBS followed by 808 nm laser irradiation for 5 min [laser power = 0.8 W (approximately 40.7 mW/mm^2)]. Data are expressed as means ± SEM; n=5 independent experiments. Statistical significance was calculated in comparison with the PBS group. *p<0.05 by Student's t-test. (c) Anticancer effects of various samples after each treatment. Data are expressed as the mean ± standard error of the mean (SEM; n=5 biologically independent tests). ***p<0.001 by Student's t-test. ICG, CPT, and GO concentration: 0.5 mg/mL; CA concertation: 5×10^7 CFU/mL. (d) Kaplan–Meier survival curves of Colon-26-tumor-bearing mice (n=5 biologically independent mice) after tumor implantation for 40 d. Statistical significance is calculated by comparison with the PBS group. ***p<0.001 by Log-rank (Mantel–Cox) test. The CPT–CA–GO group had 100% survival rate for at least 40 d. (e) Magnified view of tumor volume changes during the initial six days of each treatment. Data are represented as mean ± standard errors of the mean (SEM); n=5 independent experiments. ***p<0.001 (Student's t-test for CPT–CA–GO) and **p<0.01 (Student's t-test for CA–GO). (F) Photos of the mice after each treatment. Red arrows represent the location of recurrent cancer.

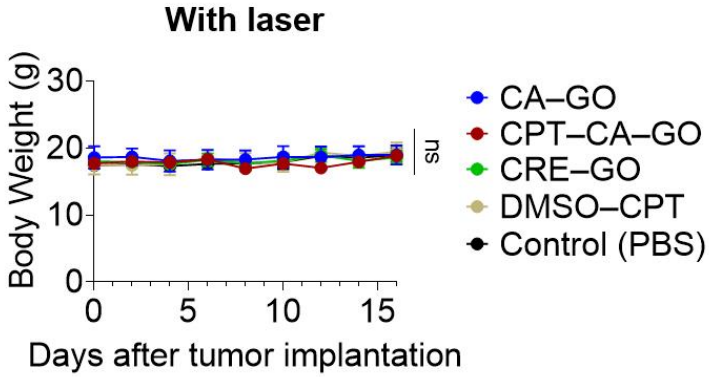

Figure 3.9. The average mouse body weight after treatment with laser irradiation during the treatment period. ns, not significant by Student's t-test versus control.

The overall health of the mice was closely monitored, with no significant changes in the average body weight in any group (**Figure 3.9**). A notable achievement of this study is the use of low-power (0.8 W; approximately 40.7 mW/mm^2) 808 nm NIR radiation in conjunction with a single intravenous injection dose of low-concentration sample, which resulted in substantial tumor eradication and complete recovery immediately after five laser irradiations for a very short time for each cycle.

3.4.4 Mechanistic insights

Finally, we investigated the anticancer mechanism of the laser-induced CPT–CA–GO nanohybrids (**Figure 3.10**). Histological examination using hematoxylin and eosin (H&E) staining revealed striking differences in tissue architecture across the treatment groups (**Figure 3.10**). The specimen treated with laser-induced CPT–CA–GO displayed widespread tissue destruction, characterized by loose, disorganized, and necrotic tumor structures, consistent with a robust therapeutic effect. In contrast, samples from the CRE–GO-, DMSO–CPT-, and PBS-treated groups exhibited tightly packed, intact tumor tissues, indicating minimal therapeutic impact with or without laser irradiation.

Apoptotic and immune cell markers were assessed using immunohistochemistry (IHC), which provided further evidence of the efficacy of CPT–CA–GO. Markers associated with apoptosis, such as TUNEL and caspase-3, were prominently expressed in the CPT–CA–GO group, indicating extensive tumor cell apoptosis, particularly after laser irradiation (**Figure 3.10**). This was accompanied by substantial immune cell infiltration, as reflected by the increased expression of markers for T cells (CD3), B cells (CD19), neutrophils (CXCR4), macrophages (F4/80), and natural killer (NK) cells (NKp46). Conversely, the CRE–GO-, DMSO–CPT-, and PBS-treated groups exhibited minimal expression of immune and apoptotic markers, indicating negligible immune cell recruitment and tumor cell death. Statistical analysis of the intensity of color development unequivocally demonstrated that laser-induced CPT–CA–GO induced a potent anti-tumor response through synergistic immune activation and apoptosis induction owing to heat generation (**Figure 3.11**).

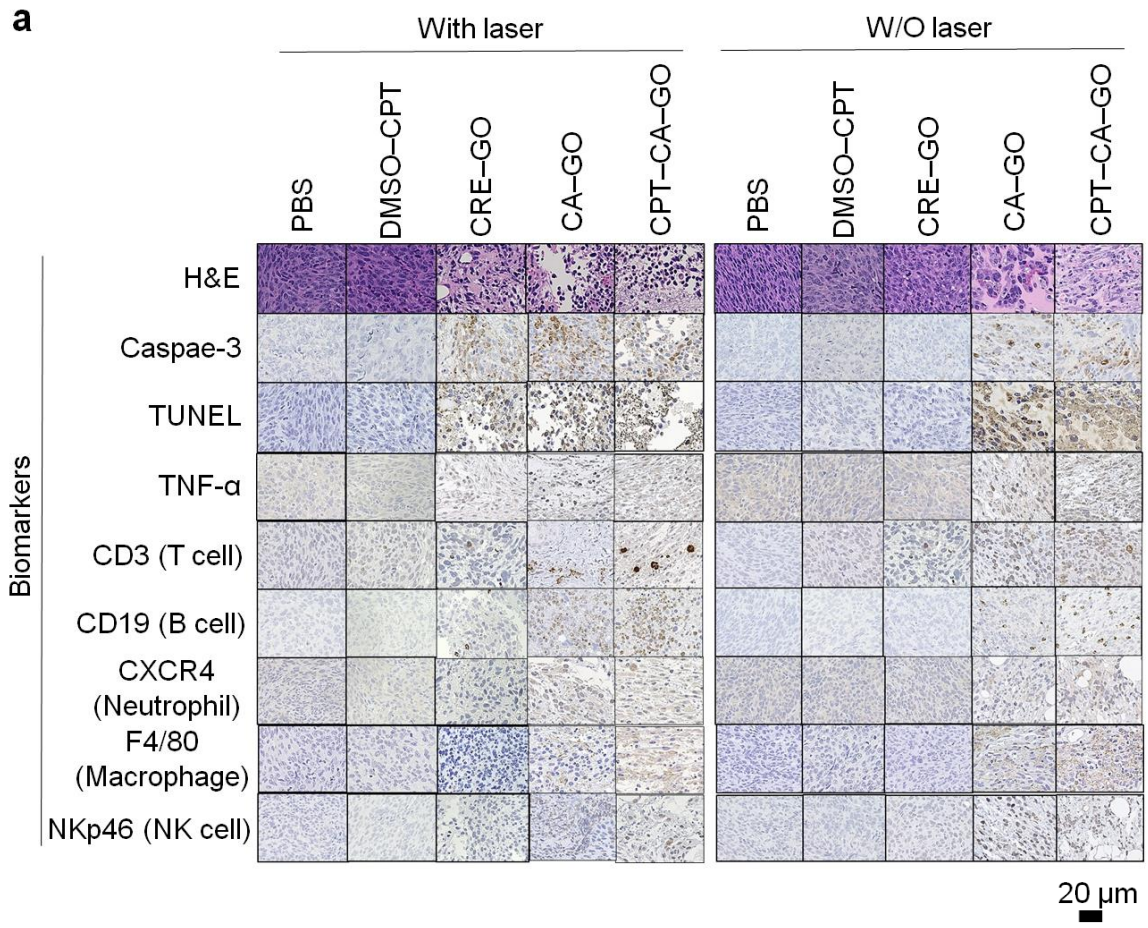

Figure 3.10. Mechanism of tumor suppression by laser-driven nanohybrids. (a) H&E-, TUNEL-, and IHC (Caspase-3, TNF-α, CD3, CD19, CXCR4, F4/80, and NKp46)-stained tumor tissues collected from different groups of mice on day 1 after their respective treatments.

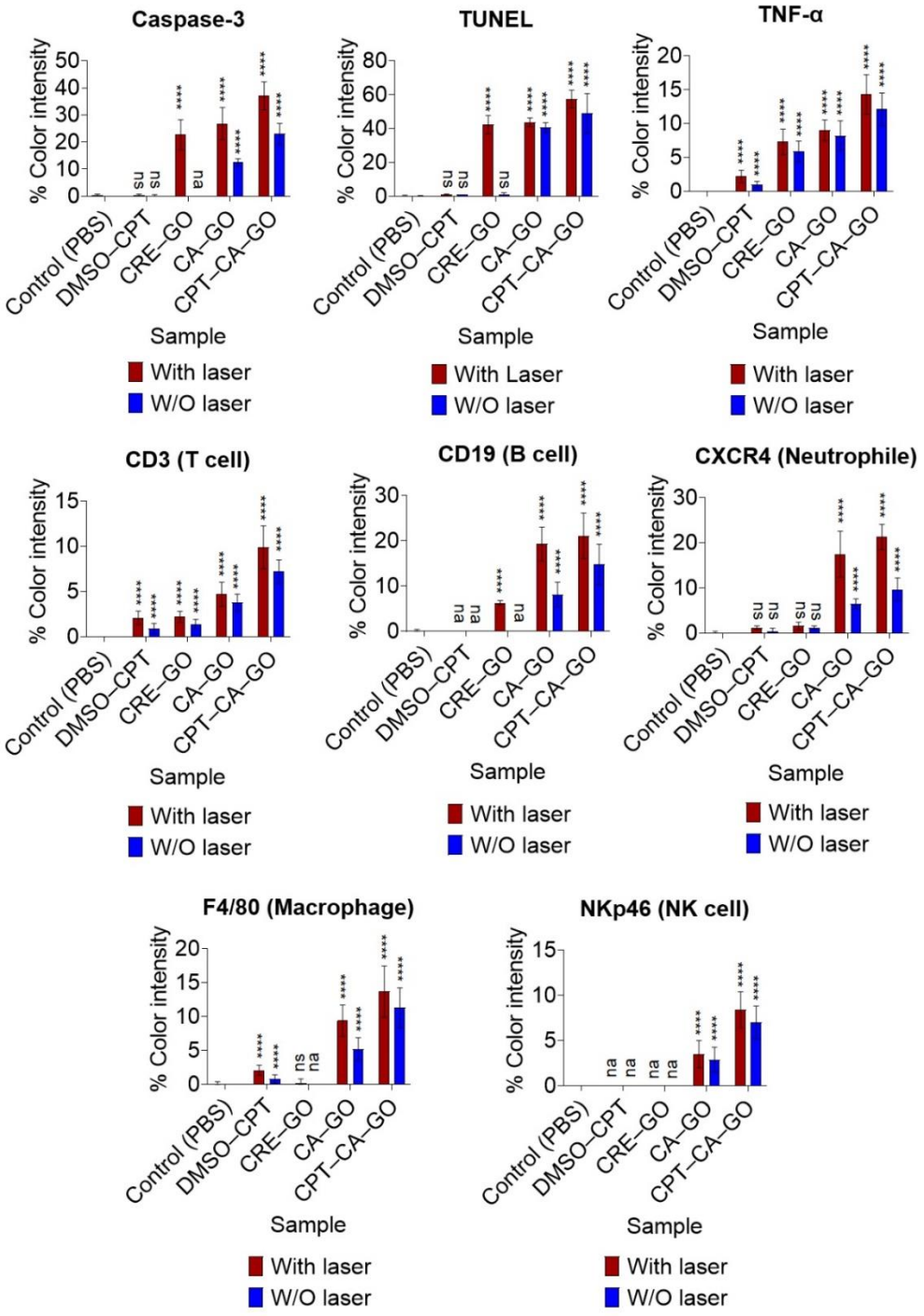

Figure 3.11. Intensity of color development in various immunohistochemical (IHC) slides as a comparison of control and treated samples. Data are represented as mean ± standard error of the mean (SEM); n = 10 independent areas (region of interest) in each tumor tissue collected from the groups of mice 1 day after treatments. Statistical significance was calculated in comparison with the control group. ns, not significant; na, not available; and ****p<0.0001 by Student's t-test.

Nevertheless, H&E analysis of the tissues of the harvested vital organs, heart, liver, lungs, kidneys, and spleen, revealed no significant abnormalities or evidence of toxicity in the CPT–CA–GO-treated group (**Figure 3.12**). The structural integrity of the tissues remained intact, with no observable signs of inflammation, necrosis, or other pathological changes. Blood tests also indicated no significant physiological alterations in mice following CPT–CA–GO treatment (**Table 3.3**).

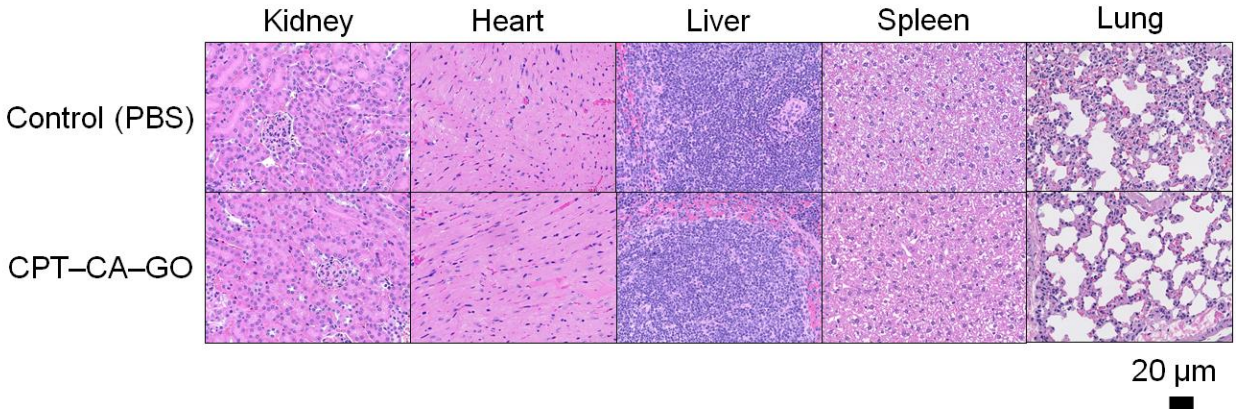

Figure 3.12. H&E staining in conventional organs sectioned after intravenous injection of camptothecin-incorporated *Cutibacterium acnes*-modified graphene oxide (CPT–CA–GO) or PBS after 14 days.

Table 3.3. Blood test of the BALB/c mice 7 days after i.v. injection of CPT–CA–GO.

Measured Value	Entry	Unit	Treated	Control	P value
CBC	WBC	$\times 10^2/\mu L$	54.8 ± 9.52	59.80 ± 12.15	> 0.05
	RBC	$\times 10^4/\mu L$	827.4 ± 45.29	871.20 ± 9.44	> 0.05
	HGB	g/dL	14.42 ± 0.61	14.96 ± 0.25	> 0.05
	HCT	%	43.06 ± 2.45	45.22 ± 0.61	> 0.05
	MCV	μm^3	52.06 ± 0.91	51.30 ± 1.08	> 0.05
	MCH	pg	17.44 ± 0.52	17.16 ± 0.32	> 0.05
	MCHC	g/dL	33.54 ± 0.68	33.46 ± 0.30	> 0.05
	RDW	%	14.1 ± 0.38	14.04 ± 0.52	> 0.05
	PLT	$\times 10^4/\mu L$	67.96 ± 3.54	70.44 ± 7.18	> 0.05
	MPV	μm^3	5.62 ± 0.13	5.68 ± 0.19	> 0.05
	PCT	%	0.38 ± 0.01	0.40 ± 0.03	> 0.05
	PDW	%	10.74 ± 0.17	10.74 ± 0.43	> 0.05
Biochemical parameters	TP	g/dL	4.56 ± 0.20	4.58 ± 0.13	> 0.05
	ALB	g/dL	3.12 ± 0.084	3.10 ± 0.12	> 0.05
	UN	mg/dL	28.32 ± 3.167	26.92 ± 6.79	> 0.05
	CRE	mg/dL	0.106 ± 0.01	0.11 ± 0.02	> 0.05
	Na	mEq/L	147.2 ± 1.30	148.20 ± 1.30	> 0.05
	K	mEq/L	20.5 ± 0.79	20.14 ± 1.16	> 0.05
	Cl	mEq/L	107.2 ± 2.17	106.60 ± 1.95	> 0.05
	AST	IU/L	43.2 ± 3.42	45.80 ± 5.17	> 0.05
	ALT	IU/L	21 ± 1.87	22.60 ± 2.30	> 0.05
	LDH	IU/L	141.4 ± 6.80	190.40 ± 42.62	> 0.05
	AMY	IU/L	2431.6 ± 296.53	2329.60 ± 281.39	> 0.05
	CK	IU/L	48.4 ± 7.13	48.00 ± 3.39	> 0.05
	γ-GT	IU/L	< 3	< 3	> 0.05

Data are represented as means ± standard errors of the mean (s.e.m.); n = 5 biologically independent mice. Statistical analyses comprise the two-way ANOVA test.

Abbreviations: ALB, albumin; ALT, alanine transaminase; AMY, amylase; AST, aspartate aminotransferase; BUN, blood urea nitrogen; Cl, chlorine; CK, creatine kinase; CRE, creatinine; HCT, hematocrit; HGB, hemoglobin; K, potassium; LDH, lactate dehydrogenase; MCH, mean corpuscular hemoglobin; MCHC, mean corpuscular hemoglobin concentration; MCV, mean corpuscular volume; MPV, mean platelet volume; Na, sodium; PCT, plateletcrit; PDW, platelet distribution width; PLT, platelet; RBC, red blood cell; TP, total protein; WBC, white blood cell; γ-GT, γ-glutamyl-transferase.

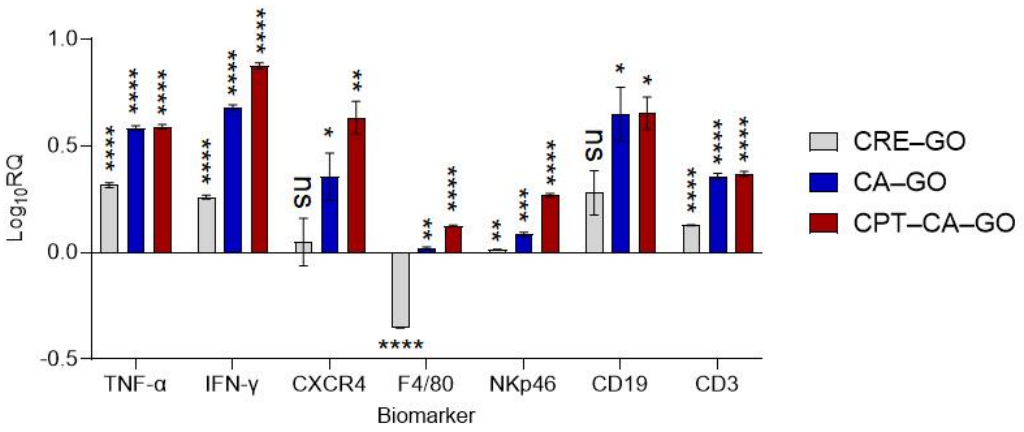

Figure 3.13. Quantification of markers related to immune cells and cytokines by qPCR after intravenous administration with CRE–GO, CA–GO or CPT–CA–GO for 24 h. The mRNA expression of CD19, CD3, CXCR4, F4/80, NKp46, and cytokines (IFN-γ and TNF-α) are shown as fold changes (log_{10} relative quantification [RQ]) relative to the control group (non-treatment). GAPDH gene expression was used as an internal control. Data are represented as means ± SEMs; n = 3 independent tumor tissues. Statistical significance was calculated by comparison with the non-treatment group. ns, not significant, *, $p < 0.05$, **, $p < 0.01$, ***, $p < 0.001$, and ****, $p < 0.0001$, by Student's two-sided *t* test.

The qPCR assay also supported that all immune cells including T cells (CD3), B cells (CD19), neutrophils (CXCR4), macrophages (F4/80), and NK cells (NKp46) were activated with increasing inflammatory cytokine TNF-α and IFN-γ in a solid tumor 24 h after i.v. administration of CA–GO or CPT–CA–GO (**Figure 3.13).**

These results indicate that the CA significantly shape the tumor microenvironment, affecting immune responses and inflammation, which influence therapeutic responses. Collectively, we verified that the photothermal and chemotherapeutic abilities of CPT–CA–GO played a significant role in the therapeutic outcomes for tumor cell destruction and cytotoxic immune cells could be actively recruited in the tumor microenvironment by CPT–CA–GO to effectively destroy targeted cancerous tumors (**Figure 3.14**). These findings strongly suggest that the CPT–CA–GO nanohybrid is highly biocompatible and does not induce off-target organ damage, indicating its potential for safe therapeutic applications.

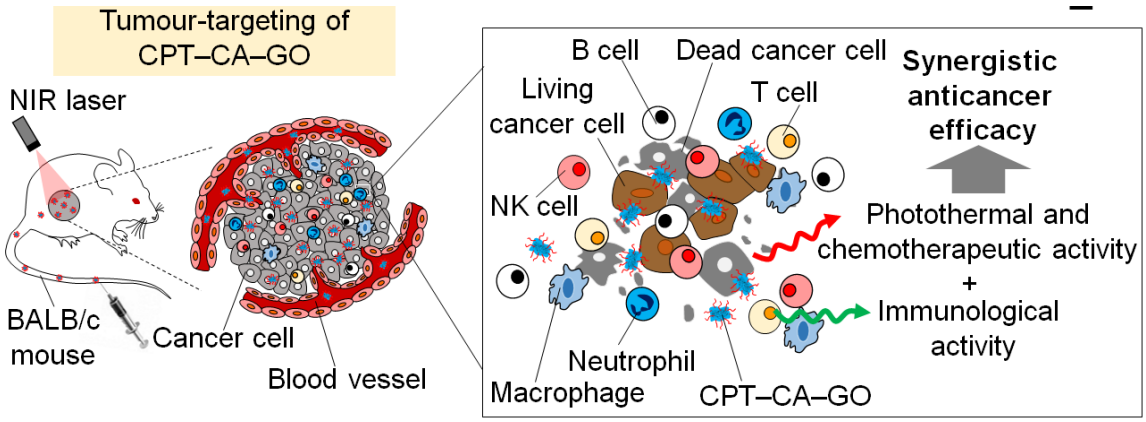

Figure 3.14- Scheme of the proposed mechanism.

3.5 Conclusion

In summary, we explored the immunological benefits of bacterial component-integrated GO nanohybrid delivery as part of a broad strategy for enhancing tumor immunogenicity and improving treatment efficacy. These findings demonstrated that the synergistic combination of GO, CA, and CPT enhanced bioavailability and triggered a robust immune response with single-dose administration. Cancer is a progressive, complex disease. The multidimensional approach is thus essential to combat various aggressive cancers.[33] This study focused on this approach, where CPT effectively targeted tumors locally, whereas GO enhanced tumor heating through photothermal effects. Simultaneously, the immune system was effectively activated by the components of CA, offering a promising approach for advanced cancer therapy. This study contributes to the growing interest in nanomedicine and immunotherapy as effective strategies that hold great promise for improving patient outcomes and paving the way for the development of immune-enhancing therapies and nanohybrid-based treatments in oncology. Modification of GO with functional molecules is a versatile platform with unique properties that find broad applications in various fields, including biomedicine.[34–36] Many researchers have attempted the potential chemical reactivity of GO and explored issues that hamper precise control of its

functionalization.[11] Further exploration of the modification and remote-controlling performances of GO nanohybrids with functional bioactive molecules for the development of an innovative treatment modality for diseases is important. Conventional functionalization of GO requires a complicated multistep of organic synthesis and purification process. Moreover, the relevance of immune cells-mediated cancer treatment with GO nanotechnology is still challenging, although immunogenicity of GO itself has actively been investigated[3] and nanoregulation of immunity[37,38] is one of the key factors to conquer cancer. We believe that our proposed method overcomes these fundamental issues of the previous research because the current work could actually make sense at least in terms of the development of simpler functionalization of GO nanohybrids without any complicated organic syntheses at all. Furthermore, the functional GO nanohybrids could be spatiotemporally evoked by biologically penetrable near-infrared laser and anticancer drugs for effective tumor regression in mice, with the help of immunological responses thanks to various bacterial immune stimulants decorated on the GO surface by a simple technique. As a result, complete tumor responses of tumors could be observed by GO nanohybrids in a light-activatable manner. These findings provide a strong basis for further investigations into the optimization and clinical translation of this nanomedicinal strategy.

3.6 References

[1] N. Kumar, S. Fazal, E. Miyako, K. Matsumura, R. Rajan, Avengers against cancer: A new era of nano-biomaterial-based therapeutics, Materials Today 51 (2021) 317–349. https://doi.org/10.1016/j.mattod.2021.09.020.

[2] T. Zhang, Graphene: From Theory to Applications, Graphene: From Theory to Applications (2022) 1–142. https://doi.org/10.1007/978-981-16-4589-1.

[3] M. Orecchioni, C. Ménard-Moyon, L.G. Delogu, A. Bianco, Graphene and the immune system: Challenges and potentiality, Adv Drug Deliv Rev 105 (2016) 163–175. https://doi.org/10.1016/J.ADDR.2016.05.014.

[4] Z. Gu, S. Zhu, L. Yan, F. Zhao, Y. Zhao, Graphene-Based Smart Platforms for Combined Cancer Therapy, Advanced Materials 31 (2019) 1800662. https://doi.org/10.1002/ADMA.201800662;JOURNAL:JOURNAL:15214095;PAGEGROUP:STRING:PUBLICATION.

[5] A.M. L Oliveira, M. Machado, G.A. Silva, D.B. Bitoque, J. Tavares Ferreira, L. Abegão Pinto, Q. Ferreira, Graphene Oxide Thin Films with Drug Delivery Function, (2022). https://doi.org/10.3390/nano.

[6] D.F. Báez, Graphene-Based Nanomaterials for Photothermal Therapy in Cancer Treatment, Pharmaceutics 15 (2023). https://doi.org/10.3390/pharmaceutics15092286.

[7] A.M. Itoo, S.L. Vemula, M.T. Gupta, M.V. Giram, S.A. Kumar, B. Ghosh, S. Biswas, Multifunctional graphene oxide nanoparticles for drug delivery in cancer, Journal of Controlled Release 350 (2022) 26–59. https://doi.org/10.1016/j.jconrel.2022.08.011.

[8] M. Hoseini-Ghahfarokhi, S. Mirkiani, N. Mozaffari, M.A. Abdolahi Sadatlu, A. Ghasemi, S. Abbaspour, M. Akbarian, F. Farjadian, M. Karimi, Applications of graphene and graphene oxide

in smart drug/gene delivery: Is the world still flat?, Int J Nanomedicine 15 (2020) 9469–9496. https://doi.org/10.2147/IJN.S265876.

[9] C. Xenodochidis, K. Hristova-Panusheva, T. Kamenska, P.B. Santhosh, T. Petrov, L. Stoychev, J. Genova, N. Krasteva, Graphene Oxide Nanoparticles for Photothermal Treatment of Hepatocellular Carcinoma Using Low-Intensity Femtosecond Laser Irradiation, Molecules 29 (2024). https://doi.org/10.3390/molecules29235650.

[10] S.A. Chechetka, B. Pichon, M. Zhang, M. Yudasaka, S. Bøgin-colin, A. Bianco, E. Miyako, Multifunctional Carbon Nanohorn Complexes for Cancer Treatment, (2015). https://doi.org/10.1002/asia.201403059.

[11] V. Georgakilas, M. Otyepka, A.B. Bourlinos, V. Chandra, N. Kim, K.C. Kemp, P. Hobza, R. Zboril, K.S. Kim, Functionalization of graphene: Covalent and non-covalent approaches, derivatives and applications, Chem Rev 112 (2012) 6156–6214. https://doi.org/10.1021/CR3000412/ASSET/IMAGES/MEDIUM/CR-2012-000412_0059.GIF.

[12] S.S.V.V. Chintalapati, S. Iwata, M. Miyahara, E. Miyako, Tumor-isolated Cutibacterium acnes as an effective tumor suppressive living drug, Biomedicine and Pharmacotherapy 170 (2024). https://doi.org/10.1016/j.biopha.2023.116041.

[13] Y. Goto, S. Iwata, M. Miyahara, E. Miyako, Discovery of Intratumoral Oncolytic Bacteria Toward Targeted Anticancer Theranostics, Advanced Science 10 (2023). https://doi.org/10.1002/advs.202301679.

[14] M. Miyahara, Y. Doi, N. Takaya, E. Miyako, Photocatalytic scaffolds enhance anticancer performances of bacterial consortium AUN, Chemical Engineering Journal 499 (2024) 156378. https://doi.org/10.1016/J.CEJ.2024.156378.

[15] H. Sudo, N. Tokunoh, A. Tsujii, S. Kawashima, Y. Hayakawa, H. Fukushima, K. Takahashi, T. Koshizuka, N. Inoue, The adjuvant effect of bacterium-like particles depends on the route of administration, Front Immunol 14 (2023). https://doi.org/10.3389/fimmu.2023.1082273.

[16] I.A. Hajam, P.A. Dar, G. Won, J.H. Lee, Bacterial ghosts as adjuvants: Mechanisms and potential, Vet Res 48 (2017). https://doi.org/10.1186/s13567-017-0442-5.

[17] Y. Shoenfeld, N. Agmon-Levin, "ASIA" - Autoimmune/inflammatory syndrome induced by adjuvants, J Autoimmun 36 (2011) 4–8. https://doi.org/10.1016/j.jaut.2010.07.003.

[18] L.F. Liu, S.D. Desai, T.K. Li, Y. Mao, M. Sun, S.P. Sim, Mechanism of action of camptothecin, in: Ann N Y Acad Sci, New York Academy of Sciences, 2000: pp. 1–10. https://doi.org/10.1111/j.1749-6632.2000.tb07020.x.

[19] K. Ariga, Nanoarchitectonics: what's coming next after nanotechnology?, Nanoscale Horiz 6 (2021) 364–378. https://doi.org/10.1039/D0NH00680G.

[20] X. Zou, S. Wei, J. Jasensky, M. Xiao, Q. Wang, C.L. Brooks, Z. Chen, Molecular interactions between graphene and biological molecules, J Am Chem Soc 139 (2017) 1928–1936. https://doi.org/10.1021/JACS.6B11226,.

[21] N. Ahmadian, F. Mehrnejad, M. Amininasab, Molecular Insight into the Interaction between Camptothecin and Acyclic Cucurbit[4]urils as Efficient Nanocontainers in Comparison with Cucurbit[7]uril: Molecular Docking and Molecular Dynamics Simulation, J Chem Inf Model 60 (2020) 1791–1803. https://doi.org/10.1021/ACS.JCIM.9B01087/ASSET/IMAGES/LARGE/CI9B01087_0014.JPEG

[22] D. Fan, Y. Cao, M. Cao, Y. Wang, Y. Cao, T. Gong, Nanomedicine in cancer therapy, Signal Transduct Target Ther 8 (2023). https://doi.org/10.1038/s41392-023-01536-y.

[23] A.I. Freeman, E. Mayhew, Targeted drug delivery, Cancer 58 (1986) 573–583. https://doi.org/10.1002/1097-0142(19860715)58:2+<573::AID-CNCR2820581328>3.0.CO;2-C.

[24] J. Li, Q. Wang, G. Xia, N. Adilijiang, Y. Li, Z. Hou, Z. Fan, J. Li, Recent Advances in Targeted Drug Delivery Strategy for Enhancing Oncotherapy, Pharmaceutics 15 (2023). https://doi.org/10.3390/pharmaceutics15092233.

[25] Z. Li, H. Lei, A. Kan, H. Xie, W. Yu, Photothermal applications based on graphene and its derivatives: A state-of-the-art review, Energy 216 (2021). https://doi.org/10.1016/j.energy.2020.119262.

[26] W. Szlasa, I. Zendran, A. Zalesińska, M. Tarek, J. Kulbacka, Lipid composition of the cancer cell membrane, J Bioenerg Biomembr 52 (2020) 321–342. https://doi.org/10.1007/S10863-020-09846-4,.

[27] D. Zink, A.H. Fischer, J.A. Nickerson, Nuclear structure in cancer cells, Nat Rev Cancer 4 (2004) 677–687. https://doi.org/10.1038/NRC1430;KWRD=BIOMEDICINE.

[28] R. Cavaliere, E.C. Ciocatto, B.C. Giovanella, B. Mondovi, G. Moricca, A. Rossi-fanelli, Md. Charles Hejdelberger, M. Margottini, SELECTIVE H E A T SENSITIVITY OF CANCER CELLS Biochemical and Clinical Studies, Public Health Service (n.d.). https://doi.org/10.1002/1097-0142(196709)20:9<1351::AID-CNCR2820200902>3.0.CO;2-.

[29] H.S. Han, K.Y. Choi, Advances in nanomaterial-mediated photothermal cancer therapies: Toward clinical applications, Biomedicines 9 (2021). https://doi.org/10.3390/biomedicines9030305.

[30] S.M. Thompson, M.R. Callstrom, K.A. Butters, B. Knudsen, J.P. Grande, L.R. Roberts, D.A. Woodrum, Heat stress induced cell death mechanisms in hepatocytes and hepatocellular

carcinoma: In vitro and in vivo study, Lasers Surg Med 46 (2014) 290–301. https://doi.org/10.1002/lsm.22231.

[31] E. Levesque, E. Martin, D. Dudau, C. Lim, G. Dhonneur, D. Azoulay, Current use and perspective of indocyanine green clearance in liver diseases, Anaesth Crit Care Pain Med 35 (2016) 49–57. https://doi.org/10.1016/j.accpm.2015.06.006.

[32] C. Schwarz, I. Plass, F. Fitschek, A. Punzengruber, M. Mittlböck, S. Kampf, U. Asenbaum, P. Starlinger, S. Stremitzer, M. Bodingbauer, K. Kaczirek, The value of indocyanine green clearance assessment to predict postoperative liver dysfunction in patients undergoing liver resection, Sci Rep 9 (2019). https://doi.org/10.1038/S41598-019-44815-X,.

[33] A. Upadhyay, Cancer: An unknown territory; rethinking before going ahead, Genes Dis 8 (2021) 655–661. https://doi.org/10.1016/j.gendis.2020.09.002.

[34] L. Feng, K. Li, X. Shi, M. Gao, J. Liu, Z. Liu, Smart pH-responsive nanocarriers based on nano-graphene oxide for combined chemo- and photothermal therapy overcoming drug resistance, Adv Healthc Mater 3 (2014) 1261–1271. https://doi.org/10.1002/ADHM.201300549;WGROUP:STRING:PUBLICATION.

[35] K. Yang, Y. Li, X. Tan, R. Peng, Z. Liu, Behavior and Toxicity of Graphene and Its Functionalized Derivatives in Biological Systems, Small 9 (2013) 1492–1503. https://doi.org/10.1002/SMLL.201201417.

[36] K. Yang, L. Feng, X. Shi, Z. Liu, Nano-graphene in biomedicine: theranostic applications, Chem Soc Rev 42 (2012) 530–547. https://doi.org/10.1039/C2CS35342C.

[37] F.Y. Wang, T. Qiu, Y. Ling, Y. Yang, Y. Zhou, Physical and Chemical Cues at the Nano–Bio Interface for Immunomodulation, Angewandte Chemie - International Edition 61 (2022) e202209499.

https://doi.org/10.1002/ANIE.202209499;JOURNAL:JOURNAL:15213773A;WGROUP:STRING:PUBLICATION.

[38] M. Yu, W. Yang, W. Yue, Y. Chen, Targeted Cancer Immunotherapy: Nanoformulation Engineering and Clinical Translation, Advanced Science 9 (2022). https://doi.org/10.1002/ADVS.202204335,.

CHAPTER 4

General conclusion

Abstract

Cancer remains one of the leading global health challenges, with conventional therapies often limited by tumor heterogeneity and systemic side effects. Despite advancements in chemotherapy and radiation, long-term survival rates remain stagnant for many cancers. Bacterial therapy offers a novel, targeted, and potentially cost-effective approach by harnessing engineered microbes to selectively attack tumors and stimulate immune responses. While concerns around safety and precision dosing persist, ongoing research into personalized and combinational treatments is promising. As scientific understanding deepens, bacterial therapy could emerge as a vital component of future cancer management, especially in low-resource settings requiring accessible solutions.

Conclusion

Bacterial therapy has emerged as a novel and promising strategy for cancer treatment, utilizing the natural abilities of certain bacteria to target and treat tumors. Among the various bacterial candidates tested in this study, *Cutibacterium acnes* (C. acnes) has shown exceptional potential due to its ability to thrive in hypoxic, low-oxygen environments characteristic of tumors. These properties allow *C. acnes* to specifically target cancer cells, offering an alternative to conventional therapies that may not effectively reach all areas of a tumor. This study investigates the tumor-suppressing effects of *C. acnes*, its ability to trigger immune responses, and its role in synergizing with advanced nanotechnologies like graphene oxide (GO) nanohybrids and chemotherapeutic agents such as camptothecin (CPT).

One of the most remarkable aspects of *C. acnes* therapy is its ability to activate the immune system. In the tumor microenvironment, *C. acnes* stimulates both innate and adaptive immune responses, recruiting various immune cells to fight the tumor. Macrophages, which are essential for recognizing and engulfing foreign pathogens or abnormal cells, are recruited in response to the bacterium. These immune cells then release cytokines that help orchestrate further immune activity. In addition to macrophages, *C. acnes* activates cytotoxic T cells, which directly attack and kill cancer cells. Natural killer (NK) cells are also brought into play; these immune cells offer a rapid response to tumor cells and are essential for mounting an early defense. This combined immune response results in a significant anti-tumor effect, not only through direct bacterial action but also by mobilizing the body's own defenses to fight the cancer.

The immune system’s activation by *C. acnes* is particularly significant in the context of tumors, which often develop mechanisms to suppress immune activity. Tumors are notorious for creating microenvironments that suppress immune responses, enabling cancer cells to evade detection and

destruction. *C. acnes* appears to counteract this by promoting immune cell infiltration and stimulating the activation of immune components that would otherwise be suppressed. The bacterium's oncolytic properties—its ability to break down tumor tissue—further support its role in cancer treatment. As it degrades the tumor, *C. acnes* opens up the tumor microenvironment, allowing immune cells to enter and attack cancerous cells more effectively (**Figure 4.1**).

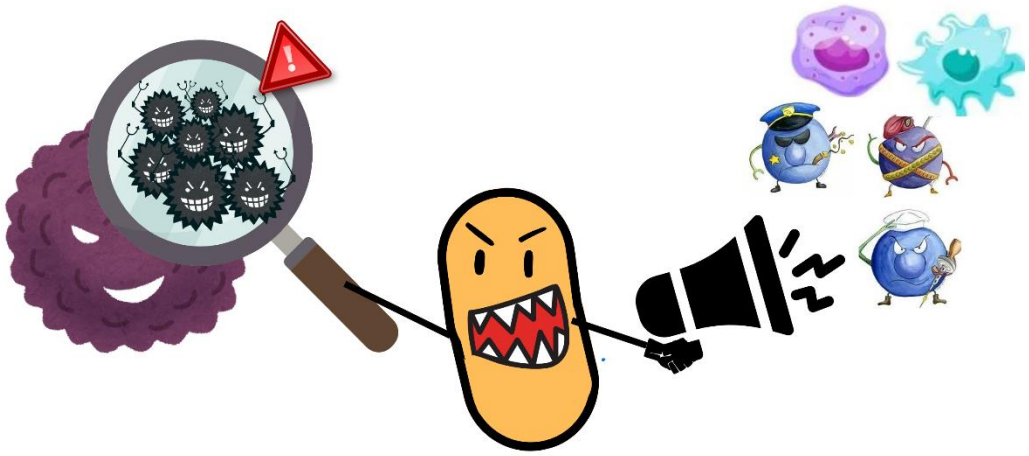

Figure 4.1- Illustration of how *C. acnes* activates the immune cells

In this study, *C. acnes* demonstrated significant tumor-suppressing effects, leading to prolonged survival in animal models. Mice treated with *C. acnes* showed superior tumor suppression compared to those treated with conventional cancer therapies, such as paclitaxel and immune checkpoint inhibitors like anti-PD-L1. Not only did *C. acnes* help destroy the tumor directly, but it also fostered an immune environment that supported long-term anti-cancer immunity. The minimal side effects observed in these treatments also make *C. acnes* a promising alternative or adjunct to traditional cancer therapies, which are often associated with severe toxicity and off-target effects.

Expanding on this promising bacterial therapy, the study also explores the integration of graphene oxide (GO) nanohybrids, which provide an advanced method of enhancing therapeutic delivery and efficacy. GO nanohybrids are a key component of nanomedicine due to their unique properties. These nanostructures are biocompatible, capable of carrying a variety of drugs, and have photothermal properties that allow them to convert near-infrared (NIR) light into heat. This feature is particularly useful in the context of cancer therapy, as it enables localized destruction of tumor cells without damaging healthy tissues.

GO nanohybrids were combined with camptothecin (CPT), a chemotherapy drug known for its ability to interfere with DNA replication in cancer cells by inhibiting topoisomerase I. The combination of GO nanohybrids and CPT provided a dual therapeutic approach, which enhanced the overall efficacy of the treatment. The nanohybrids facilitated the targeted delivery of CPT directly to the tumor, allowing for a higher local concentration of the drug and reducing the side effects associated with systemic chemotherapy. Simultaneously, the heat generated by the GO nanohybrids upon NIR light exposure induced thermal damage to tumor cells. This added layer of therapy made the tumor cells more susceptible to the chemotherapy drug, leading to a synergistic effect where both the photothermal and chemotherapy treatments worked together to destroy the cancer more effectively than either treatment alone.

Figure 4.2- Schematic of the ICG-tagged Camptothecin- *C. acnes*- Graphene oxide nanocomplex

When tested in vivo, the combination of *C. acnes*, GO nanohybrids, and CPT (**Figure 4.2**) resulted in significantly improved tumor suppression compared to the use of any one of these treatments in isolation. Tumors in animals treated with this combination shrank considerably, and the survival rates were much higher than those in groups treated with either *C. acnes* alone or the chemotherapy drug without the addition of bacteria or nanohybrids. The synergistic effect of combining immune modulation, photothermal therapy, and chemotherapy demonstrated that each component of the treatment contributed to the overall success.

Furthermore, the GO nanohybrids provided an important role in the treatment by promoting the infiltration of immune cells into the tumor. In addition to their ability to deliver the chemotherapy drug directly to the tumor, the heat generated by the nanohybrids also induced the release of tumor-associated antigens. This process helps to activate the immune system, prompting a stronger immune response to cancer cells. The local heating effect of the GO nanohybrids led to the breakdown of tumor cells, which released these antigens, further stimulating immune cells, including macrophages and T-cells, to recognize and attack the tumor. This immune boost was crucial in supporting the activity of *C. acnes*, enhancing its oncolytic effects and creating a comprehensive treatment strategy.

While the addition of GO nanohybrids and CPT to the *C. acnes* treatment enhanced the therapeutic response, it is important to note the minimal side effects observed in the combination therapy. Traditional chemotherapy often comes with significant toxicity, including immune suppression, nausea, and hair loss. However, the combination of *C. acnes*, GO nanohybrids, and CPT demonstrated an improved safety profile, with fewer adverse effects on healthy tissues. This makes the combined approach a safer, more targeted alternative to conventional therapies, which often result in long-term damage to the body's healthy cells.

In conclusion, this study highlights the potential of combining bacterial therapy with advanced nanotechnology in the treatment of cancer. *C. acnes* plays a crucial role by triggering a robust immune response, recruiting immune cells such as macrophages, cytotoxic T cells, and NK cells to target and destroy cancer cells. Its oncolytic effects are further enhanced by the addition of GO nanohybrids, which offer localized tumor destruction via photothermal therapy and improved drug delivery through the targeting of CPT directly to the tumor site. The synergistic effects of these therapies lead to more significant tumor suppression, prolonged survival, and minimal side effects compared to conventional cancer treatments.

This combined approach opens new possibilities for the future of cancer therapy, offering a safer and more effective alternative to traditional treatments. While further research is necessary to optimize this strategy and investigate its long-term effects, the results from this study suggest that bacterial therapy, when combined with nanotechnology and chemotherapy, holds great promise for transforming cancer treatment paradigms. The ability to harness the immune-modulating effects of *C. acnes* alongside the advanced drug delivery capabilities of GO nanohybrids provides a multifaceted strategy that could one day be applied in clinical settings to improve patient outcomes in cancer treatment.

List of publications related to the thesis

1. **Chintalapati, S. S. V. V.,** Iwata, S., Miyahara, M., & Miyako, E. (2024). Tumor-isolated *Cutibacterium acnes* as an effective tumor suppressive living drug. *Biomedicine and Pharmacotherapy*, 170. link $IF_{2023} = 6.9$
2. **Chintalapati, S.,** & Miyako, E. (2025). Hybrid nanoarchitectonics with bacterial component-integrated graphene oxide for cancer photothermo-chemo-immunotherapy. *Carbon*, *238*, 120252. link $IF_{2023} = 10.5$

   Press released from JAIST. Highlighted in news media (EurekAlert, AlphaGalileo, Phys Org, Nanowerk, MSN United States, Wetenschap, lab-news.de, ecancer, Graphene-Info, Energy & Capital, The Microbiologist, and Gate2Biotech, etc.)

Conferences

1. **Chintalapati S.**, Iwata, S., Miyahara, M., & Miyako, E. (2024). Tumor-isolated *Cutibacterium acnes* as an effective tumor suppressive living drug. Exponential Biomedical DX 2024 (eMEDX-24) Symposium, JAIST, Japan, December 19–20, 2024.

Awards

1. Monbukagakusho (MEXT) Scholarship for Doctoral Study by the Japanese Government; Issued by the Ministry of Education, Culture, Sports, Science and Technology, Japan (October 2022 to September 2025).

Acknowledgements

I would like to sincerely thank everyone who supported me during this research.

I am especially grateful to my supervisor, Prof. Ejiro Miyako, for his mentorship, valuable insights, and continuous encouragement. His guidance, patience, and vision were instrumental to every stage of this research.

I am grateful to the Ministry of Education, Culture, Sports, Science and Technology (MEXT), Japan, for providing the scholarship that made it possible for me to pursue my studies at the Japan Advanced Institute of Science and Technology (JAIST).

I also thank Prof. Kazuaki Matsumura for his support as my second supervisor, and Prof. Takumi Yamaguchi for his input and valuable guidance during this journey as my minor research professor.

I appreciate the help and companionship of my lab mates and lab staff, friends, and everyone in the Department of Materials Science at JAIST. Their presence made the experience more meaningful. I would also like to thank my parents, my brothers, my relatives, and my friends for their support from afar. Lastly, I would like to thank my late grandfather for believing in me and supporting me to this point. Their constant support and belief in me have brought me here.